

2005

# Investigation of residual stress and distortion due to phase transformations in LENS [i.e. Laser Engineered Net Shaping] using finite element analysis

Matthew Tomik  
*Lehigh University*

Follow this and additional works at: <http://preserve.lehigh.edu/etd>

---

## Recommended Citation

Tomik, Matthew, "Investigation of residual stress and distortion due to phase transformations in LENS [i.e. Laser Engineered Net Shaping] using finite element analysis" (2005). *Theses and Dissertations*. Paper 906.

This Thesis is brought to you for free and open access by Lehigh Preserve. It has been accepted for inclusion in Theses and Dissertations by an authorized administrator of Lehigh Preserve. For more information, please contact [preserve@lehigh.edu](mailto:preserve@lehigh.edu).

Tomik, Matthew

Investigation of  
Residual Stress  
and Distortion due  
to Phase  
Transformations  
in LENS using...

September 2005

Investigation of Residual Stress and Distortion due to  
Phase Transformations in LENS using  
Finite Element Analysis

By

Matthew Tomik

A Thesis

Presented to the Graduate and Research Committee  
Of Lehigh University  
in Candidacy for the Degree of  
Master of Science

In

Mechanical Engineering and Mechanics

Lehigh University  
2005

This thesis is accepted and approved in partial fulfillment of the requirements of the  
Master of Science.

August 12, 2005

Date

Thesis Advisor

Chairperson of Department

# Table of Contents

List of Figures .....	v
List of Tables .....	vii
Abstract .....	1
Chapter 1 - Introduction .....	2
1.1 Rapid Prototyping and LENS History .....	2
1.2 Industry Applications .....	8
1.3 Purpose of Research .....	11
1.4 Welding Research History .....	12
1.4.1 The Beginnings of Welding Research .....	12
1.4.2 Use of Computers in Welding Research .....	13
1.4.3 Development of Heat Source and Material Property Models .....	16
1.4.4 Welding Simulation Incorporating Filler Material .....	20
1.5 LENS and 3D Cladding Research .....	22
1.6 Issues and Objectives .....	26
Chapter 2 - Modeling Concerns .....	27
2.1 Introduction .....	27
2.2 Thermal Aspect .....	27
2.3 Mechanical Aspect .....	30
2.4 Metallurgical Aspect .....	32
Chapter 3 - LENS builds .....	34
3.1 Introduction .....	34
3.2 Operating Parameters .....	35
3.3 Build Progression .....	37
Chapter 4 - Modeling Using SYSWELD .....	47
4.1 Geometric Modeling Aspect .....	48
4.2 Thermal Modeling Aspect .....	52
4.3 Mechanical Modeling Aspect .....	54
4.4 Metallurgical Modeling Aspect .....	55
4.5 Temporal Modeling Aspect .....	58

Chapter 5 - Results and Discussion.....	59
5.1 Thermal Results .....	59
5.2 Mechanical Results .....	67
Chapter 6 - Conclusions and Recommendations .....	78
6.1 Conclusions.....	78
6.2 Recommendations.....	79
References.....	81
Appendix.....	83
Vita.....	99

## List of Figures

Figure 1.1 - Stereolithography Example <sup>[1]</sup> .....	4
Figure 1.2 - Photomasking <sup>[1]</sup> .....	4
Figure 1.3 - LENS 750 at Lehigh University .....	6
Figure 1.4 - LENS 750 Head and Stage .....	7
Figure 1.5 - Mold with Conformal Cooling Channel <sup>[5]</sup> .....	10
Figure 1.6 - Gaussian Heat Source Model <sup>[9]</sup> .....	18
Figure 1.7 - Conical Heat Source Model <sup>[16]</sup> .....	20
Figure 1.8 - Long Raster Pattern vs. Short Raster Pattern <sup>[19]</sup> .....	23
Figure 2.1 - Typical Steel Stress/Strain Curve .....	32
Figure 3.1 - LENS builds example .....	35
Figure 3.2 - First build set example .....	38
Figure 3.3 - Effect of changing laser power. (35, 40, 45 and 50 amp laser current shown from front-left to back-right) .....	40
Figure 3.4 - Effect of changing powder feeder RPM. (4, 6, 8 and 10 RPM shown from front-left to back-right) .....	40
Figure 3.5 - Effect of using different set build height (A is front-left and B is back-right) .....	41
Figure 3.6 - Line Build with feed rate of 4.00 mm/s .....	42
Figure 3.7 - Line Build with feed rate of 8.00 mm/s .....	43
Figure 3.8 - 6.0 - 9.5 mm/s build set (6, 8 and 10 RPM from left to right, 6.0 to 9.5 mm/s from front to back) .....	44
Figure 3.9 - Build with “wavy” defect .....	44
Figure 3.10 - “Best” build from set in Figure 3.11 .....	45
Figure 3.11 - Line build exhibiting small dip on left side .....	46
Figure 3.12 - Final build off of which the models are based .....	47
Figure 4.1 - Comparison of experimental build and model (side view) .....	49
Figure 4.2 - Comparison of experimental build and model (top view) .....	50
Figure 4.3 - Finite Element Mesh ( left: Top View, right: Front View) .....	51
Figure 5.1 - Small Weld Pool Example .....	60
Figure 5.2 - Molten Pool size at t ~ 5 seconds (S355J2G3, DC04 and X20Cr13 from left to right) .....	62
Figure 5.3 - S355J2G3 Simulation, t ~ 11.5 s .....	63
Figure 5.4 - DC04 Simulation, t ~ 11.5 .....	63
Figure 5.5 - X20Cr13 Simulation, t ~ 11.5 s .....	64
Figure 5.6 - Molten Pool size at t ~ 25 seconds (S355J2G3, DC04 and X20Cr13 from left to right) .....	65
Figure 5.7 - S355J2G3 Simulation, t ~ 25.0 s .....	66
Figure 5.8 - DC04 Simulation, t ~ 25.0 s .....	66
Figure 5.9 - X20Cr13 Simulation, t ~ 25.0 s .....	67
Figure 5.10 – S355J2G3 Simulation, t ~ 25.00 s, $\sigma_{xx}$ (MPa) .....	69
Figure 5.11 - DC04 Simulation, t ~ 25.00 s, $\sigma_{xx}$ (MPa) .....	69
Figure 5.12 - X20Cr13 Simulation, t ~ 25.00 s, $\sigma_{xx}$ (MPa) .....	70

Figure 5.13 – S355J2G3 Simulation, $t \sim 25.00$ s, $\sigma_{yy}$ (MPa) .....	70
Figure 5.14 - DC04 Simulation, $t \sim 25.00$ s, $\sigma_{yy}$ (MPa).....	71
Figure 5.15 - X20Cr13 Simulation, $t \sim 25.00$ s, $\sigma_{yy}$ (MPa).....	71
Figure 5.16 - S355J2G3 Simulation, $t \sim 25.00$ s, $\sigma_{yy}$ (MPa), bead only .....	72
Figure 5.17 – DC04 Simulation, $t \sim 25.00$ s, $\sigma_{yy}$ (MPa), bead only.....	72
Figure 5.18 - S355J2G3 Simulation, $t \sim 25.00$ s, $\sigma_{yy}$ (MPa), bead only .....	73
Figure 5.19 - S355J2G3 Simulation, $t = 60.00$ s, $\sigma_{xx}$ (MPa).....	74
Figure 5.20 - DC04 Simulation, $t = 60.00$ s, $\sigma_{xx}$ (MPa).....	74
Figure 5.21 - X20Cr13 Simulation, $t = 60.00$ s, $\sigma_{xx}$ (MPa) .....	75
Figure 5.22 - S355J2G3 Simulation, $t = 60.00$ s, $\sigma_{yy}$ (MPa).....	75
Figure 5.23 - DC04 Simulation, $t = 60.00$ s, $\sigma_{yy}$ (MPa).....	76
Figure 5.24 - X20Cr13 Simulation, $t = 60.00$ s, $\sigma_{yy}$ (MPa) .....	76
Figure 5.25 - S355J2G3 Simulation, Displacement in y direction (mm) (shifted scale)	77
Figure 5.26 - DC04 Simulation, $t = 60.00$ s, Displacement in y direction (mm).....	77
Figure 5.27 – X20Cr13 Simulation, $t = 60.00$ s, Displacement in y direction (mm).....	78



## List of Tables

Table 3.1 - LENS Operating Manual suggested parameters.....	37
Table 3.2 - Build parameters for Figure 3.5.....	41
Table 3.3 - Build parameters for Figure 3.7.....	43
Table 3.4 - Parameters of final build (Figure 3.12) .....	47
Table 4.1 - Heat source input parameters .....	52
Table 4.2 - Material Composition of S355J2G3[31] .....	56
Table 4.3 - Material Composition of DC04[32] .....	56
Table 4.4 - Material Composition of X20Cr13[33] .....	57
Table 4.5 - Experimental Build Timing.....	59
Table 4.6 - Simulation Build Timing.....	59
Table 5.1 - Thermal Results Color Index.....	61
Table 5.2 - Temperatures data ~ 5. 0s.....	62
Table 5.3 - Temperature Data ~ 11.5 s .....	64
Table 5.4 - Temperature Data ~ 25.0 s .....	67

## **Abstract**

Laser Engineered Net Shaping (LENS) is a relatively new rapid prototyping technology that creates parts using an advanced laser welding process. Since this is a new technology, many aspects of LENS created parts are still not well understood. One specific area which has been given little attention is the effect of phase transformations on residual stress and distortion. The goal of this research is to run a series of simulations to examine the impact of phase transformations on parts created by LENS.

Three finite element simulations of the LENS process were computed using the finite element welding program SYSWELD. A different material model was used for each of the two simulations to assess the effect of phase transformations in the LENS process. Thermal and mechanical simulations were run for each of the three material models. All of the models were based on representative LENS builds done at Lehigh University.

The results of the thermal simulations for each of the materials were very similar, providing a good stage on which to compare the mechanical simulations. The results of the mechanical simulation showed very little difference in residual stress or distortion between the different materials. These results indicate that phase transformations do not appear to have an affect on the residual stresses or distortion when simulating a LENS line build using these specific materials.

# Chapter 1 - Introduction

## *1.1 Rapid Prototyping and LENS History*

Laser Engineered Net Shaping (LENS) is a relatively new technology in the growing field of rapid prototyping. Rapid prototyping is the creation of a complex part directly from a solid model. More specifically, rapid prototyping uses a layer-by-layer approach to create three-dimensional parts directly from a solid model on a computer. The solid model is broken down into many thin cross sections and the part is built by depositing these thin cross sections one-on-top-of-another until the part is complete.

Rapid prototyping has several advantages over traditional manufacturing methods. Creating parts using rapid prototyping is faster and cheaper than conventional manufacturing. Rapid prototyping is also capable of making more complex parts than conventional machining due to the layer-by-layer approach. While these advantages give rapid prototyping significant potential, there are also some disadvantages. Many types of rapid prototyping are only capable of making prototypes, not fully-functional parts. The other main problem with rapid prototyping is that it usually cannot match the precision of a conventionally-machined part. This problem is primarily due to the limited experience in the various rapid prototyping methods. One would expect that with more experience will come more precise parts.

Although some of the rudimentary concepts of rapid prototyping were established in the 19<sup>th</sup> Century, modern rapid prototyping emerged in the 1980s. The origins stemmed from two different areas: photo-sculpture and topography. As early as

1860 François Willème designed a sculpting technique which used equally spaced cameras around an object. This allowed Willème to create small portions of the object which could be assembled to form the sculpture. In 1892, J.E. Blather patented a layered method for creating topographical relief maps. His method consisted of stacking contoured wax plates, one on top of another, to create a mold for a paper map.<sup>[1, 2]</sup>

Laser photolithography, the first modern form of rapid prototyping to emerge, was based on photopolymers. Laser photolithography uses a laser along with a photo-curable resin to create parts. The first commercially available rapid prototyping machine was 3D Systems' Stereolithography Apparatus in 1988 (See Figure 1.1). Other similar laser photolithography systems became available around 1990. For example, one system used a transparent plate underneath the part allowing a laser to scan from below the part. Another variation used a stationary laser and moved the part to achieve the X-Y scanning capability. Also developed around 1990 was another rapid prototyping technique called photomasking (See Figure 1.2). This system uses a light source to solidify a photopolymer; however, a mask is used to selectively apply the light to given areas.<sup>[1-3]</sup>

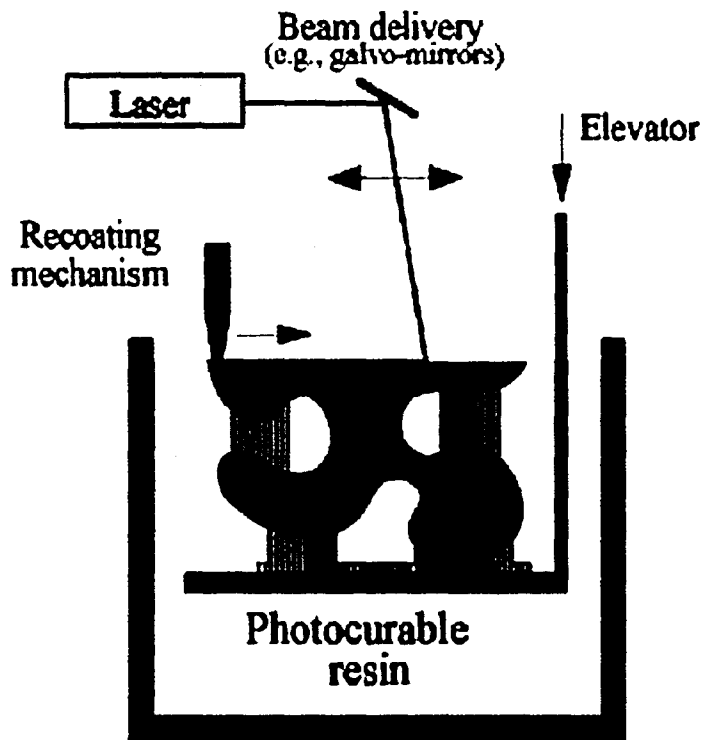


Figure 1.1 - Stereolithography Example<sup>(1)</sup>

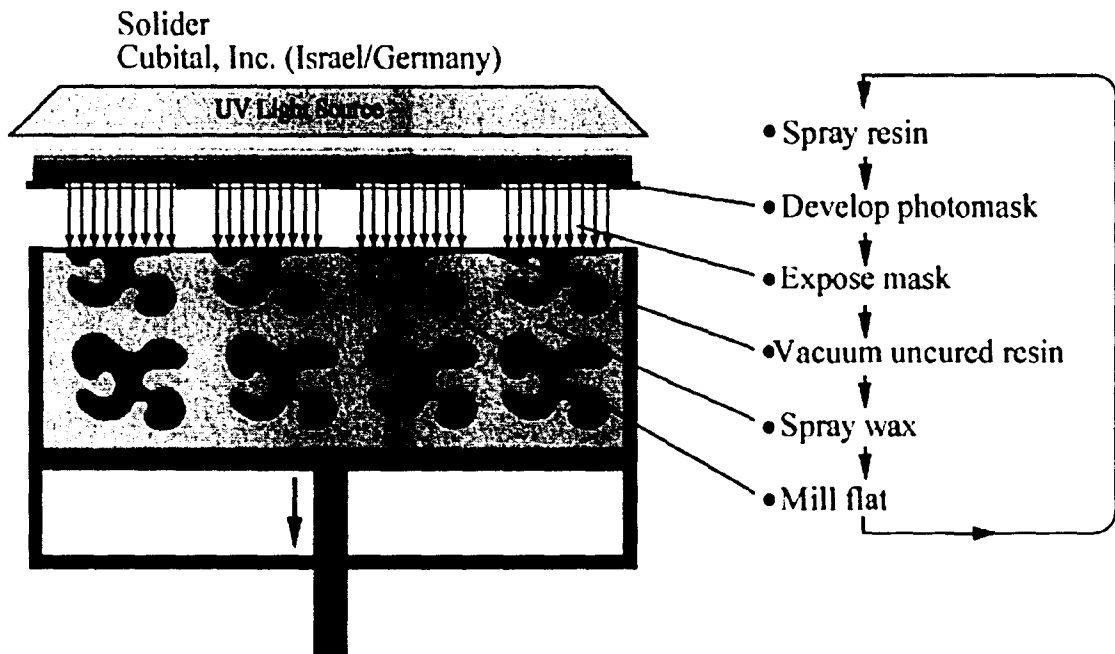


Figure 1.2 - Photomasking<sup>(1)</sup>

While laser photolithography was the first type of rapid prototyping available commercially, other types were being developed around the same time period. These

other types are classified in three main categories: powder, lamination, and deposition. Powder rapid prototyping is named as such because it uses powder for its stock material. Lamination rapid prototyping uses sheets of material to create parts. The process works by cutting two-dimensional cross-sections into the sheet, then stacking and adhering the sheets one-on-top-of-another. Lastly, deposition rapid prototyping uses various methods to add material to the part in designated areas. For example, Fused Deposition Molding extrudes a polymer, in a very controlled fashion to create parts. Overall, many concepts rapid prototyping methods are being investigated. <sup>[1, 2]</sup>

LENS is a 3D-cladding rapid prototyping method, which falls under the powder rapid prototyping category. Figure 1.3 shows Lehigh University's Optomec LENS 750 without the front cover. It uses a laser beam in conjunction with powdered metal and a metal substrate. A 700 watt Nd:YAG laser is focused on the metal substrate creating a weld pool. Four copper nozzles feed powder to the weld pool, creating the desired material build-up. The stage, on which the metal substrate is mounted, scans in the x and y-directions to build the part up in the desired areas and create a cross section. The three-dimensional part is created by adding layer upon layer in this same fashion until the piece is complete. A better view of the LENS 750 head, including the stage, can be seen in Figure 1.4. The head assembly is located inside a glove box with a controlled atmosphere (oxygen between 3-5 ppm) to minimize defects in the part. LENS, in particular, has many advantages over both traditional manufacturing and other forms of rapid prototyping. LENS, unlike some rapid prototyping methods, is capable of making fully-functional parts for load bearing applications. It is also able to make more

complicated parts and make parts faster and cheaper than conventional machining. In addition, LENS is capable of creating functionally-graded materials. Lastly, LENS-created parts have improved properties because they are essentially heat treated during part creation. [3, 4]

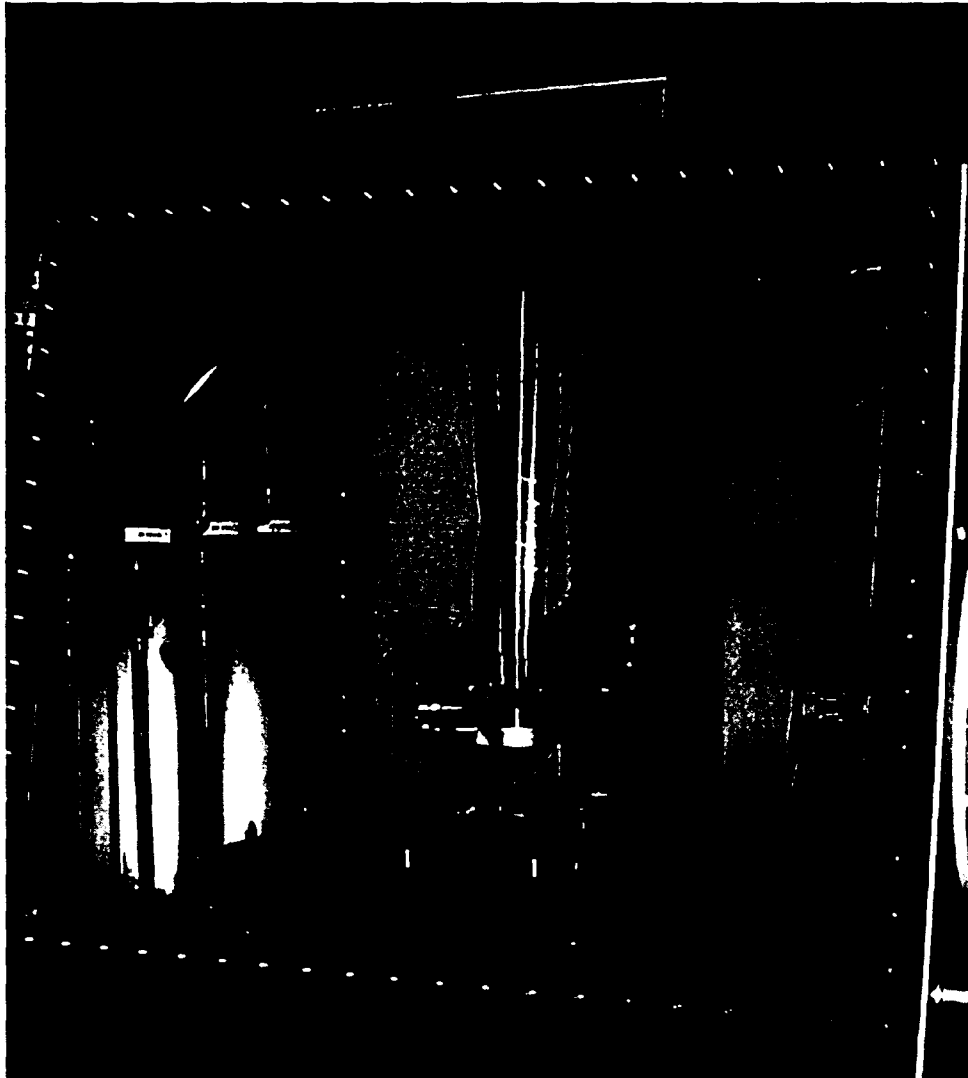


**Figure 1.3 - LENS 750 at Lehigh University**

complicated parts and make parts faster and cheaper than conventional machining. In addition, LENS is capable of creating functionally-graded materials. Lastly, LENS-created parts have improved properties because they are essentially heat treated during part creation. [3,4]

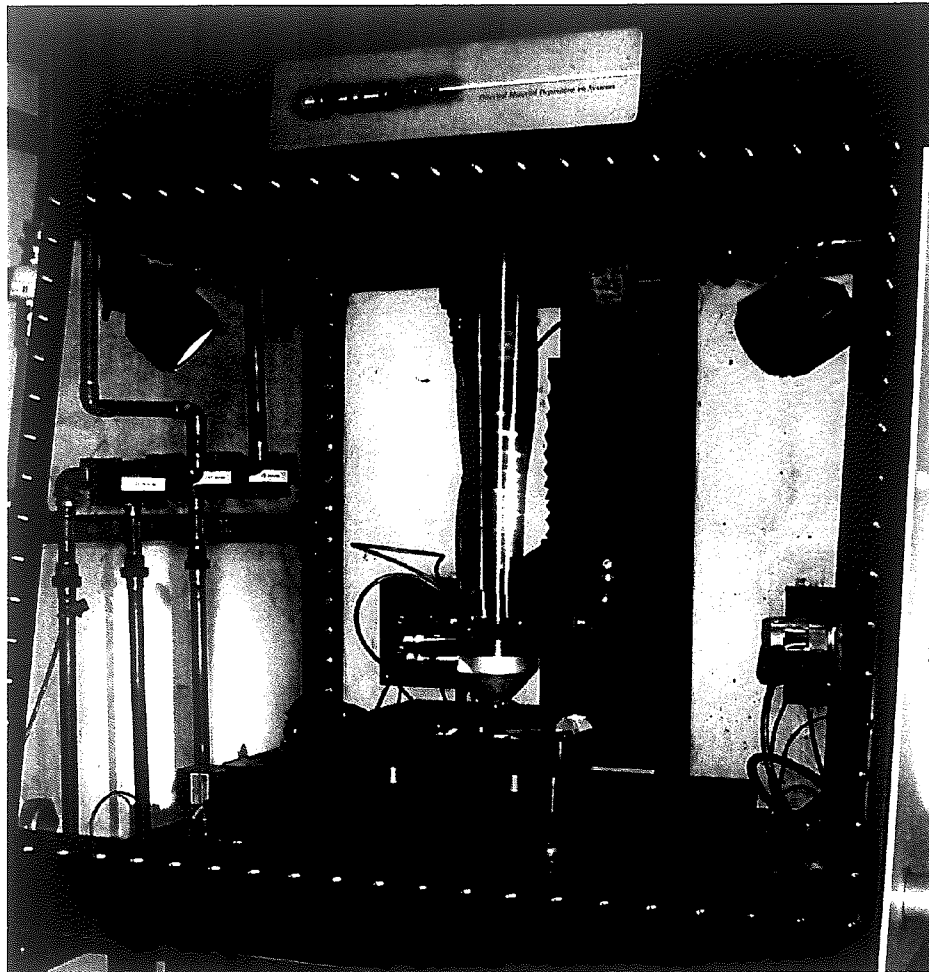


**Figure 1.3 - LENS 750 at Lehigh University**



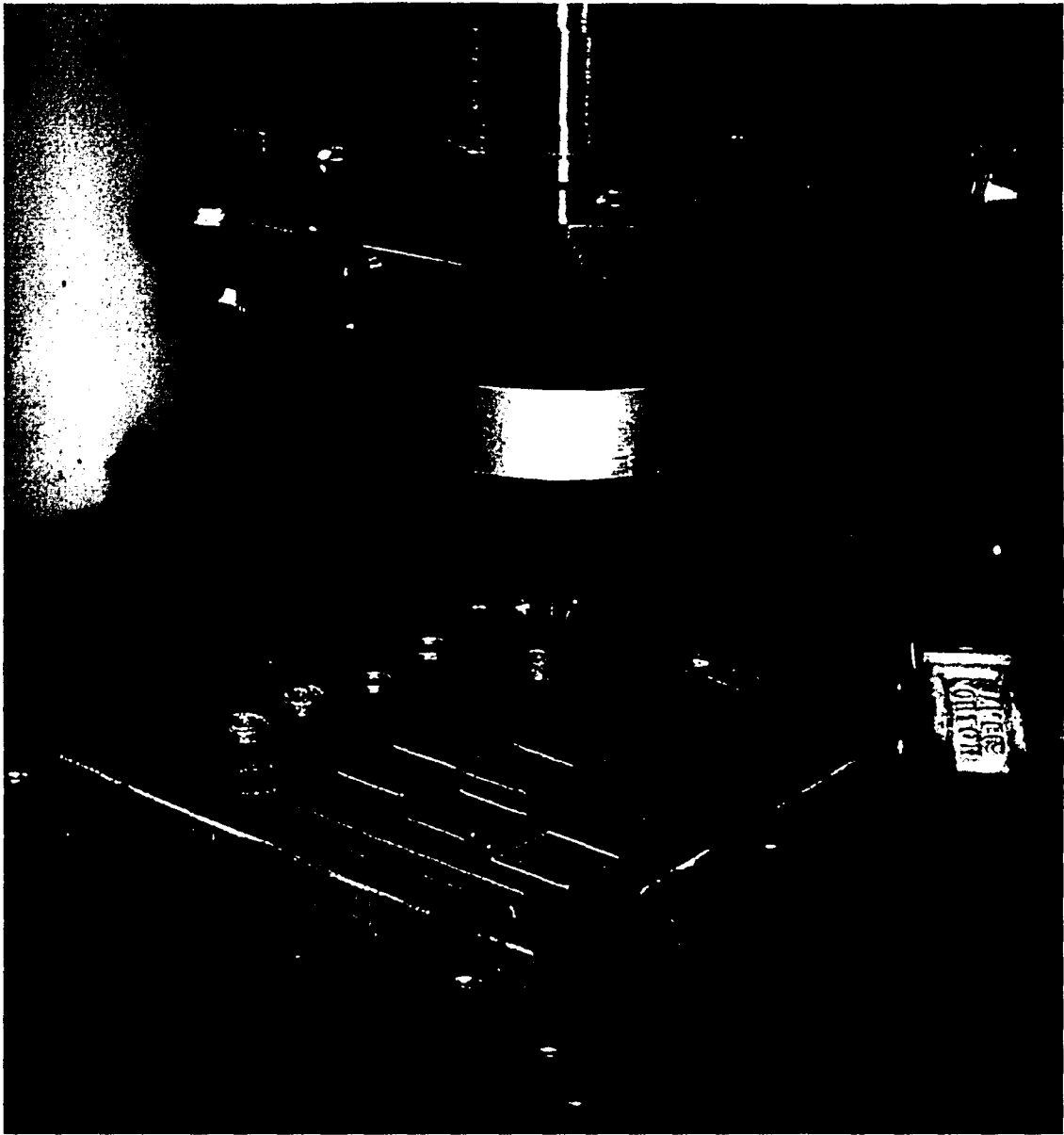


**Figure 1.4 - LENS 750 Head and Stage**

It should be noted that while this study focuses on LENS in particular, it should also be applicable for other 3D cladding rapid prototyping machines. Two specific examples are Directed Light Fabrication (DLF) developed at Los Alamos National Laboratory and Controlled Metal Build Up (CMB) developed at Fraunhofer Institute for Production Technology. Both of these processes are similar to LENS and may benefit from this study. <sup>[1, 2]</sup>



Figure 1.4 - LENS 750 Head and Stage

It should be noted that while this study focuses on LENS in particular, it should also be applicable for other 3D cladding rapid prototyping machines. Two specific examples are Directed Light Fabrication (DLF) developed at Los Alamos National Laboratory and Controlled Metal Build Up (CMB) developed at Fraunhofer Institute for Production Technology. Both of these processes are similar to LENS and may benefit from this study. <sup>[1, 2]</sup>

Development of the LENS began in 1993 at Sandia National Laboratories in Albuquerque, NM. The LENS was developed under a Cooperative Research and Development Agreement (CRADA) formed in 1997 between 3M, Honeywell, Optomec, Wyman-Gordon, Laser Fare, KAPL, NASA, and Ford, among others. In 1998, the first commercial LENS was delivered to a consumer. Currently, the LENS machine is in its third-generation and further development is still being pursued. <sup>[4]</sup>

## ***1.2 Industry Applications***

The fast and cost-efficient creation of prototypes is a major application for LENS and other rapid prototyping systems. However, the unique properties of 3D cladding provide interesting and useful opportunities in other areas. One capability of 3D cladding methods is the capacity to make fully-functional metal parts, not just prototypes. Another advantage of LENS is the very small heat affected zone it produces during operation. A third, advanced, capability possible with LENS, and other 3D-cladding methods, is the creation of parts with very complex geometry. Lastly, these rapid prototyping methods are capable of making parts with functionally-graded materials. The capabilities of LENS, and 3D cladding in general, have a large potential to not only address rapid prototyping needs, but to provide new solutions in other manufacturing areas as well. <sup>[5]</sup>

Making fully-functional metal parts with a process like LENS has several advantages. The first advantage is that parts created using LENS may be tested. This is very useful for parts which need to carry a load. Since LENS is capable of making fully-functional parts, it is ideal for short-run production. The small number of parts

can be made without wasting time and money on setup and tooling or mold creation. Lastly, the ability to make fully functional parts is ideal for applications where storing a lot of stock material is difficult. On a deployed submarine, for example, it is very inconvenient to store large quantities of stock material or to have material delivered in the case of a malfunctioning part. An onboard LENS machine would allow the submarine to easily create replacement parts on its own without having to store vast amounts of material.<sup>[5]</sup>

The heat affected zone in a welding type operation is where the part has reduced strength and cracking can more easily occur. LENS achieves improved material properties by greatly reducing the size of the heat affected zone. The LENS heat affected zone is reduced because of the rapid melting and solidifying process, as well as the very precise application of heat. This property of LENS is very important for many repair applications. For example, compressor and turbine blades are very costly items to produce because of the tight tolerances and complex metallurgy. Repairing these items would save a lot of money, but it is difficult to maintain the tolerances and metallurgy through conventional welding repair. LENS is capable of repairing these types of parts because the small heat affected zone minimizes the residual stress and deformation. In addition, LENS actually deposits material that has the same microstructure as the original blades, further enhancing the repair quality.<sup>[5]</sup>

The layer-by-layer technique used by LENS allows it to create parts that may not be possible to create through conventional machining. While there are many areas that could make use of this, one of the most prominent is the injection molding industry. One part, which cannot be made by traditional machining techniques, is a mold with

conformal cooling channels. Conformal cooling channels, shown in Figure 1.5, are passages inside the mold that follow the contours of the mold cavity and are very effective cooling the mold. In industry it is very desirable to cool molds rapidly because it is usually the longest time delay during the injection-molding cycle. Reducing the cycle time is highly desirable because it reduces cycle time and part cost.<sup>[5]</sup>

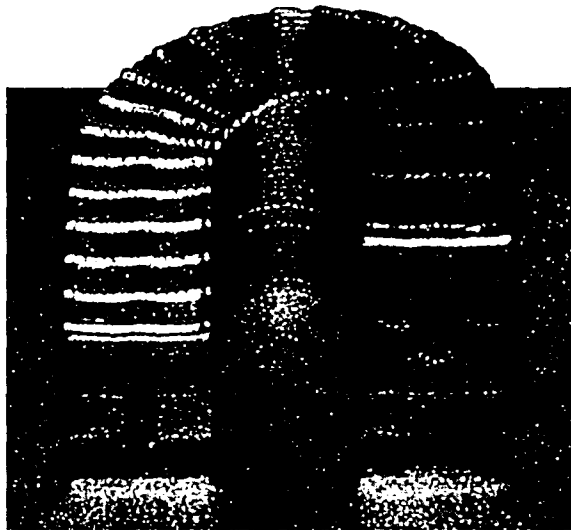


Figure 1.5 - Mold with Conformal Cooling Channel<sup>[5]</sup>

Lastly, the capability of LENS to make functionally graded parts also provides unique and interesting opportunities. Since LENS uses powder as its stock material, it can change powder composition during part creation by switching from one material to another. This is very useful in mold creation as well as things like car or bicycle frame creation. Functionally-graded materials can enhance the important, and previously discussed, mold cooling. For example, LENS can be used to manufacture a mold comprised of both steel and copper. The steel can be deposited in the areas of the mold that require good mechanical properties and the copper in areas that require good thermal properties. Using this type of setup allows for the creation of molds with much

better thermal performance and minimal loss in mechanical performance. As another example, in the fabrication of a bicycle frame, functionally graded materials can be used to provide increased strength in high stress areas. LENS is capable of constructing a bicycle frame from steel and depositing a high-strength material like titanium in the areas likely to see higher stresses.<sup>[5]</sup>

All these properties demonstrate that LENS and 3D cladding are useful for much more than just rapid prototyping. The unique properties of LENS allow it to fabricate fully-functional, highly-complex, functionally-graded parts with improved material properties. LENS and 3D cladding have great potential to improve the many aspects of manufacturing as it is known today.

### ***1.3 Purpose of Research***

Less than ten years old, LENS, and other 3D-cladding systems, have yet to realize their potential. While LENS makes it possible to create parts that have conformal cooling channels or functionally graded material, it is more complicated than simply pressing a button and watching the part appear. It is necessary to understand the thermal and mechanical aspects taking place in order to optimize the building process. Parameters such as laser power and powder feed rate, among others, need to be set to the right level to optimize build time and the properties of the part. The purpose of research on LENS is to more completely understand all aspects of the process. A thorough understanding will allow more precise control of the parts that are created. The overall goal of LENS research is to use this improved understanding to realize all the potential uses of LENS.

## ***1.4 Welding Research History***

### **1.4.1 The Beginnings of Welding Research**

Since 3D cladding is closely related to laser welding, much of the research done on welding can also be applied to LENS and 3D cladding. In the late 1930s Rosenthal<sup>[6]</sup> first developed a way to calculate the thermal distribution in welds. His method applied Fourier's basic theory of heat flow to a moving heat source. Although Rosenthal's method was fairly simple, it provided useful results and a good starting point for future heat flow analysis. His method gives accurate results in the areas where the temperature remained below 20 percent of the material's melting point. However, his method is subject to increasing error when approaching the heat source. <sup>[3]</sup>

Due to its simplicity, Rosenthal's model allowed him to calculate the thermal history of a weld analytically. His analysis used not only a point heat source and constant material properties, but also assumed a quasi-stationary state<sup>[6]</sup>. Quasi-stationary heat flow occurs when the temperature distribution becomes constant with respect to the heat source. This allows the use of a moving coordinate system that travels with the heat source. The quasi-stationary flow means that at every position, the temperature distribution will be the same relative to the heat source, allowing easy calculation of thermal history. The advantage of using quasi-stationary flow is that the model is much easier to solve. However, the disadvantage is that it only applies to the middle of longer welds. Short welds and the beginning and ending of all welds most certainly do not exhibit quasi-stationary heat flow characteristics.

While most early welding models in the United States used the quasi-stationary flow assumption, according to Masubuchi,<sup>[7]</sup> research in Japan was focusing on heat

flow in the non-stationary state. In the 1930s and 1940s, Tanaka, Naka, and Masubuchi investigated modeling this non-stationary state heat flow in welding. From the late 1940s-to-late-1950s, Nippes and Savage studied the heat affected zone in welds, in particular, the cooling rates. Also in the late 1950s, Suzuki researched the heat affected zone in high strength steels. Nippes and Savage, as well as Suzuki, concluded that their models have two main deficiencies. The first problem with their models was the point heat source did not sufficiently represent the actual heat source, creating an inaccurate thermal history for the heat affected zone. The second problem was high thermal gradients in the heat affected zone coupled with constant thermal properties for the material in the model did not suffice. Although these problems were recognized, they were hard to correct. <sup>[7]</sup>

Introducing a more accurate heat source model and non-constant thermal properties into welding models makes the analysis significantly more complicated. The use of non-constant thermal properties alone transforms the fundamental equation for heat transfer in solids from a linear to a non-linear problem. Solution of non-linear equations analytically is difficult, and, in many cases, impossible. Thus, a problem existed: current models were not accurate enough while more accurate models were too complex to be solved. The answer to this problem came in the form of computers, which made it possible to solve these complicated models. <sup>[7]</sup>

#### **1.4.2 Use of Computers in Welding Research**

According to Masubuchi, computers began being used for solving welding heat flow problems around 1965. In 1967, University of Wisconsin researchers Myers<sup>[8]</sup> *et*



*al.*, used computers to solve for the heat flow in welding. Although the model they used still employed the simplifications of a point heat source and constant material models, it was one of the first documented applications of using a computer to solve a weld model. Then in 1969, Pavelic<sup>[9]</sup> *et al.*, also at the University of Wisconsin, used a computer to solve a more complicated welding model that included a more advanced heat source model. He used the finite difference method to create equations and used the computer to solve them numerically. Pavelic was able to obtain much greater accuracy than previous models; however his model was still lacking a non-constant material model. Also, Pavelic's model was only a two dimensional analysis.

In the early 1970s computers were being used for analyzing welding by both McDonnell Douglas Astronautics Company and M.I.T.<sup>[7]</sup> The research at McDonnell Douglas, conducted by Stoeckinger,<sup>[10]</sup> was mostly concerned with determining the amount of heat delivered by the source rather than the actual thermal history of the weld. However, his research did use non-constant material models and a three dimensional welding model. Stoeckinger concluded that one could indeed accurately predict the amount of heat which enters the weld pool. He based this conclusion on a comparison of temperatures predicted by his simulation with temperatures recorded by thermocouples during welding. Stoeckinger's research model was capable of predicting the amount of heat delivered but was deficient in being able to predict the thermal history of the entire weld. He assumed the heat source had constant power over an area, which was not ideal according to Pavelic.<sup>[9]</sup> Stoeckinger's comparison of experimental versus simulated data was not done in the weld pool, but the comparison closest to the weld did show the greatest amount of error.

In 1975, following Stoeckinger's lead, Paley and Hibbert<sup>[11]</sup> focused on the temperature history of the weld in "Computation of Temperatures in Actual Weld Designs". Like Stoeckinger, Paley and Hibbert used a three-dimensional model with non-constant material properties. The heat source model they used not only applied heat to the surface, but to the whole element inside the fusion line. In order to compare experimental data to simulation data, Paley and Hibbert superimposed the simulated isotherms onto the corresponding macrosection of the actual weld. While this method of comparison is easy to understand, it is difficult to quantify. A more accurate heat source model would most likely improve the accuracy of this model.

In 1983, Goldak<sup>[12]</sup> *et al.* developed a new model for welding heat sources. Goldak's main concern in his paper was modeling the welding heat source accurately. He developed a double ellipsoid heat source model for his simulations. Goldak compared his model to previous ones by looking at both cooling time and temperature distribution near the heat source. He showed that his model was indeed more accurate than previous welding models, including Rosenthal's. However, the model still differed from experimental results by five percent. Goldak suggests this may be due to the fact that his model neglects longitudinal heat flow since it is only a two-dimensional model.

In 1979, ESI software decided to develop a program to numerically simulate welding through use of finite element analysis. In 1981, the first version of this software, called SYSWELD, was available. Development of this software made it possible to model welding processes without developing code to solve the finite element equations. Currently, SYSWELD is able to perform welding simulations using a complex heat source model, such as the double ellipsoid, and use three dimensional

models. Thus, all the shortcomings of the models done previously may be avoided when using SYSWELD. SYSWELD, like most software programs, has been updated and improved significantly since its original release in 1981. <sup>[13]</sup>

### **1.4.3 Development of Heat Source and Material Property Models**

While Rosenthal's initial 1930s research was very successful, it was only a beginning. The goal of modeling welding procedures is to obtain a precise knowledge of the thermal history of the welded part. Knowledge of the thermal history, and how that specific material is affected by the thermal events, allows the prediction of part microstructure. Rosenthal's research was not accurate enough for use in predicting micro-structural changes in the material. His model had two major short-comings: the heat source model and the material properties model. Rosenthal used a point source to model the heat source. Unfortunately, a point source does not resemble an actual welding heat source, and models everything from a laser heat source to an arc welding heat source the same. This is the biggest cause of the large error near the heat source in Rosenthal's model. Furthermore, Rosenthal's material properties are faulty as they are independent of temperature. Metal properties are directly affected by temperature and this assumption causes inaccuracies in both thermal and mechanical calculations. With knowledge of the accuracy problems in Rosenthal's model, researchers began developing better welding models. <sup>[9]</sup>

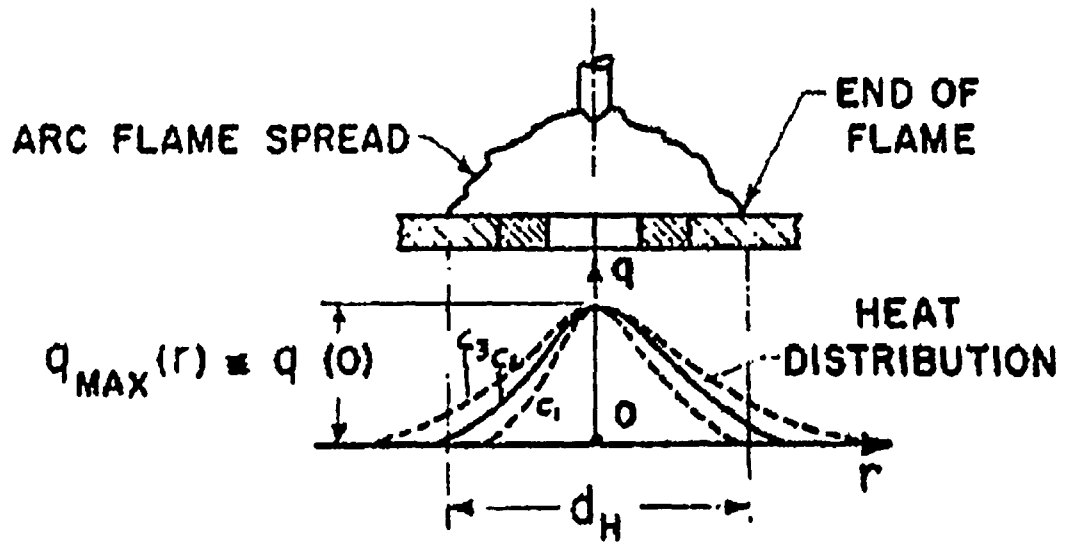
The first step towards an improved heat source model was taken in 1969 by Pavelic *et al.* Pavelic investigated this welding simulation problem as well, and suggested modeling a normal circular heat source with a Gaussian distribution of

specific heat flux about the surface. The equation for the distribution proposed by Pavelic is:

$$q(r) = q(0)e^{-Cr^2} \quad (2.1)$$

Where:  $q(r)$  = surface flux at radius  $r$  ( $W/m^2$ )  
 $q(0)$  = maximum heat flux (at source center) ( $W/m^2$ )  
 $C$  = concentration coefficient ( $m^{-2}$ )  
 $r$  = radial distance from source center ( $m$ )

This equation is shown graphically in Figure 1.6. Changing the concentration coefficient,  $C$ , allows modeling of heat sources that are more or less dispersed. This model showed significant improvement over the point heat source model used by Rosenthal. Compared to experimental data cited by Pavelic, Rosenthal's model predicted 46 percent below the experimental peak temperature and the Gaussian model was off by a much smaller 4.7 percent.



$$c_1 > c_2 > c_3$$

$d_H \equiv$  HOT SPOT (DIA.)

$C \equiv$  CONCENTRATION COEFFICIENT

Figure 1.6 - Gaussian Heat Source Model<sup>[9]</sup>

In 1975, Friedman<sup>[14]</sup> applied Pavelic's heat source model to a moving coordinate system. In 1978, Krutz and Segerlind<sup>[15]</sup> modified Friedman's equation slightly to fit their needs. Their resulting equation relating flux to radius and time is:

$$q(r,t) = \frac{3Q}{\pi R^2} e^{(-3r/R)^2} e^{-3\left(\frac{Vt-\tau}{R}\right)^2} \quad (2.2)$$

- Where:
- $q(r,t)$  = surface heat flux at radius  $r$  and time  $t$  ( $W/m^2$ )
  - $r$  = radial distance from heat source center (m)
  - $t$  = time (s)
  - $Q$  = total heat input (W)
  - $R$  = maximum radius (m)
  - $V$  = heat source velocity (m/s)
  - $\tau$  = lag factor (m)

Conversion of this 2D Gaussian distribution model to a moving coordinate system helps simplify the complex welding model.

Although the 2D Gaussian distribution model showed significant improvement over the previous heat source model, it was not complete. Heat sources tend not only to apply heat to the surface, but penetrate through to the underlying layers. Since Pavelic’s model is only two-dimensional, it fails to address this “digging” action of most heat sources. After consideration by other researchers of hemispherical and ellipsoidal power density distributions, Goldak *et al.* proposed a double ellipsoidal power density distribution model for heat sources. This model is more accurate for both penetrative and non-penetrative heat sources. Its advantage over the ellipsoidal model is that it is capable of modeling non-axisymmetric heat sources in addition to symmetric ones.

While the double ellipsoid model is still used, a more accurate model exists for high powered lasers such as the one used by LENS. For this specific type of laser, a more accurate model is the 3D conical Gaussian heat source model. This more closely matches the deeper penetration exhibited by high powered lasers. The equation for this heat source model is:

$$q(r, z, t) = - \frac{9Q}{\pi(r_c^2 z_i + z_i r_i^2 + r_c r_i z_i - r_c^2 z_c - z_c r_i^2 - z_c r_i r_c)} e^{-3 \frac{r^2}{r_0(z)^2}} \quad (2.3)$$

Although most sources do not mention when and where the 3D conical Gaussian heat source model was developed, it seems to be the standard for laser and electron beam sources. SYSWELD, in fact, has this model built into the software and recommends that it be used for sources such as a laser or electron beam. <sup>[16]</sup>

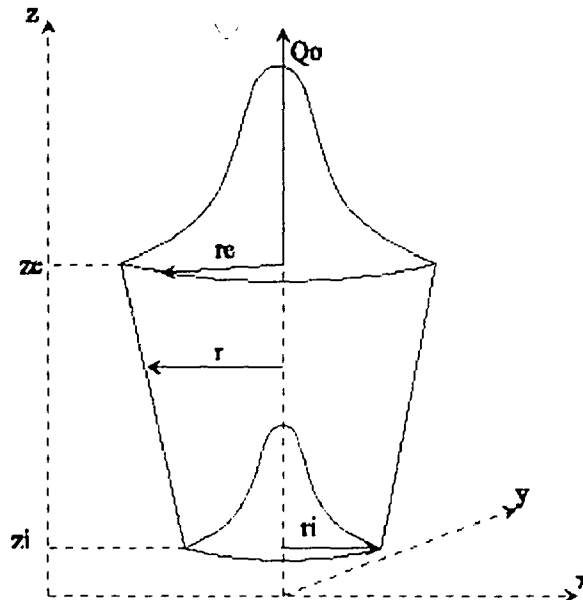


Figure 1.7 - Conical Heat Source Model<sup>[16]</sup>

Many researchers after Rosenthal continued to model the material properties independent of temperature. Metal characteristics like thermal diffusivity and thermal conductivity change with temperature and should be modeled as such in order to accurately simulate a welding operation. Stoeckinger was the first researcher to use a more accurate material model. Goldak went further than Stoeckinger by modeling the material properties using data gathered by the British Iron and Steel Research Association (BISRA). He also used numbers to approximate thermal conductivity in the liquid range and heat of fusion and heat of transformation.<sup>[12]</sup> However, this seems to be the last step taken in regards to material modeling.

#### 1.4.4 Welding Simulation Incorporating Filler Material

All of the welding research mentioned so far has been concerned with the simplest case: a heat source traveling across a metal substrate. However, these models fail to incorporate an important part of the welding process: filler material. Since the

actual weld bead consists mostly of the filler material, it is necessary to model the welding with the simultaneous appearance of the filler material. In the case of LENS, the entire part is built out of the filler material; so including it in the model is essential.

According to Hoadley and Rappaz,<sup>[17]</sup> very few models of laser cladding were published before 1991. Hoadley mentions Weerasinghe and Steen, who developed a model of laser cladding by powder injection which used the finite difference method. Their study included the powder absorbing energy from the laser while in the air, reducing the energy absorbed by the substrate. Their model assumed the powder melted instantaneously on contact with the clad surface, not allowing for mixing in the melt pool. However, according to Hoadley, not accounting for mixing means flow in the weld pool must be convected away by the melted powder, requiring a full solution of the Navier-Stokes equations. Another investigation was done in this area by Kar and Mazumder,<sup>[18]</sup> who examined the dissolution of powder through a diffusion mechanism for mass transport through use of a one dimensional model.

In 1991, Hoadley and Rappaz published an article detailing their research on thermal modeling of laser cladding by powder injection. Their finite element model was two dimensional and quasi-stationary. They also used a 2-D Gaussian distribution heat source model. Unlike previous researchers, Hoadley and Rappaz assumed mixing instantaneously distributed the powder throughout the melt pool. They did not solve for fluid flow specifically but assuming instantaneous mixing accounts some degree of convective heat transfer. This method greatly simplifies the necessary input parameters in comparison to Weerasinghe and Steen's model. The simplified input parameters make it possible to implement real processing conditions into the cladding model. Their



results had good correlation between the clad height predicted by the model and the actual values obtained through experiment.

### ***1.5 LENS and 3D Cladding Research***

Since the development of layered manufacturing processes like LENS, more research has been devoted to modeling and understanding these new processes. At the 1999 Solid Freeform Fabrication Symposium, Nickel *et al.*<sup>[19]</sup> presented their work on residual stress accumulation and part distortion in layered manufacturing. Their work began by developing an analytical model to determine the effect of the number of layers and layer thickness on part warping. The results of the analytical model showed that creating parts using more thin layers as opposed to fewer thicker layers reduced part deflection. Additionally, a finite element model along with experimental analysis was used to further investigate part distortion. The research concluded that the geometry of the deposition pattern significantly affects part distortion. The results showed that larger distortion occurs with the use of a long raster pattern as opposed to a short raster pattern, shown in Figure 1.8. Both the experimental and finite element analysis agreed with this conclusion. While the results of this study are useful, assessment of the finite element model is not possible because details were not provided in the paper.

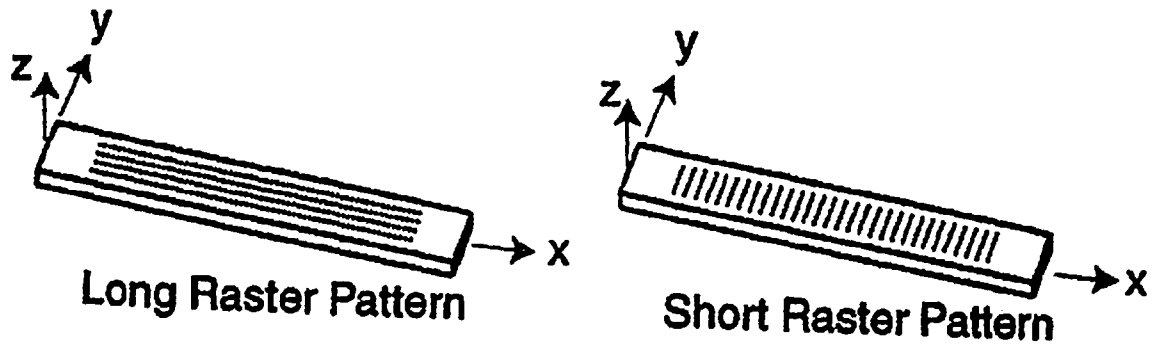


Figure 1.8 - Long Raster Pattern vs. Short Raster Pattern<sup>[19]</sup>

Also in 1999, Griffith et al.<sup>[20]</sup> closely examined the thermal history of parts made by the LENS process. A variety of thermal measurement techniques were used to determine the temperature history of the parts. The first method was the use of fine diameter Type C thermocouples whose diameter is only 10  $\mu\text{m}$ . This analysis showed that subsequent builds on the top, reheated the layer with the thermocouple to 800°C after seven layers, and to 600°C after 11 layers. The paper mentions that repeated elevation to temperatures above 600°C can age or temper the material, causing reduced hardness. Testing of the fabricated parts indeed verified reduced hardness in layers that experienced repeated temperature elevation. This study also recorded residual stresses on a hollow box using a technique called holographic-hole drilling. An unusual, biaxial stress state was found in the fabrication plane of the part, in which the stress in the welding direction was in tension while the stress in the vertical direction was in compression. After using thermocouples, a few non-invasive methods for determining temperature history were examined. The first method, digital IR imaging, uses infrared radiation emitted by heated objects to determine temperature. In Griffith's research, this method was unable to give absolute temperatures due to the unknown emissivity of the fabricated part. The second method, high speed visible imaging, uses a high speed

camera combined with standard pyrometric techniques. The two methods corresponded well with each other and showed promise for implementing some type of feedback control for LENS.

Hofmeister *et al.*<sup>[21]</sup> combined thermal imaging, microstructural analysis, and finite element modeling to try to understand the thermal behavior of the LENS process. Results from the thermal imaging showed that gradients in the previous build layer reached a maximum of  $400^{\circ} \text{K mm}^{-1}$  and were below  $200^{\circ} \text{K mm}^{-1}$  behind the heat source. At-and-below the melting temperature, cooling rates almost reached  $1000^{\circ} \text{K s}^{-1}$ . Further data collected showed that the molten pool size continued to increase with laser power up to 275 W. Once the laser power surpassed 275 W, the molten pool temperature increased without a significant increase in size. Increasing power above 275 W significantly decreased the cooling rate at the solid-liquid interface and in the solid itself. The microstructural analysis showed that the decreased cooling rates due to the higher laser power caused coarser microstructures by allowing more time for grain growth. The finite element model presented by Hofmeister uses element birthing in order to simulate the LENS process. Element birthing is when elements begin as inactive and are activated in order to simulate material buildup from the injection of powder. While element birthing is an important concept in LENS modeling, mention of any thermal history results in the paper was neglected.

Vasinonta *et al.*<sup>[22]</sup> developed non-dimensional plots, which they term “process maps” for the LENS process. The main purpose of these maps is to graphically represent the correlation between process parameters and melt pool size during solid freeform fabrication processes. Two different simulations were conducted, one with

temperature dependent material properties and one with constant properties. The research indicates that melt pool size is not significantly affected by uniformly preheating the substrate on which the part is to be made. Though, Vasinonta also suggests that uniform preheating is a good possibility for reducing residual stresses and warping.

Similar to Vasinonta's research, Brice *et al.*<sup>[23]</sup> looked at the effects of process variables on laser deposited metal. Brice analyzed the effect of six process variables on sample height and sample porosity. The six variables used in the experiment are travel speed, laser power, stand-off distance, hatch width, layer thickness, and powder flow-rate. The influence of these variables was assessed by means of a screening factorial design of experiments procedure. The results indicated that while standoff distance was not deemed crucial in either height or porosity, powder flow rate was crucial in achieving an acceptable deposit.

The most recent comprehensive finite element analysis of the LENS process was done in 2002 by Mengel<sup>[3]</sup> at Lehigh University. His model used a conical heat source model, specifically for deep penetrating sources like a laser or electron beam. The material modeled was AL6XN, a stainless steel, and non-constant material properties were used. Also included in this model was element birthing, in order to effectively simulate addition of filler material. In the setup of the model, Mengel goes to great lengths to understand many thermal and mechanical issues involved with modeling the LENS process. Mengel's simulation only included two build layers because he assumed that more layers would be somewhat trivial, but would require much more storage space and computation time. Overall, his research provided a successful

simulation of two LENS passes and an excellent starting point for continued research in this area.

### ***1.6 Issues and Objectives***

The main objective of the research in this study is to develop a finite element model of the LENS process to understand and quantify the effect of phase transformations on LENS fabricated parts. A complete understanding of the important aspects in LENS will provide a better capability to make complex parts. More specifically, this research will look at the deformation and residual stress caused by phase transformations. This study is also concerned with the impact of excluding phase transformations for the simulation altogether.

Several issues exist in modeling the LENS process with phase transformations; specifically: geometry, heat source modeling, material properties modeling. The layer thickness and width, as well as the finite element mesh, need careful consideration. Another issue is the modeling of the heat source. Furthermore, while a heat source model has been discussed in some detail, the specific model and power need to be considered for this model. A third consideration needs to be made for the material models being used. Even though material models have been examined rather cursorily, they obviously play a large role in phase transformation characteristics. The last main issue in this study is the comparison of materials that have residual stresses due to phase transformations to those that do not. The problem is that it is not possible to simply turn off and on phase transformations. This is because material properties do not only depend on temperature, but time as well. In order to incorporate the dependence on

temperature and time, phases must be used. Completely different material models must be used, which makes the comparison difficult.

## **Chapter 2 - Modeling Concerns**

### ***2.1 Introduction***

In order to develop a comprehensive finite element model of the LENS process, many things must be considered. While the previous chapter detailed past welding and cladding research, this chapter will be more concerned with aspects that directly affect modeling LENS. This chapter will look at the concerns associated with the thermal, mechanical, and metallurgical aspects of modeling, and the options available for dealing with each of these concerns.

### ***2.2 Thermal Aspect***

There are two main ways to model the welding process: two-dimensionally and three-dimensionally. A two-dimensional model requires minimal time and storage space. The time savings is significant, typically being one or two orders of magnitude. Although the two-dimensional simulation is faster and smaller in terms of storage, it sometimes lacks sufficient accuracy for predicting the heat flow in welding simulations. Specifically, when the welding speed is low, the two-dimensional model suffers in accuracy because it does not allow for any heat flow parallel to the welding direction.

In his Masters Thesis, Mengel simulated a weld using both two-dimensional and three-dimensional models for comparison purposes. For slow welding speeds of 0.2 and 1.0 mm/s the three dimensional model never reached melting temperature because

of heat transfer in all directions. In contrast, the two-dimensional model did achieve melting temperatures, showing that the two-dimensional model is inaccurate for those particular welding speeds. Comparing the different models at a weld speed of 5.0 mm/s shows good agreement between the two models with the two-dimensional model showing only slightly higher temperatures in the fusion zone. Results from welding speeds of 25.0 mm/s and higher show nearly identical results between the two models in comparison. Overall, this study found that weld speeds below 5.0 mm/s seem to require a three-dimensional model for any degree of accuracy.

Another thermal aspect of importance is the heat source model. The most rudimentary model is the point source model, which gives accurate results only for regions far enough away from the heat source. The next model developed was the 2D Gaussian model followed by the Goldak's double ellipsoid model. In this case, the most logical choice for a heat source model is the conical heat source, which many researchers use when studying laser welded parts. However, the type of the heat source is not the only thing that needs consideration when modeling LENS. All of the other parameters of the heat source model are important to the accuracy of the simulation. More specifically, the parameters  $r_c$ ,  $r_i$ ,  $z_c$ ,  $z_i$ , and  $Q$  ( eq. 2.3) all need to be determined in order to model the source correctly.

An additional thermal aspect of importance is heat of fusion. Heat of fusion is the energy required to transform a material from its solid state to its liquid state. It is important to understand the various ways of modeling this effect and the impact it has on the results. Two typical ways of accounting for heat of fusion are: adjusting the enthalpy directly and changing the values of specific heat in the melting range.

According to Mengel's research, both methods of implementing the heat of fusion seem to provide similar results. He also compared models with and without the heat of fusion taken into account. Including the heat of fusion lowered the peak temperature and the average molten pool temperature around 100°C and reduced the size of the molten pool by around six percent.

Another area that needs consideration is fluid flow in the weld pool. The fluid flow in the weld pool is affected by magnetohydrodynamic effects, Lorentz forces, Marangoni forces, and buoyancy forces.<sup>[24-26]</sup> Modeling this precisely is a difficult task and is often the sole objective of a research project. Since fluid flow in the molten pool is not the focus of this research, the thermal effects of fluid flow will be approximated. By increasing the thermal conductivity of the material above the melting temperature, the convective mixing in the weld pool can be reasonably modeled without severely complicating the model. The increased thermal conductivity will let the heat in the weld pool transfer more quickly, mimicking, to an extent, the effect of weld pool mixing. It is suggested by Lueng *et al.*<sup>[27]</sup> that the thermal conductivity above the melting temperature be increased by an order of magnitude to achieve this effect.

Lastly, the material models are important in terms of the thermal aspect of the simulation. The previous chapter details the movement from constant material properties to the more accurate approach of temperature dependent properties. The next step for material modeling in the thermal sense is to include the effect of phase changes on the thermal material properties. Using SYSWELD, it is possible to create material models that include phase changes. Also, the material models provided by SYSWELD already include phase changes in the models.



## ***2.3 Mechanical Aspect***

While knowledge of the thermal history of a weld is useful, most often the real purpose of welding simulations is the mechanical simulation. Residual stress and distortion are the overriding concerns in most welding applications, especially 3D cladding. This section will attempt to detail the main areas which need to be addressed when solving the mechanical portion of the simulation.

Along with the thermal simulation, the first area to be considered during the mechanical simulation is whether the model should be done in two or three dimensions. As with the thermal calculations, the benefits of a two-dimensional approach are reductions in computation time, storage space, and complexity. However, two-dimensional models usually assume plane strain, which does not allow for displacement in the welding direction. This is a problem since displacement in the welding direction certainly does exist and can be seen in results from three dimensional models. Mengel found that assuming these displacements do not occur causes the compressive stresses seen before the heat source arrival, as well as the overall final residual stresses, to be over estimated. Like the thermal model, the two dimensional mechanical model is more accurate with faster weld speeds.

The other problem with the plane strain model is the boundary conditions it imposes. By not allowing displacement in the welding direction, both ends of the welded part are forced to remain stationary. This essentially puts a rigid boundary condition on the two ends, when, during most welding operations, the part is free to expand in the welding direction. A two-dimensional alternative is the generalized plane strain model which allows the entire plane to move in the out of plane direction, in this

case in the welding direction. This method alleviates the boundary condition problem imposed by the plane strain model. In his investigation of longitudinal stress, Mengel found that the generalized plane strain method agreed well with the three-dimensional model and became stable while the plane strain method did not stabilize. While the generalized plane strain model provided accurate results for the longitudinal stress, it is limited to modeling in regions far removed from end effects.

The modeling decisions based on the thermal simulation must be considered in the mechanical simulation as well. Mengel showed that while thermal results differ substantially when modeling with and without the heat of fusion, mechanical results do not, when dealing with a material without phase transformations. He also demonstrated that adjusting the thermal conductivity to account for fluid flow in the weld pool has a large effect on thermal results, but is not noticeable in the mechanical results. Again, this was only shown to be true when dealing with materials that do not exhibit solid phase transformations.

Another area that needs to be considered in the mechanical model is the material behavior model. While properties like yield stress and elastic modulus are easily specified, plastic strain hardening behavior is difficult to describe numerically. A typical stress strain curve is shown in Figure 2.1. The simplest model used is elastic perfectly plastic. This model assumes that once the yield strength has been reached, stress will remain constant while strain increases. However, most materials, including metals, experience increased stress during plastic deformation, making the perfectly plastic model inaccurate. Therefore a strain hardening model must be used to more accurately describe the material properties. SYSWELD usually uses either a kinematic

or isotropic model to simulate strain hardening. Isotropic strain hardening coincides with an expansion to the elasticity domain and kinematics strain hardening coincides with a translation of the elasticity domain. The kinematic strain hardening model is suggested for cyclic applications, such as LENS modeling. Overall, the entire mechanical material model is extremely important because it directly affects the results of the mechanical simulation.<sup>[28]</sup>

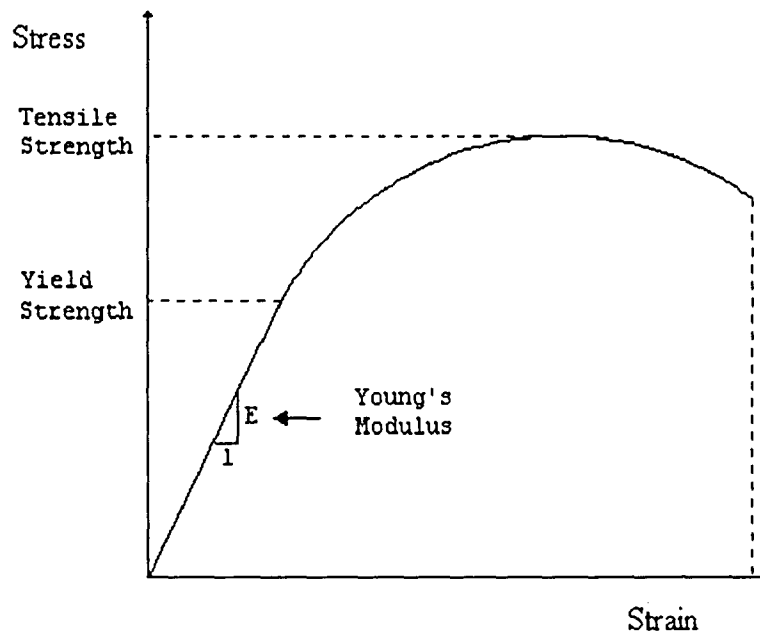


Figure 2.1 - Typical Steel Stress/Strain Curve

## ***2.4 Metallurgical Aspect***

Although the metallurgical aspects affect both the thermal and mechanical models, it needs separate consideration because it is the focal point of this study. As mentioned earlier, the latent heat associated with solid phase transformations affects the thermal calculation. The mechanical calculation is also affected by solid phase transformations. Materials, namely steels, which exhibit solid phase transformations,

have very different material properties depending on their phase. The problem with the metallurgical aspect of modeling is that it is extremely complex.

The difficulty of modeling the metallurgical aspect of materials begins with the complicated nature of metallurgy itself. The first problem is the difficult nature of obtaining the material properties desired for the metallurgical model. Measuring a multitude of properties at each material phase is necessary for an accurate model. Unfortunately this is not an easy task and is compounded by the fact that some of these phases are unstable and difficult to maintain. In addition, even the tightest specification materials can often have significant differences in properties. Very tightly specified steels can have continuous cooling transformation diagrams (CCT diagrams) which differ by an order of magnitude in some cases. Of course these differences in the steel can alter results to a significant degree.<sup>[29]</sup> Overall, simulations that include material models with phase transformations will suffer in accuracy because of this inability to precisely model the metallurgy.

The complexity of modeling phase transformations accurately limits the options that can be considered for the metallurgical aspect of the simulation. For example, SYSWELD is capable of using two different approaches for calculating metallurgical transformations during a simulation. One approach includes the Johnson-Mehl-Avrami type transformation kinetics and uses data from a continuous cooling transformation (CCT) diagram. The second approach is used by Nancy Metal Materials Engineering and Science Laboratory and is based on isothermal transformation diagrams. Ideally, the effect of these two approaches would be analyzed so that the advantages and drawbacks of both would be understood. Unfortunately, this examination is beyond the

scope of this research because it would require developing a CCT diagram and a isothermal transformation diagram for a material through experimental measurements.<sup>[28]</sup>

The easiest way to include metallurgical transformations without dealing with the complexities of performing experimental measurements is by using pre-defined material properties. SYSWELD contains data for five metals: one aluminum and four steels. However, there are a couple problems that come along with using pre-defined material properties. The first problem is that using pre-defined materials severely limits the materials available for use in the simulation. With only four steels available in SYSWELD, options are very limited when trying to compare a simulation to an experiment or another simulation. The second problem is that the method by which the material properties were obtained is unknown. This makes it difficult to determine the accuracy of the material properties provided. Overall, using pre-defined materials will not allow determination of the exact effects of metallurgical transformations in LENS, but it will provide the means to estimate them. This should provide an indication to the relative importance of including metallurgical transformation models in LENS and welding simulations.

## **Chapter 3 - LENS builds**

### ***3.1 Introduction***

In general, when doing any kind of simulation, the best way to create an accurate model is to base it on experimental data. For development of this 3D cladding

simulation, actual line builds were created by LENS, some of which are shown in Figure 3.1. Several build parameters can be changed in the LENS process, which alters the resulting build. These parameters, along with the geometries of the LENS builds, were recorded and incorporated in the model. This ensures that the foundation of the LENS model is solidly rooted in experimental builds.

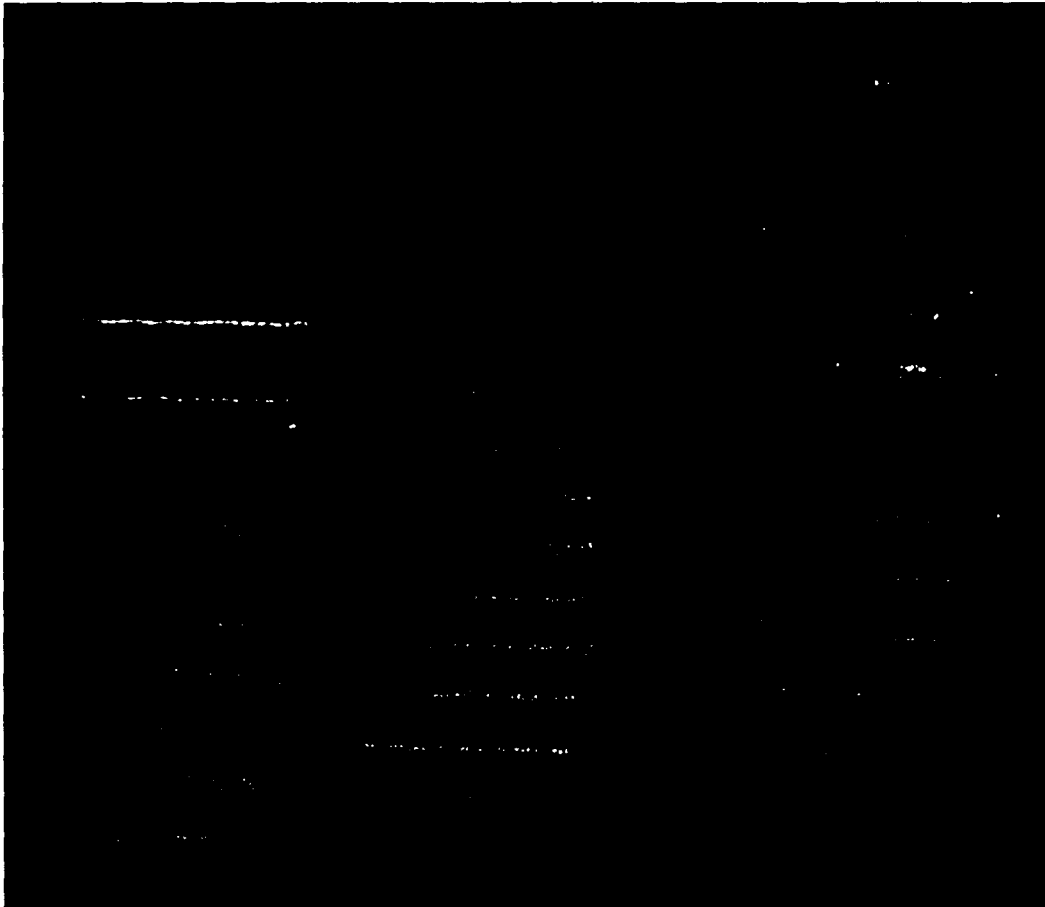


**Figure 3.1 - LENS builds example**

### ***3.2 Operating Parameters***

When creating parts with LENS, there are a number of operating parameters that may be changed. Understanding the effects of these parameters on the resulting build is quite important. The main parameters in LENS that can be adjusted are: 1) Laser

simulation, actual line builds were created by LENS, some of which are shown in Figure 3.1. Several build parameters can be changed in the LENS process, which alters the resulting build. These parameters, along with the geometries of the LENS builds, were recorded and incorporated in the model. This ensures that the foundation of the LENS model is solidly rooted in experimental builds.

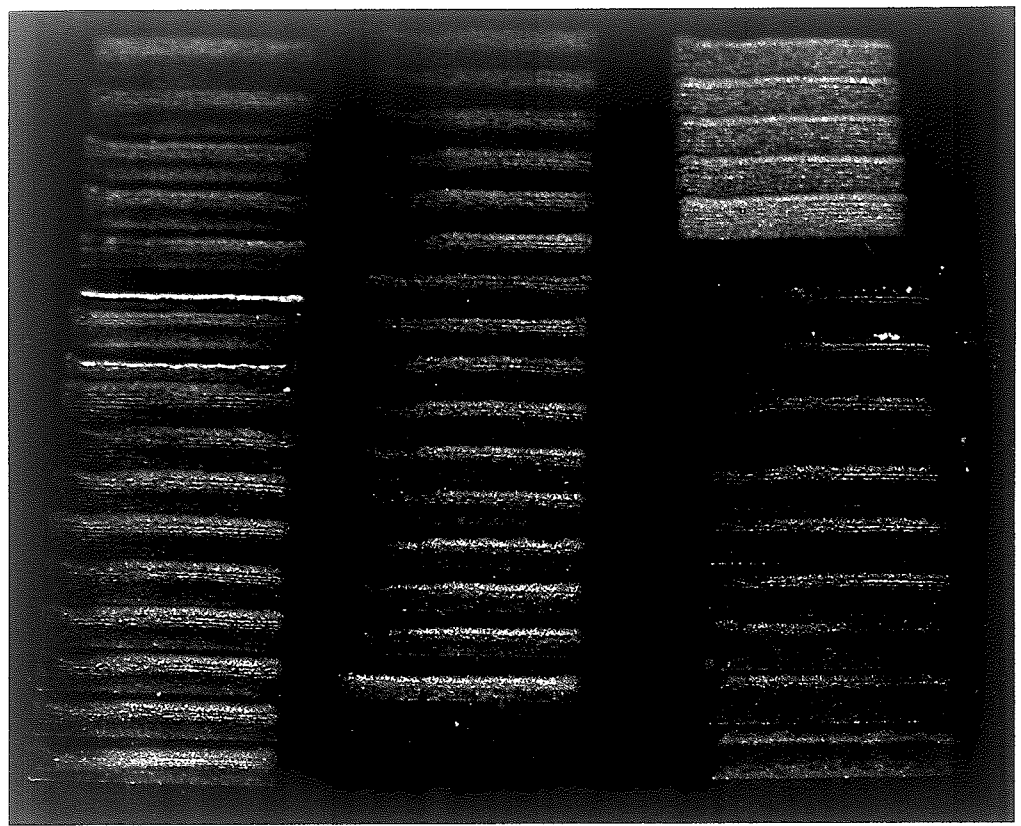


Figure 3.1 - LENS builds example

### 3.2 Operating Parameters

When creating parts with LENS, there are a number of operating parameters that may be changed. Understanding the effects of these parameters on the resulting build is quite important. The main parameters in LENS that can be adjusted are: 1) Laser

Power, 2) Powder Feeder RPM, 3) Feed Rate, 4) Layer Height, 5) Hatch Width, and 6) Layer Build Path. Laser power changes the electrical energy going to the laser, changing the output energy of the laser (the laser powers listed assumes 220V). The importance of laser power is quite direct; too much and the molten pool will become too large, too little and there will not be a molten pool at all. Powder feeder RPM adjusts the amount of build material flowing through the copper nozzles and at the molten pool. Because of the powder feed setup, calculating mass flow rate is very difficult to achieve and the somewhat arbitrary "Powder Feeder RPM" must be used. The feed rate is the speed at which the stage, what the part is mounted on, moves during building. Set layer height is a complicated parameter and is based on other parameters. When using LENS, one can not specifically program it to make a build 0.1 inches tall. Actual layer height is based on the previously mentioned parameters like laser power, powder feeder RPM, and feed rate. The set layer height must closely match the actual layer height or the laser will become out of focus. Hatch width is similar to build height in that one cannot program it specifically to make a desired hatch width. It depends on the same parameters as build height. This study will not concern itself with hatch width because it is only necessary in building solid objects, like a cube. Lastly, layer build path is the route, in the X-Y plane, that the laser follows to build the given layer. For example, consider two circular channels built using LENS. The first, every layer is made in a clockwise direction. The second has odd layers built in the clockwise direction and the even layers built in the counter-clockwise direction. This is an example of using different layer build paths.



### 3.3 Build Progression

For simplicity, the first experimental LENS builds used the parameters outlined in Lehigh University's LENS Operating Manual,<sup>[30]</sup> a guide supplied to LENS operators at Lehigh. The manual suggests using the parameters outlined in Table 3.1. It should be noted that the numbers given in the manual are in inches, but must be converted to millimeters since that is what SYSWELD uses. The manual also suggests using a hatch width of 0.015 inches, but hatch width is not an input used when creating a line build. Layer build path is a complicated parameter when creating most parts. However, when creating each layer of a line build, only two build paths are used: left to right or right to left. While there are a number of possible ways to create line builds using these two paths, this study only looked at two: bidirectional and unidirectional. In a bidirectional build, the odd layers are built left to right and the even layers built right to left. In a unidirectional build, every layer is built in the same direction as the first layer. While the manual does not specifically suggest using a bidirectional build method, the program for creating line builds automatically creates them with a bidirectional build pattern.

Laser Power	Powder Feeder RPM	Feed Rate	Set Layer Height	Build Path
7700 Watts (35 amps)	5	16.933 mm/s	0.254 mm	Bidirectional

Table 3.1 - LENS Operating Manual suggested parameters

The first line builds, which were made using the suggested parameters, had a number of flaws. An example of one of these builds can be seen in Figure 3.2. The most obvious problem is that the ends of the build are much taller than the middle part of the build. Not only are the ends taller, but they are slightly wider as well. Another

flaw with this build, which cannot be seen by looking at the resulting part, is that the set layer height was much larger than the actual layer height, causing the laser to go out of focus during the build. The build in Figure 3.2 was supposed to reach a height of 25.4 mm, but only managed to achieve a height of around 5.0 mm at the center due to the inaccurate layer height setting. The increased buildup near the ends is most likely due to a combination of the bidirectional build path, the high feed rate, and the set layer height. When using a bidirectional build pattern, the laser tends to linger on the ends of the line build, causing more buildup. The high feed rate exaggerates this lingering effect because the time spent building in the middle is much lower percentage-wise than it would be with a slower feed rate. Lastly, the set layer height adds to this flaw by allowing deposition to continue at the raised ends when deposition has ceased in the middle part of the build due to the laser being out of focus.

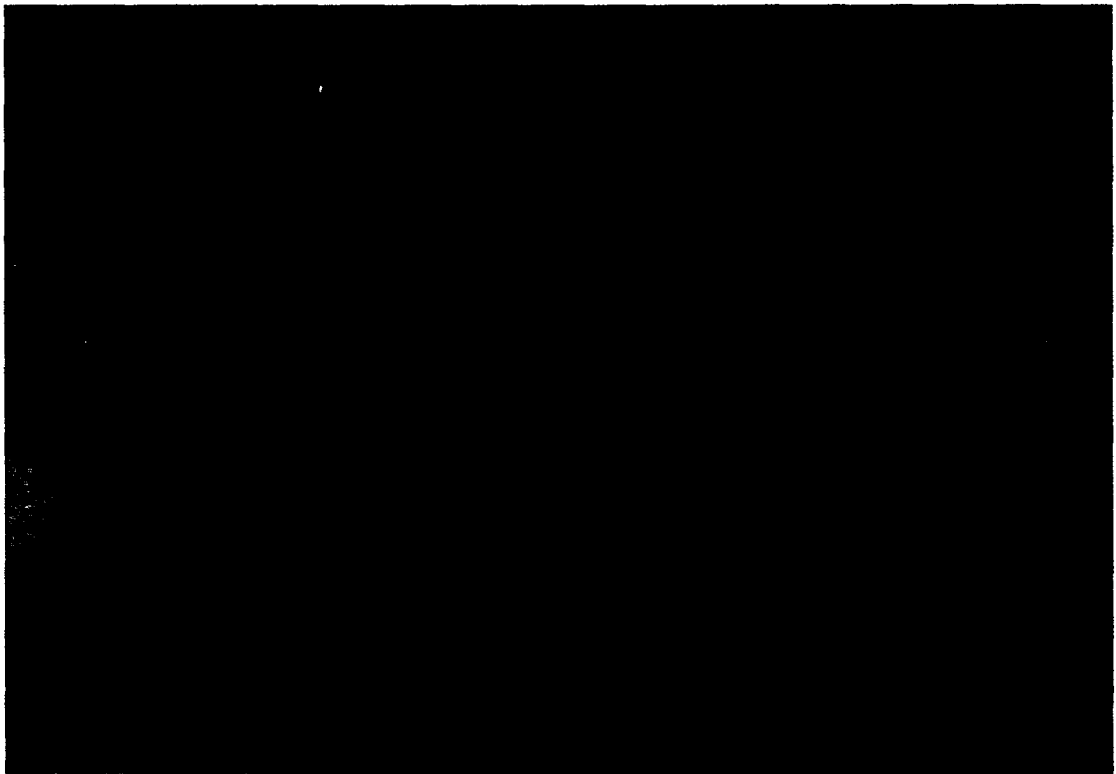


**Figure 3.2 - First build set example**

flaw with this build, which cannot be seen by looking at the resulting part, is that the set layer height was much larger than the actual layer height, causing the laser to go out of focus during the build. The build in Figure 3.2 was supposed to reach a height of 25.4 mm, but only managed to achieve a height of around 5.0 mm at the center due to the inaccurate layer height setting. The increased buildup near the ends is most likely due to a combination of the bidirectional build path, the high feed rate, and the set layer height. When using a bidirectional build pattern, the laser tends to linger on the ends of the line build, causing more buildup. The high feed rate exaggerates this lingering effect because the time spent building in the middle is much lower percentage-wise than it would be with a slower feed rate. Lastly, the set layer height adds to this flaw by allowing deposition to continue at the raised ends when deposition has ceased in the middle part of the build due to the laser being out of focus.

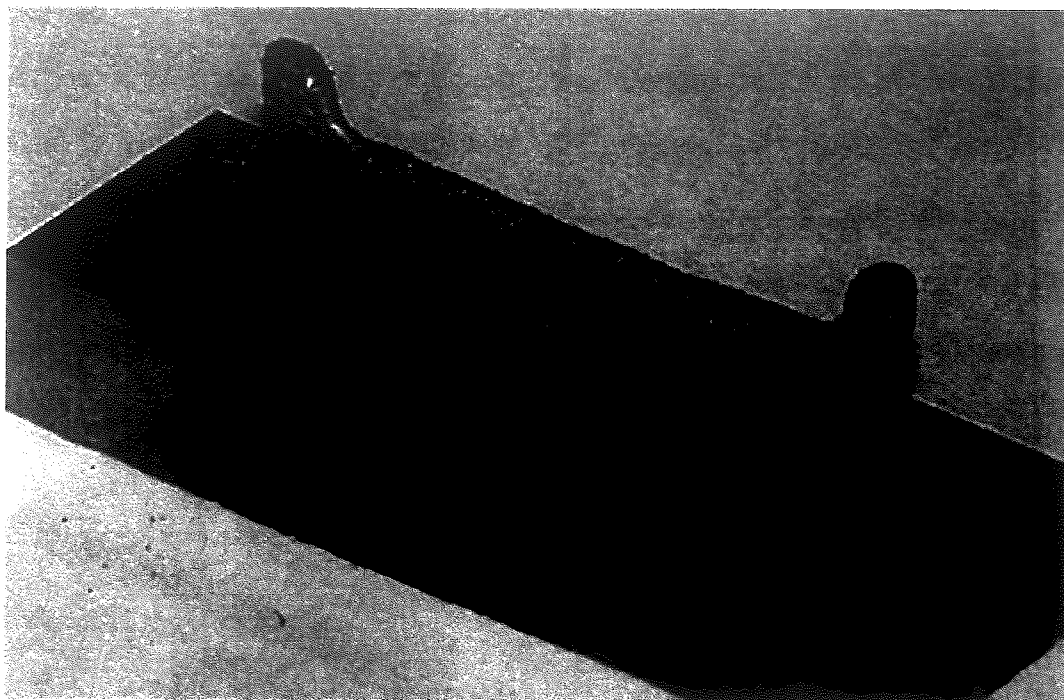


**Figure 3.2 - First build set example**

The second set of builds used the same feed rate and build path, but changed laser power, powder feeder RPM, and set layer height. Unfortunately, the causes of the increased build-up on the ends of the line build were not completely understood during the build progression, and therefore, the feed rate and build path were not changed first. Laser current was the first parameter changed, with current varying from 35 to 50 amps (Figure 3.3). Increasing the laser power enlarged the build width and build height, which reduced the excessive build-up on the ends to a small degree. However, even at full laser power, the ends were still raised above the middle of the build. Increasing the powder feeder RPM had a similar effect to the increased laser power: wider and taller build layer, but only small improvement in keeping the middle height equal to the ends. The powder feeder RPM was varied from four to ten, and is shown in Figure 3.4. Lastly, the set layer height was varied from 0.1 mm to 0.25mm. This set of builds showed the importance of correctly matching the set layer height to the actual layer height. If the set layer height is too high, after a few passes the laser will become focused too far above the part to create a molten pool. If the set layer height is too small, the growth of the part will be stunted. A good example of the effect of set layer height can be seen in Figure 3.5. The build parameters for Figure 3.5 are shown in Table 3.2. By increasing the set layer height from 0.15 mm to 0.20 mm, the total height of the build increased from 7.62 mm to 8.76 mm.

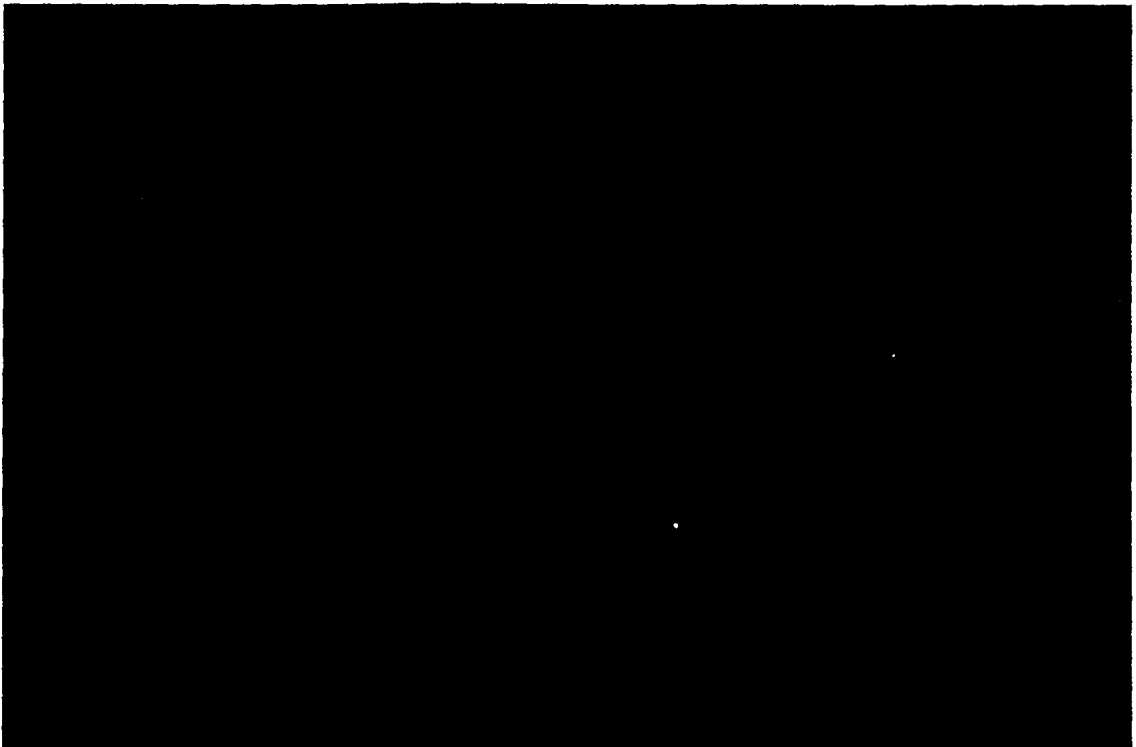


**Figure 3.3 - Effect of changing laser power. (35, 40, 45 and 50 amp laser current shown from front-left to back-right)**



**Figure 3.4 - Effect of changing powder feeder RPM. (4, 6, 8 and 10 RPM shown from front-left to back-right)**



Figure 3.3 - Effect of changing laser power. (35, 40, 45 and 50 amp laser current shown from front-left to back-right)

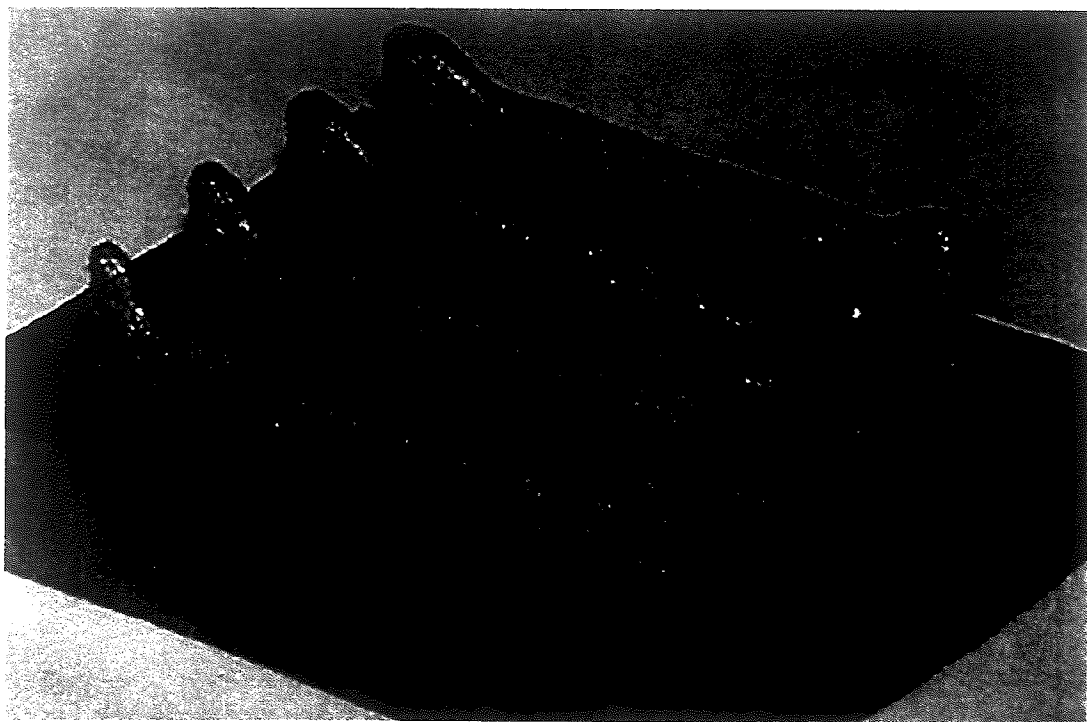


Figure 3.4 - Effect of changing powder feeder RPM. (4, 6, 8 and 10 RPM shown from front-left to back-right)



**Figure 3.5 - Effect of using different set build height (A is front-left and B is back-right)**

Build	Laser Power	Powder Feeder RPM	Feed Rate	Set Layer Height
A	9900 Watts (45 amps)	10	16.933 mm/s	0.15 mm
B	9900 Watts (45 amps)	10	16.933 mm/s	0.20 mm

**Table 3.2 - Build parameters for Figure 3.5**

In the next group of builds, the feed rate parameter was altered. The effect of reducing the feed rate from 16.9 mm/s to 4.0 mm/s was very dramatic. The reduction in feed rate created a much thicker and taller build (Figure 3.6). The change in feed rate also significantly reduced the problem of excessive buildup on the ends of the part. The ends were only very slightly higher and wider than the center of the part. Another build, shown in Figure 3.7, with a feed rate of 8.0 mm/s was also performed, and again, only had slight problems with excessive build near the ends. This particular build

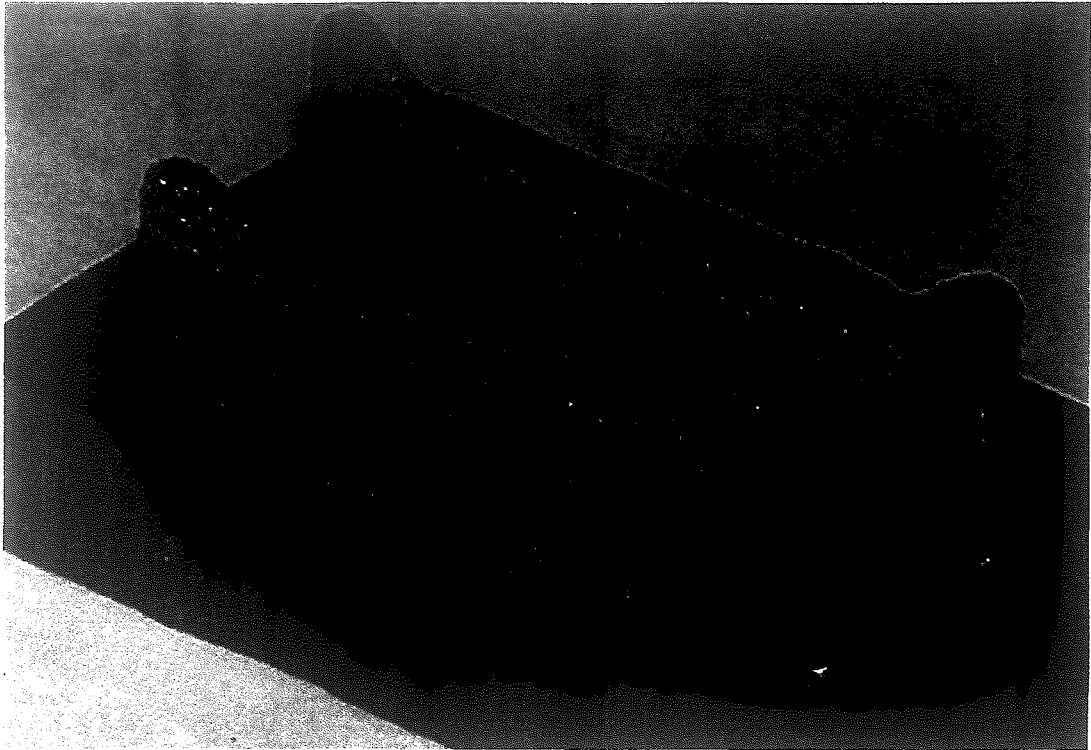


Figure 3.5 - Effect of using different set build height (A is front-left and B is back-right)

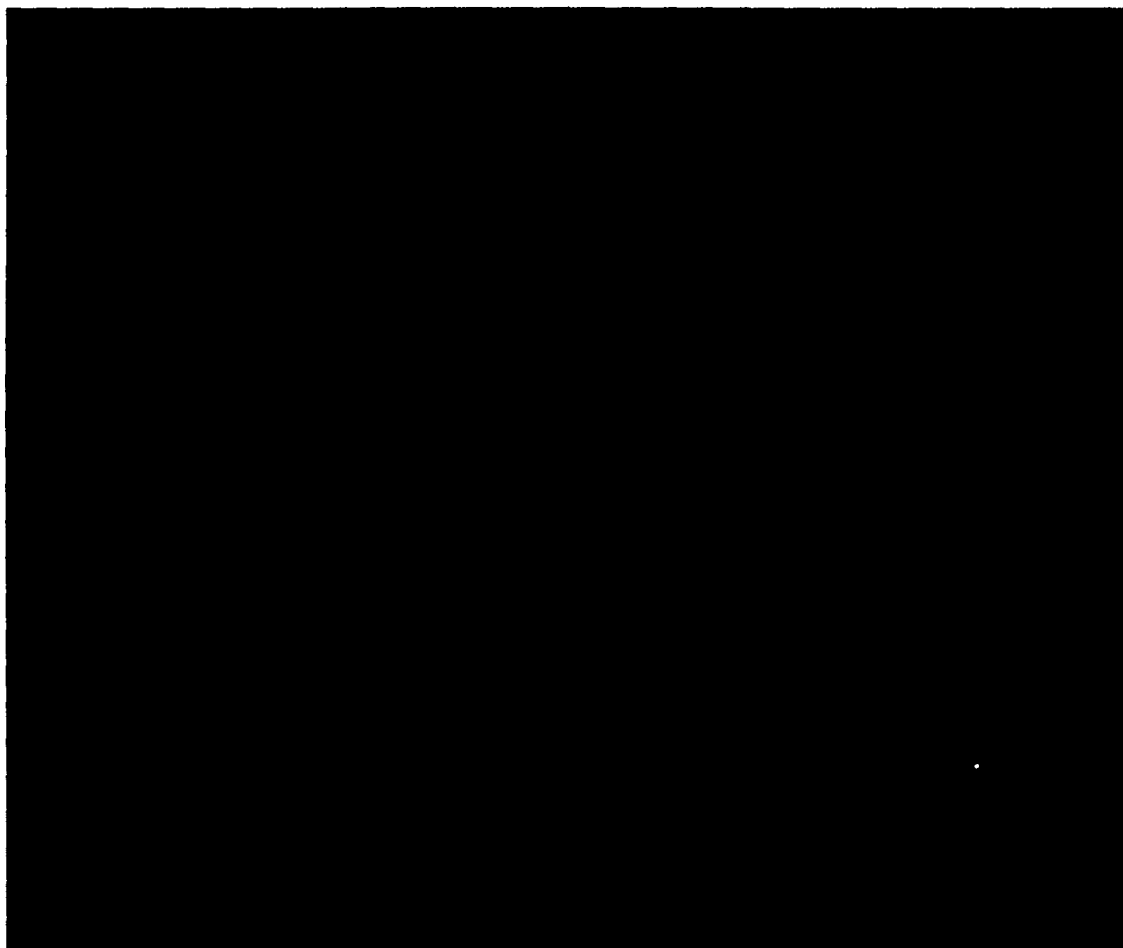
Build	Laser Power	Powder Feeder RPM	Feed Rate	Set Layer Height
A	9900 Watts (45 amps)	10	16.933 mm/s	0.15 mm
B	9900 Watts (45 amps)	10	16.933 mm/s	0.20 mm

Table 3.2 - Build parameters for Figure 3.5

In the next group of builds, the feed rate parameter was altered. The effect of reducing the feed rate from 16.9 mm/s to 4.0 mm/s was very dramatic. The reduction in feed rate created a much thicker and taller build (Figure 3.6). The change in feed rate also significantly reduced the problem of excessive buildup on the ends of the part. The ends were only very slightly higher and wider than the center of the part. Another build, shown in Figure 3.7, with a feed rate of 8.0 mm/s was also performed, and again, only had slight problems with excessive build near the ends. This particular build



(Figure 3.7) was deemed the most ideal build to date and the build parameters (Table 3.3) were used as a basis for the next large set of builds.



**Figure 3.6 - Line Build with feed rate of 4.00 mm/s**

(Figure 3.7) was deemed the most ideal build to date and the build parameters (Table 3.3) were used as a basis for the next large set of builds.

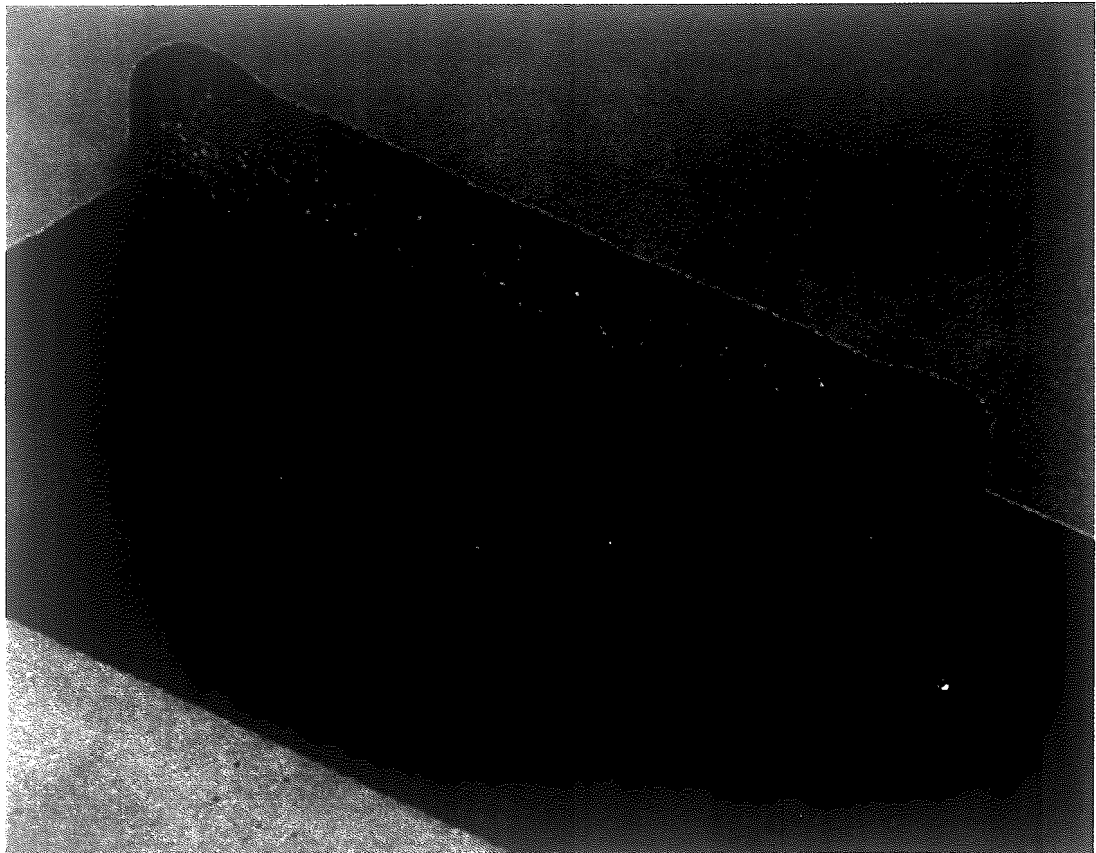


Figure 3.6 - Line Build with feed rate of 4.00 mm/s



**Figure 3.7 - Line Build with feed rate of 8.00 mm/s**

Laser Power	Powder Feeder RPM	Feed Rate	Set Layer Height	Build Path
8800 Watts (40 amps)	8	6.00 mm/s	0.3 mm	Bidirectional

**Table 3.3 - Build parameters for Figure 3.7**

The next set of builds started with the parameters show in Table 3.3 and expanded in several areas in an attempt to find the optimum build parameters. In order to limit the variables and runs that would be needed, the laser power was limited to 8800 Watts (40 amps). The set layer height was also set constant to 0.3 mm, which is what was measured from the build in Figure 3.7, and each build was 20 layers tall. Since more experimentation had been done regarding powder feeder RPM, only three cases were examined in this build set: 6, 8 and 10 RPM. The feed rates examined were



**Figure 3.7 - Line Build with feed rate of 8.00 mm/s**

Laser Power	Powder Feeder RPM	Feed Rate	Set Layer Height	Build Path
8800 Watts (40 amps)	8	6.00 mm/s	0.3 mm	Bidirectional

**Table 3.3 - Build parameters for Figure 3.7**

The next set of builds started with the parameters show in Table 3.3 and expanded in several areas in an attempt to find the optimum build parameters. In order to limit the variables and runs that would be needed, the laser power was limited to 8800 Watts (40 amps). The set layer height was also set constant to 0.3 mm, which is what was measured from the build in Figure 3.7, and each build was 20 layers tall. Since more experimentation had been done regarding powder feeder RPM, only three cases were examined in this build set: 6, 8 and 10 RPM. The feed rates examined were

every 0.5 mm/s from 6.0 to 9.5 mm/s. This group of builds can be seen in Figure 3.8. During this set of builds, a “wavy” defect was observed, which had not been seen before. (Figure 3.9) The cause of the wavy defect is unclear. After measuring the thickness and height of each build, as well as visually examining each one, it was determined that the build, shown in Figure 3.10, using a powder feeder RPM of 8 and a feed rate of 6.0 mm/s, produced the best build. This build was chosen because the top was relatively flat and the problem of excessive build on the ends was very minimal.



**Figure 3.8 - 6.0 - 9.5 mm/s build set (6, 8 and 10 RPM from left to right, 6.0 to 9.5 mm/s from front to back)**

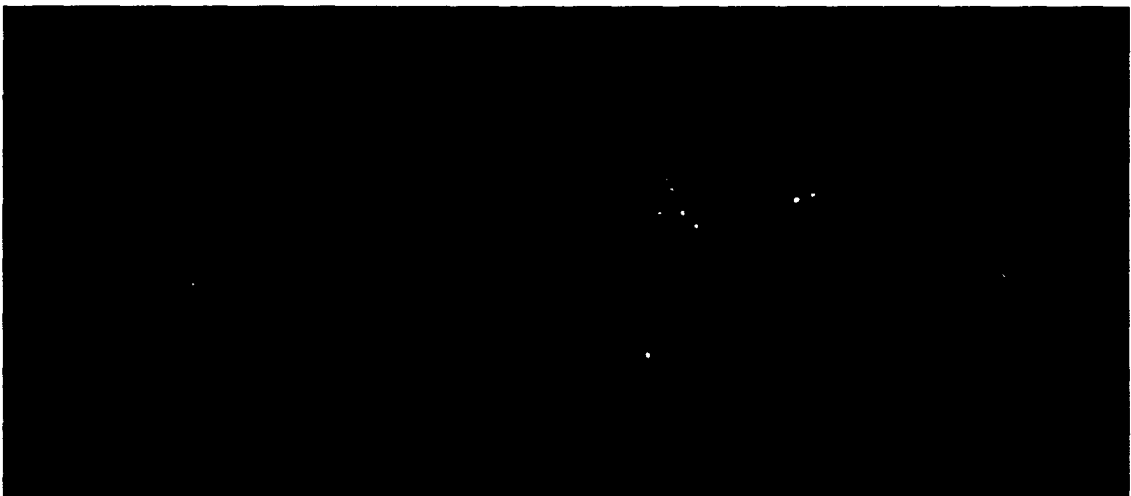


**Figure 3.9 - Build with “wavy” defect**

every 0.5 mm/s from 6.0 to 9.5 mm/s. This group of builds can be seen in Figure 3.8. During this set of builds, a “wavy” defect was observed, which had not been seen before. (Figure 3.9) The cause of the wavy defect is unclear. After measuring the thickness and height of each build, as well as visually examining each one, it was determined that the build, shown in Figure 3.10, using a powder feeder RPM of 8 and a feed rate of 6.0 mm/s, produced the best build. This build was chosen because the top was relatively flat and the problem of excessive build on the ends was very minimal.

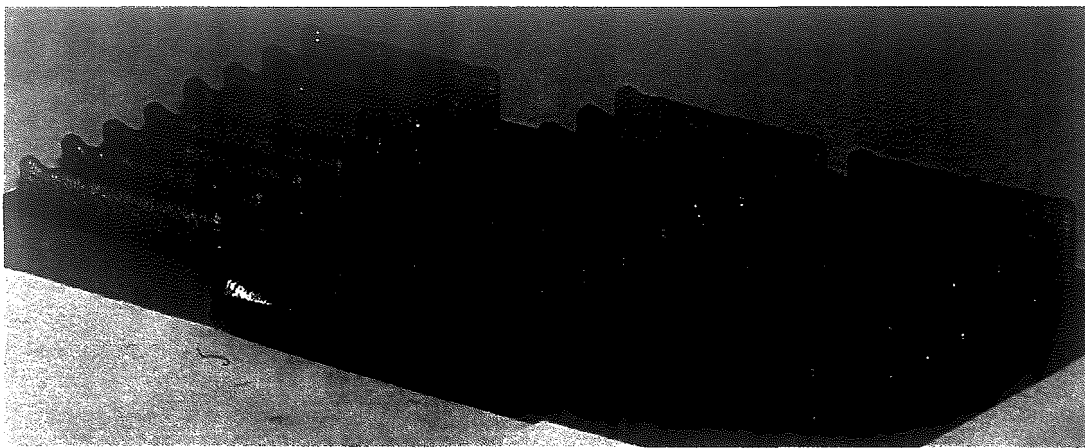


**Figure 3.8 - 6.0 - 9.5 mm/s build set (6, 8 and 10 RPM from left to right, 6.0 to 9.5 mm/s from front to back)**



**Figure 3.9 - Build with “wavy” defect**



**Figure 3.10 - “Best” build from set in Figure 3.11**

The last set of builds essentially fine tuned the parameters of the build seen in Figure 3.10. While the feed rate and powder feeder RPM were kept constant, the set layer height was adjusted to match the measured layer height. Changing the set layer height from 0.3 mm to 0.4 mm hardly changed the overall build height. Two small concerns still existed in looking at the first couple builds during this set, an example of which is shown in Figure 3.11. The first concern was the ends were still slightly higher and thicker than the rest of the piece. The second concern was the small dip on the left side of the part, near the end. The first concern was addressed by altering the build path from bidirectional to unidirectional. This finally got rid of the extra buildup on the ends of the part. By watching the build closely, it was determined that the dip was caused by inadequate heat at the beginning of the first layer. To address this issue, two things were done. First, a pass was made without the powder feeders on, essentially preheating the substrate material. Second, a small delay was added to the program in order to ensure the stage did not begin movement before the laser was turned on. The

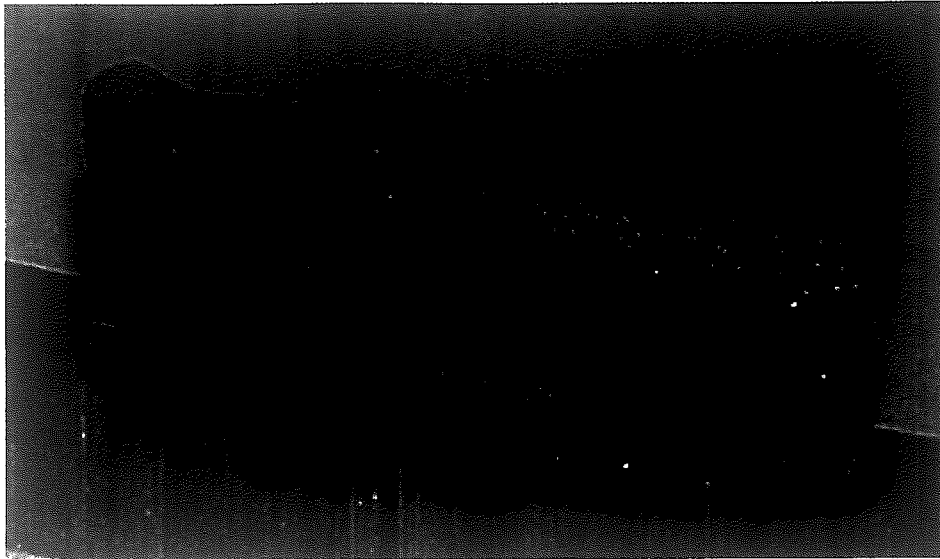


**Figure 3.10 - "Best" build from set in Figure 3.11**

The last set of builds essentially fine tuned the parameters of the build seen in Figure 3.10. While the feed rate and powder feeder RPM were kept constant, the set layer height was adjusted to match the measured layer height. Changing the set layer height from 0.3 mm to 0.4 mm hardly changed the overall build height. Two small concerns still existed in looking at the first couple builds during this set, an example of which is shown in Figure 3.11. The first concern was the ends were still slightly higher and thicker than the rest of the piece. The second concern was the small dip on the left side of the part, near the end. The first concern was addressed by altering the build path from bidirectional to unidirectional. This finally got rid of the extra buildup on the ends of the part. By watching the build closely, it was determined that the dip was caused by inadequate heat at the beginning of the first layer. To address this issue, two things were done. First, a pass was made without the powder feeders on, essentially preheating the substrate material. Second, a small delay was added to the program in order to ensure the stage did not begin movement before the laser was turned on. The



resulting and final build is shown in Figure 3.12, which is the build used as the basis for the finite element simulation. The final build was 20 layers tall, and took about 130 seconds to build. The build parameters for this build are detailed in Table 3.4.

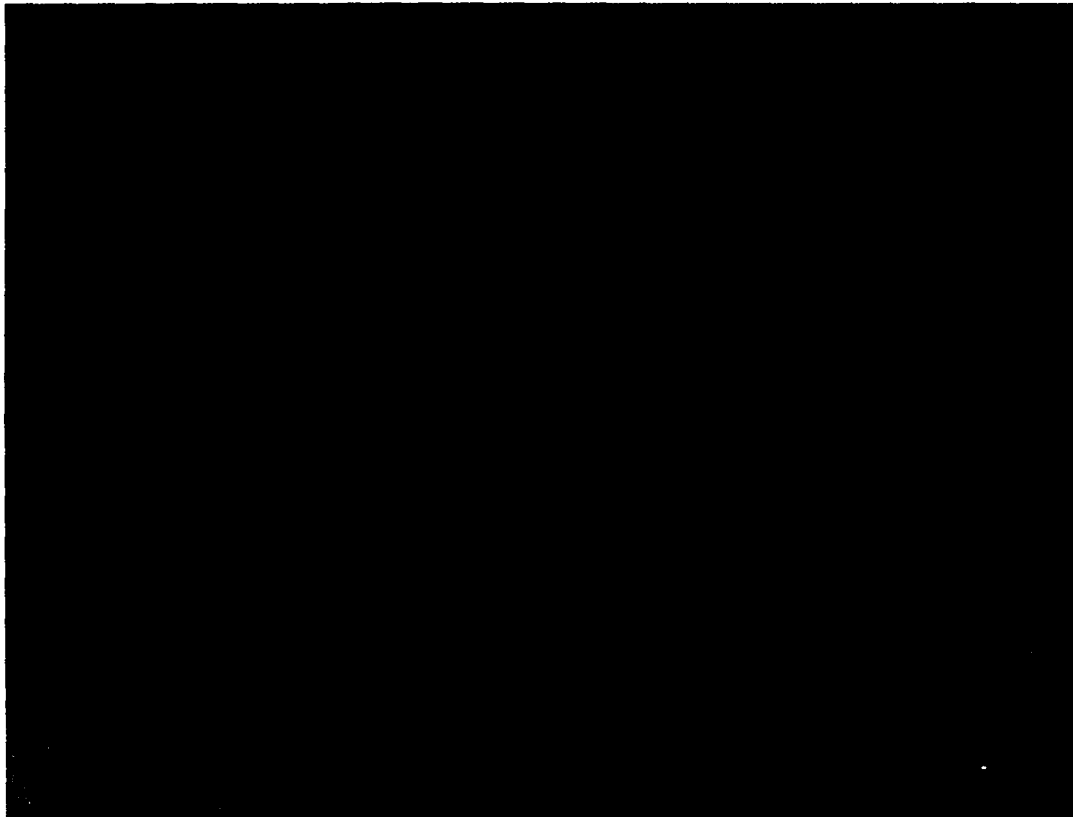


**Figure 3.11 - Line build exhibiting small dip on left side**

resulting and final build is shown in Figure 3.12, which is the build used as the basis for the finite element simulation. The final build was 20 layers tall, and took about 130 seconds to build. The build parameters for this build are detailed in Table 3.4.



**Figure 3.11 - Line build exhibiting small dip on left side**

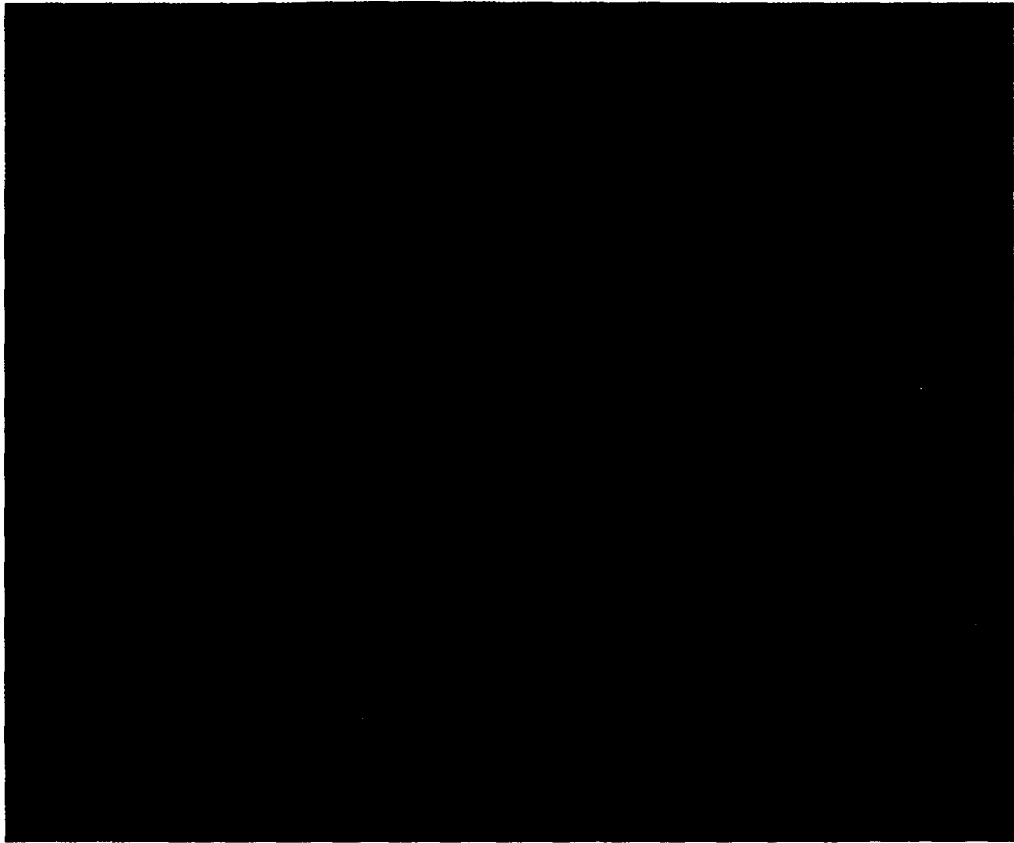


**Figure 3.12 - Final build off of which the models are based**

Laser Power	Powder Feeder RPM	Feed Rate	Set Layer Height	Build Path
8800 Watts (40 amps)	8	6.0 mm/s	0.40 mm	Unidirectional

**Table 3.4 - Parameters of final build (Figure 3.12)**

## **Chapter 4 - Modeling Using SYSWELD**

In order to estimate distortion and residual stress due to solid phase transformations, an accurate model must be created. In creating this model, all aspects of the LENS process must be considered in order to achieve the best model possible. The many aspects of LENS can be grouped into four modeling areas: geometric, thermal, mechanical, and metallurgical. These areas must not only be considered individually, but also as a whole since choices in one area may affect another. While many of the ideas have been discussed in previous chapters, they will now be

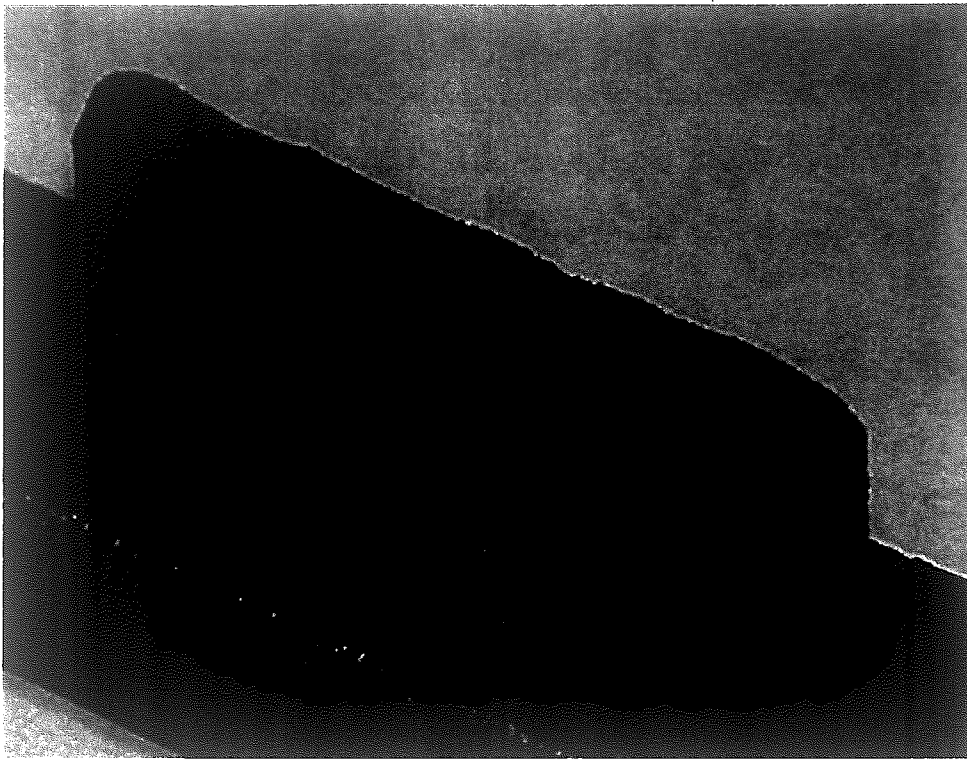


**Figure 3.12 - Final build off or which the models are based**

Laser Power	Powder Feeder RPM	Feed Rate	Set Layer Height	Build Path
8800 Watts (40 amps)	8	6.0 mm/s	0.40 mm	Unidirectional

**Table 3.4 - Parameters of final build (Figure 3.12)**

## **Chapter 4 - Modeling Using SYSWELD**

In order to estimate distortion and residual stress due to solid phase transformations, an accurate model must be created. In creating this model, all aspects of the LENS process must be considered in order to achieve the best model possible. The many aspects of LENS can be grouped into four modeling areas: geometric, thermal, mechanical, and metallurgical. These areas must not only be considered individually, but also as a whole since choices in one area may affect another: While many of the ideas have been discussed in previous chapters, they will now be

considered with respect to this particular study. In addition, a temporal section will be included in this chapter. The temporal section will compare the experimental timing to that of the simulation. Modeling LENS will be done using SYSWELD because it is the most capable welding simulation program and also because it is the program most familiar to the Mechanical Engineering department at Lehigh University.

#### ***4.1 Geometric Modeling Aspect***

As discussed previously, the first important decision when modeling is whether to use two or three dimensions. In this study, the welding velocity is 6.00 mm/s. Although reduced time and storage is beneficial, accurate calculation of longitudinal heat flow and stress is more important. Therefore, a three-dimensional model will be used to simulate LENS.

Once the number of dimensions is determined, the geometry of the weld base and each deposit layer (bead) must be created. The dimensions of the substrate material for the experimental builds was 175 mm long x 175 mm wide x 6.35 mm tall. Modeling this entire weld base would require very high storage space and would increase solution times considerably. Since the thermal history of the weld base is not important, the weld base dimensions were trimmed to 35 mm long x 15 mm wide x 6 mm tall. This change does affect the heat flowing away from the weld, making it necessary to alter the boundary conditions of the trimmed weld base so that it dissipates heat similarly to the actual weld base.

The geometry of the deposit layers is important, first and foremost, because it is the actual “part” being created. It is also important because this is where the highest

thermal gradients will exist, and most likely the largest stresses and distortions. The width and height of each layer in the model is 1.40 mm and 0.40 mm, respectively, to match those of the experimental build. However, the build length was modeled at only 25 mm long even though the experimental builds were 25.4 mm long. This change should make minimal difference since it is only shorter by 1.6 percent. This change was made to simplify the mesh. The rounded shape on the top of the build, seen during the experimental builds, was included in the LENS model (Figure 4.1). Another difference between the experimental builds and the model is the rounded ends, which can be seen in Figure 4.2. Modeling a rounded end along with a rounded top would seriously complicate creating the geometry and would also put a strain on SYSWELD's meshing capabilities. Therefore, the bead ends were left squared in the simulation.

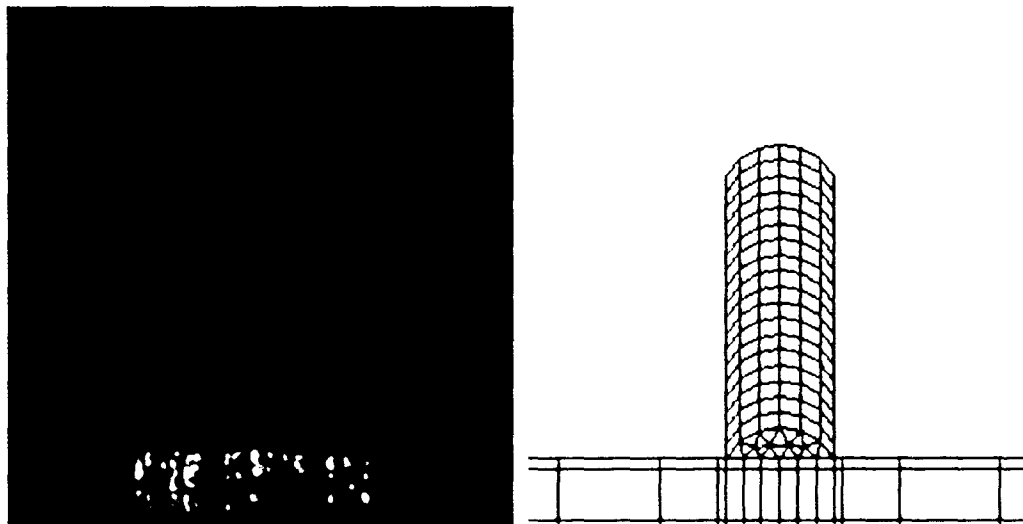


Figure 4.1 - Comparison of experimental build and model (side view)

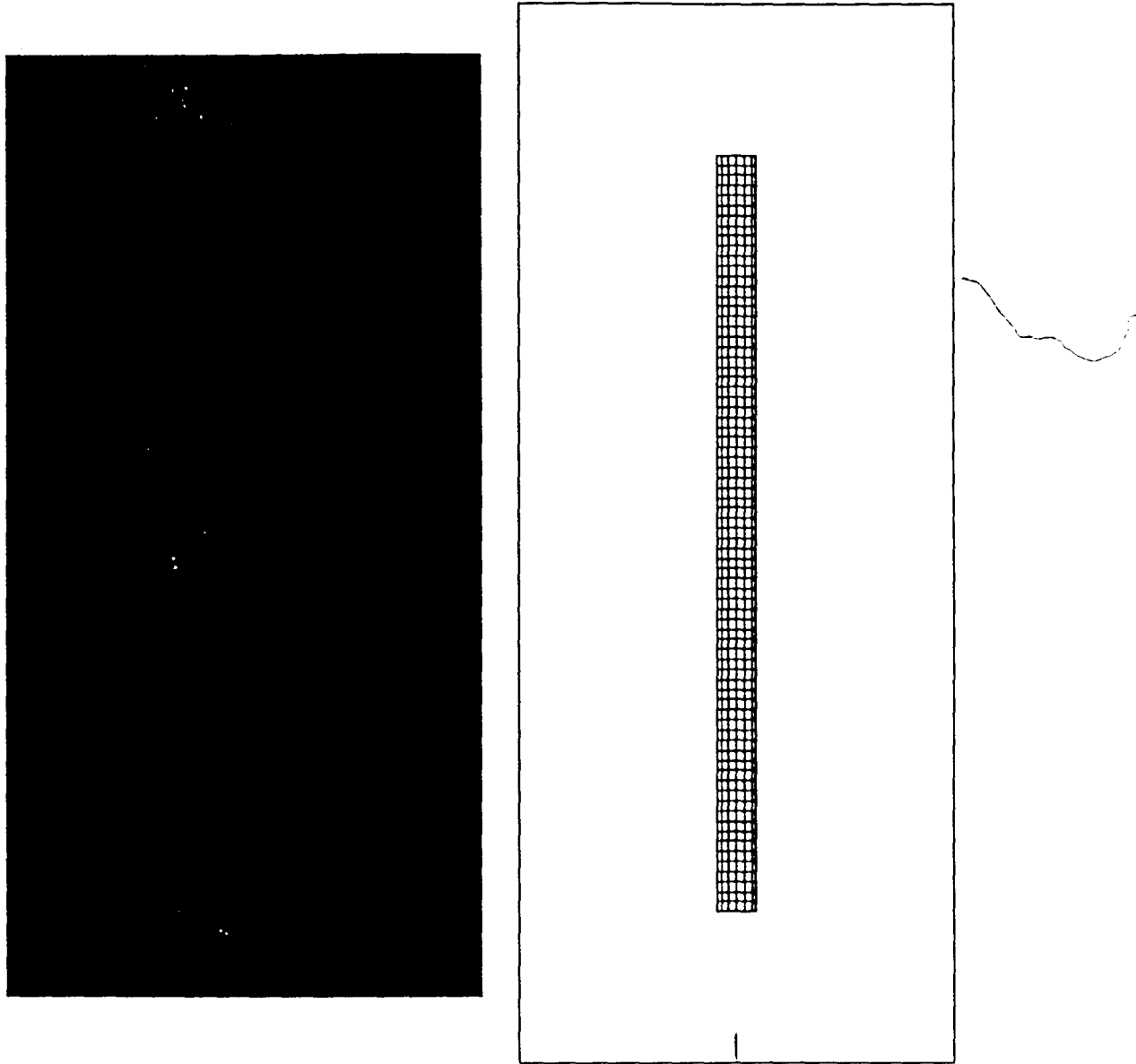
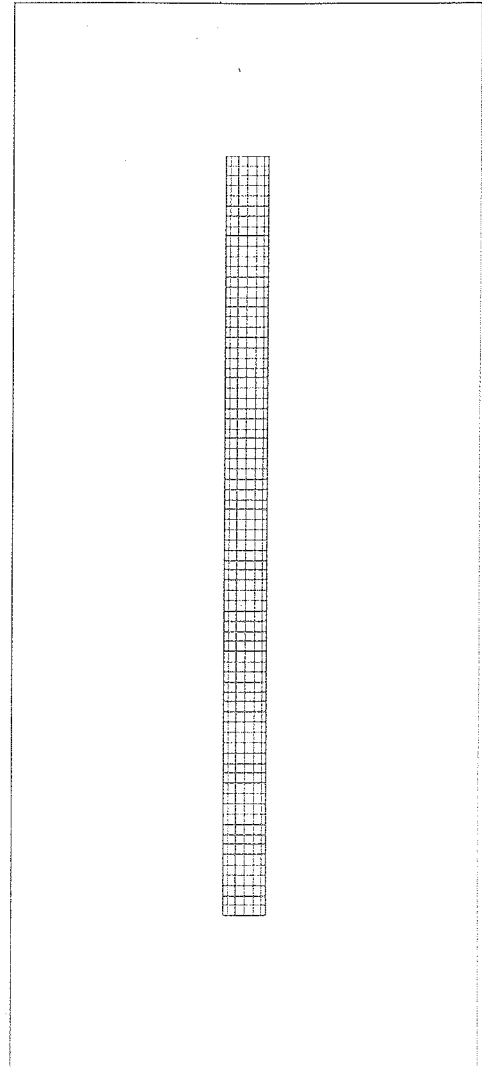
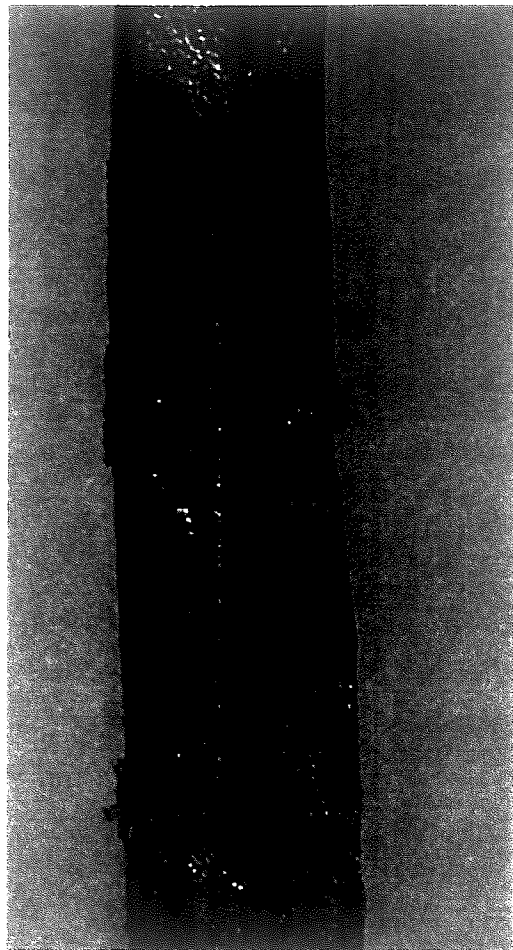


Figure 4.2 - Comparison of experimental build and model (top view)

Furthermore, the number of layers included in the model is important. Initially, 20 layers were modeled to match number of layers in the experimental builds. However, even running the simulation with activating only 10 of these 20 layers, requires two weeks of computation time. In order to reduce the computation time, seven layers were modeled, and only four of them were activated. This dramatically reduced the computation time to around three days. Obviously, the drawback of using a



**Figure 4.2 - Comparison of experimental build and model (top view)**

Furthermore, the number of layers included in the model is important. Initially, 20 layers were modeled to match number of layers in the experimental builds. However, even running the simulation with activating only 10 of these 20 layers, requires two weeks of computation time. In order to reduce the computation time, seven layers were modeled, and only four of them were activated. This dramatically reduced the computation time to around three days. Obviously, the drawback of using a



smaller number of layers is the model is not fully developed and may not produce the results a full, 20 layer model, would.

Once the geometry is in place, the next step is meshing. This essentially divides the geometry into finite sections, called elements, which then will be used in the finite element analysis. The mesh density refers to the size of the elements in a certain region of the model. If the mesh density is too high, it will cause the simulation to run slower than necessary and it will require excessive storage space. If the mesh density is too low, the simulation will not finish because it will not converge to a solution. Areas with higher thermal and stress gradients will require finer meshes than areas that will experience minimal thermal or stress gradients. The mesh used for this simulation can be seen in Figure 4.3.

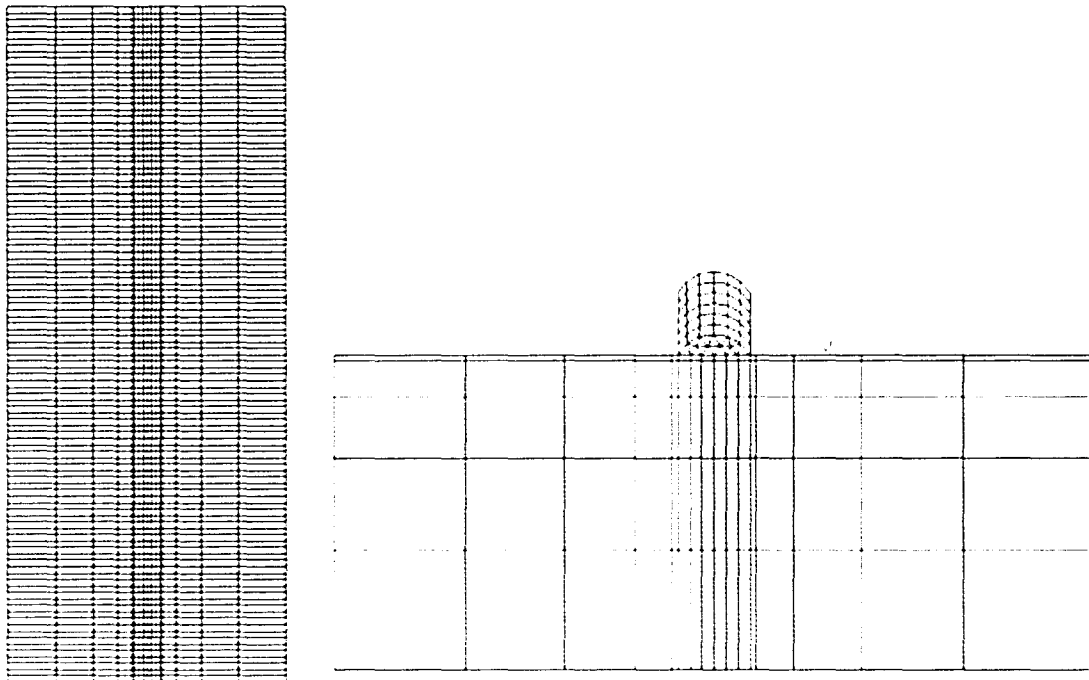


**Figure 4.3 - Finite Element Mesh ( left: Top View, right: Front View)**

The heat source model used in the simulation is the 3D conical Gaussian model. This choice was made mainly because this is what was recommended by the

SYSWELD Help Manual for modeling laser heat sources.<sup>[16]</sup> The heat source parameters are given in Table 4.1. The laser intensity was adjusted slightly to compensate for the different melting temperatures of the materials.

(Q)	R <sub>e</sub>	R <sub>i</sub>	Z <sub>e</sub>	Z <sub>i</sub>
850 W/mm <sup>3</sup>	0.7 mm	0.55 mm	0.4 mm	0.0 mm

**Table 4.1 - Heat source input parameters**

The last part of the model geometry is the element activation/deactivation portion, which is very helpful in simulating material deposition. Without it, a new geometry would have to be created to account for each additional piece of deposited material. Fortunately, by using element activation/deactivation this can be avoided. First, the entire geometry, including all of the deposit material, is created. Then, the deposit material is initially deactivated, giving it the properties of air. Once the simulation begins, the deposit material is activated as the heat source approaches, simulating material deposition in welding. For this study, the elements are activated before the heat source arrives to prevent instability in the solution. Also, boundary conditions for the specific bead being activated are neglected to prevent instability.

## ***4.2 Thermal Modeling Aspect***

After the geometry of the model is established, the thermal aspects need to be addressed. First of all, it should be noted that the initial thermal material properties are taken from the material models built into SYSWELD. As mentioned previously, fluid flow in welding, heat of fusion, and latent heat due to phase changes should be taken into consideration. The fluid flow in the weld pool is accounted for by following Leung's recommendation of increasing the conductivity of the material ten fold when at

the melting temperature. Fortunately, the heat of fusion and latent heat due to phase changes are accounted for directly by the material models developed by SYSWELD.

The change in weld base geometry also needs to be taken into account in the thermal area of the model. Although reducing the weld base geometry significantly reduces computation time and storage space, it causes several difficulties with the thermal computation. Without the extra material surrounding the weld, the heat is not able to dissipate as fast as it otherwise would, artificially inflating the thermal history of the part. In order to compensate, the radiative and convective heat transfer coefficients were increased to five and four times their normal rates, respectively. These values are obtained through comparison of numerous simulations to the experimental builds. These increased values are only used for the boundary conditions for the weld base. In the same vein, the radiative coefficient for the beads was increased by 25 percent. This increase accounts for the boundary conditions of the activating bead being neglected, as noted at the end of section 4.1.

The last consideration for the thermal aspect of the model is attempting to accurately mimic the experimental builds. During the initial simulations, the weld pool started out as a fraction of the layer width and by the end, enlarged to over five times the layer width. While the weld pool increases as the build progresses, the initial simulations grossly overestimated the effect. In order to correct this problem, several measures were taken. The first was increasing the boundary conditions of the base of the part. This helped to some extent, but the problem still existed. Finally, the preheating pass described in the LENS build section was included in the model. This addition finally produced a thermal simulation with reasonable weld pool sizes in both

the first and final passes. Once this was achieved, the model laser power was fine tuned to obtain thermal results similar to the ones observed in the experimental builds.

### ***4.3 Mechanical Modeling Aspect***

In this study, there are no experimental mechanical results to compare simulation results against. So, unlike the thermal simulation, it is not possible to adjust certain properties to make the results from the model more closely match those of the experiments. Yet, there are decisions regarding the mechanical model that need to be made.

The first decision to make is whether to model in two or three dimensions. The decision to model in three dimensions has already been mentioned, but much of the reasoning was due to the mechanical aspect of the simulation. The most accurate prediction of longitudinal stress is through the use of a three dimensional model. Since longitudinal stress is considered an important quantity in this study, sacrificing accuracy for speed was not desirable in this case. Also, three dimensional models are slightly more accurate for stress in other directions as well, making the extra dimension worthwhile.

Another important matter for the mechanical model is the strain hardening model which will be used. In the Modeling Concerns chapter, the kinematic strain hardening model is recommended for cyclic applications, including welding. However, the material models included in SYSWELD use the isotropic strain hardening model. While it is possible to change the strain hardening model, the effects of making this change are unknown and it makes the most sense to use the model provided by

SYSWELD. Overall, throughout this study, the mechanical model is left alone for the most part, with any necessary changes being done in the thermal model.

#### ***4.4 Metallurgical Modeling Aspect***

As discussed in the modeling concerns chapter, the metallurgical aspect is quite complex. To minimize this complexity, the material models developed by SYSWELD will be used in the simulation. The SYSWELD material models all include the metallurgy of the materials. All of these models include the previously mentioned Johnson-Mehl-Avrami type transformation kinetics, which uses data from CCT diagrams. For the most part, these material models were generally left untouched. The only small changes made are to the conductivity. Even though SYSWELD has four steel material models, three were used in this study. The fourth material had substantially different in a couple different areas, and was therefore excluded. One of the problematic aspects of using the material models developed by SYSWELD is they are European standard materials and do not directly correlate to American standard materials.

The first material model is S355J2G3, which is part of Euronorm 10025 or EN 10025 Steel Norms. Unfortunately, this material has no American equivalent. The composition of this material is shown in Table 4.2. It is a hot rolled, non-alloy, structural steel. The yield stress can range from 275 – 355 MPa (Mega Pascal). The tensile strength can range from 450 – 680 MPa.<sup>[31]</sup> The material model provided by SYSWELD does include numbers for tensile and yield stress, and extracting those numbers is rather difficult since each phase has a range of yield strengths depending on

the temperature. The model of S355J2G3 has a melting point of 1450°C. The model also has four different phases and a thermal conductivity of 0.033 Watts/meter Kelvin at temperatures above 1450°C. This is a material that will undergo solid phase transformations, possibly influencing residual stress and distortion in parts created with LENS.<sup>[31]</sup>

Element	Carbon	Manganese	Silicon	Phosphorus	Sulfur	Nitrogen
Percentage	0.20	1.60	< 0.55	0.035	0.035	0.00

Table 4.2 - Material Composition of S355J2G3[31]

The second material model is DC04, which is part of EN 10277 Steel Norms. This material can be loosely compared with the ASTM SAE 1006 steel, but there are some differences in chemical composition. The composition of DC04 is shown in Table 4.3. It is a cold-rolled low-carbon steel. The yield stress can range from 140 – 210 MPa and the tensile strength can range from 270 – 350 MPa.<sup>[32]</sup> As with the previous material, extracting the yield stress from the material model is extremely difficult. The modeled melting temperature for DC04 is 1505°C. This material model has six phases and a thermal conductivity of 0.032 W/mK above the melting temperature. This material will undergo solid phase transformations, which may alter residual stress and part distortion.<sup>[32]</sup>

Element	Carbon	Manganese	Phosphorus	Sulfur
Percentage	0.08	0.040	0.030	< 0.030

Table 4.3 - Material Composition of DC04[32]

The third material is X20Cr13, which is part of the EN 10088 Steel Norms. This material is the rough equivalent of AISI 420. This is a stainless steel, and its composition is shown in Table 4.4. The yield strength can vary from 350 – 550 Mpa and the tensile strength ranges from 650 – 880 MPa.<sup>[33]</sup> The modeled melting

temperature for X20Cr13 is 144°C. This material has only two phases and a thermal conductivity of 0.0332 W/mK above the melting temperature. This material, as a stainless steel, should experience minimal effects from phase transformations.<sup>[33]</sup>

Element	Carbon	Chromium	Silicon	Manganese	Molybdenum	Vanadium
Percentage	< 0.20	12.0 – 14.0	< 1.0	< 1.0	0.70	0.20

Table 4.4 - Material Composition of X20Cr13[33]

The material models provided by SYSWELD contain two major parts, the thermal properties and the mechanical properties. The thermal properties included in the model are thermal conductivity, specific heat, and density. The mechanical properties included in the model are Young's modulus, Poisson's ratio, yield strength, coefficient of thermal expansion, and slope, which refers to the slope of the stress/strain curve. All of these properties are dependent on the temperature and phase of the material.

Although using the material properties provided by SYSWELD is more convenient, there are several drawbacks. One of the major drawbacks is that the properties are just given, without any information as to how they were obtained. They do not come with any information about the accuracy of the properties, making it difficult to define the accuracy of the simulation results. For example, all but two of the properties defined for each material have the exact same values in all phases but one. Whether this is a crude estimate of the properties or an accurate representation of their characteristics is hard to know. The second problem is the materials themselves are hard to compare. Each material has a different melting temperature, yield strength and conductivity. This makes it impossible to run an ideal "scientific" experiment with only one variable. However, this drawback is not as bad as one might think: finding any two

steels with identical properties except for solid phase transformations is quite difficult. The last problem is using steels with European standards makes attempting to verify the simulations through experimentation extremely difficult. Since comparison with experimental builds is beyond the scope of this study, this is not extremely detrimental either. Overall, because of the use of material properties provided by SYSWELD, the comparison between materials with, and without, solid phase transformations cannot be exact. The goal of this study is to estimate the magnitude of effect from solid phase transformations and give an idea of the importance of including them in the simulation.

#### ***4.5 Temporal Modeling Aspect***

The primary focus of the simulation timing is keeping it the same as the timing in the experimental builds. The timing for the experimental builds is shown in Table 4.5. The time not accounted for on the chart is when the laser is returning to the left side to begin the next build. Each layer deposited takes 4.233 s (25.4 mm long at a feed rate of 6 mm/s) and each return takes 2.116 s (25.4 mm long at 12 mm/s). In total, to make a deposit and return is 6.35 seconds. The timing for the SYSWELD model is shown in Table 4.6. The main difference is that the passes in the simulation are only 25.0 mm, and therefore only take 4.166 seconds to build and 2.083 seconds to return. The only other difference is that the first bead in the simulation is does not start directly after the end of the preheat pass. This is to make the numbers simpler and also avoid starting a time step at a repeating decimal.



Bead	Start Position	Start Time	Stop Position	Stop Time
Preheat	Right	0.000 s	Left	4.233 s
1	Left	4.233 s	Right	8.466 s
2	Left	10.583 s	Right	14.816 s
3	Left	16.933 s	Right	21.166 s
4	Left	23.283 s	Right	27.516 s

**Table 4.5 - Experimental Build Timing**

Bead	Start Position	Start Time	Stop Position	Stop Time
Preheat	Right	0.000 s	Left	4.166 s
1	Left	4.200 s	Right	8.366 s
2	Left	10.450 s	Right	14.616 s
3	Left	16.700 s	Right	20.866 s
4	Left	22.950 s	Right	27.116 s

**Table 4.6 - Simulation Build Timing**

Lastly, a cooling period was added to the end of the simulation to allow most of the heat from the laser to dissipate. The cooling period started at 27.116 seconds and lasted until 60.000 seconds.

## **Chapter 5 - Results and Discussion**

### ***5.1 Thermal Results***

In this particular study, the thermal results are the only basis for comparison between the LENS model and the experimental builds. Although no specific thermal data was recorded from the experimental builds, the size and shape of the weld pool was observed during the builds. Ideally, the thermal simulation results would closely resemble the experimental observations. In addition, the thermal results for the different materials would also be proportional to one another, providing better means of comparison.

The first observation from the experimental builds was that the size of the weld pool was rather small during the first pass. The small weld pool caused a narrow build during the first pass, as shown in Figure 5.1. The other important observation from the experimental builds was the relative size of the weld pool as the line builds progressed. The weld pool slightly increased in size as the build progressed. From observations, the weld pool size did not exceed 0.7 mm wide, 0.8 mm tall or 1.4 mm long.

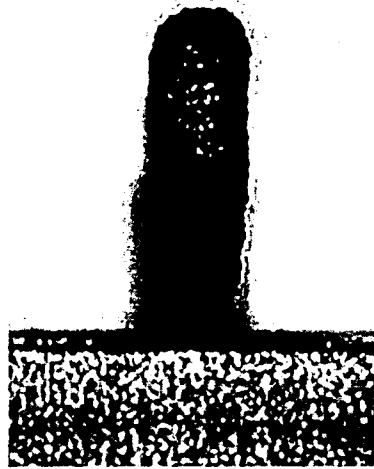


Figure 5.1 - Small Weld Pool Example

The observations from the experimental builds were used to fine tune the thermal simulation results. The boundary conditions and laser power were adjusted so that the weld pool retained an appropriate size during the course of the simulation. All of these adjustments were done with the simulation for S355J2G3 steel. Once accurate parameters were established for this material, the parameters were then transferred to the other material simulations as well. If any further adjustments needed to be made for the simulations with the other materials, only the laser power was changed.

The thermal results for the materials S355J2G3, DC04, and X20Cr13 are compared in the following figures. The thermal results will follow the color index that

is shown in Table 5.1. Figure 5.2 shows a section view of the weld pool, at about 5.00 seconds, for all the material simulations. Although the size of the molten pool is not exactly the same, the results are very similar. The regions in the orange and yellow ranges are very similar. Another way to compare these simulations is by looking at the maximum temperatures (Table 5.2). It is somewhat surprising to see that the S355J2G3 model had the highest maximum temperature with respect to its melting temperature when it had the smallest molten pool. This demonstrates the difficulty of comparing one material to another. Increasing the laser power in the S355J2G3 model would make the maximum temperature further above the melting point. In general, when comparing different materials, getting the results to correlate exactly is an unreasonable expectation. Further evidence of this is the fact that the user cannot control the time steps taken by the simulation. The times shown in Table 5.2 were the closest to 5.00 seconds for each of the simulations. In general, emphasis will be placed on the overall trend of the simulations, not the specific comparison of a given number for a specific time step.

Color	Shade (in black and white)	Temperature Range
Red	Dark Grey	Melting and above
Orange	Light Grey	1150°C – Melting
Yellow	White	850°C – 1150°C
Olive	Light Grey	600°C – 850°C
Green	Grey	400°C – 600°C
Turquoise	Light Grey	200°C – 400°C
Light Blue	Grey	20°C – 200°C
Royal Blue	Dark	20°C and Below

Table 5.1 - Thermal Results Color Index

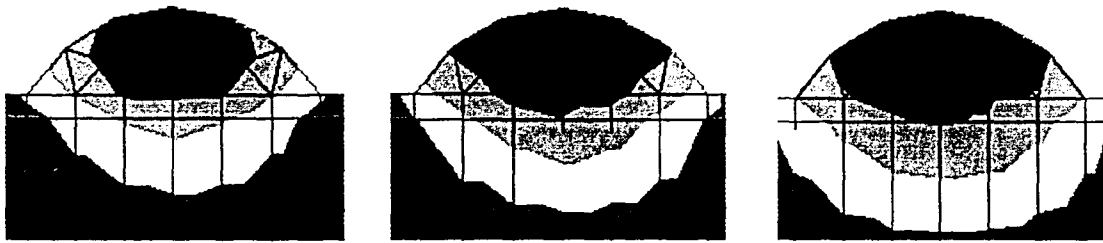


Figure 5.2 - Molten Pool size at t ~ 5 seconds (S355J2G3, DC04 and X20Cr13 from left to right)

Material	S355J2G3	DC04	X20Cr13
Max Temp @ t ~ 5.00 s	1534.65°C	1579.78°C	1520.05°C
Melting Temp	1450°C	1505°C	1444°C
Difference	84.65°C	74.78°C	76.05°C
Time Step	5.06 s	5.00 s	5.03 s

Table 5.2 - Temperatures data ~ 5.0s

Thermal results for the three simulations, at a time near 11.500 seconds, are shown in Figures 5.3 – 5.5. Table 5.3 shows the temperature data for the three simulations. The relative size and shape of the weld pool is very similar for all three cases. In addition, the maximum temperature relative to the melting temperature is very similar for all three simulations as well. The only noticeable difference is in the temperatures of the base of the part. This is most likely due to the differing thermal conductivities of the materials. This is not a large concern in any case because the thermal history of the base is of minimal importance.

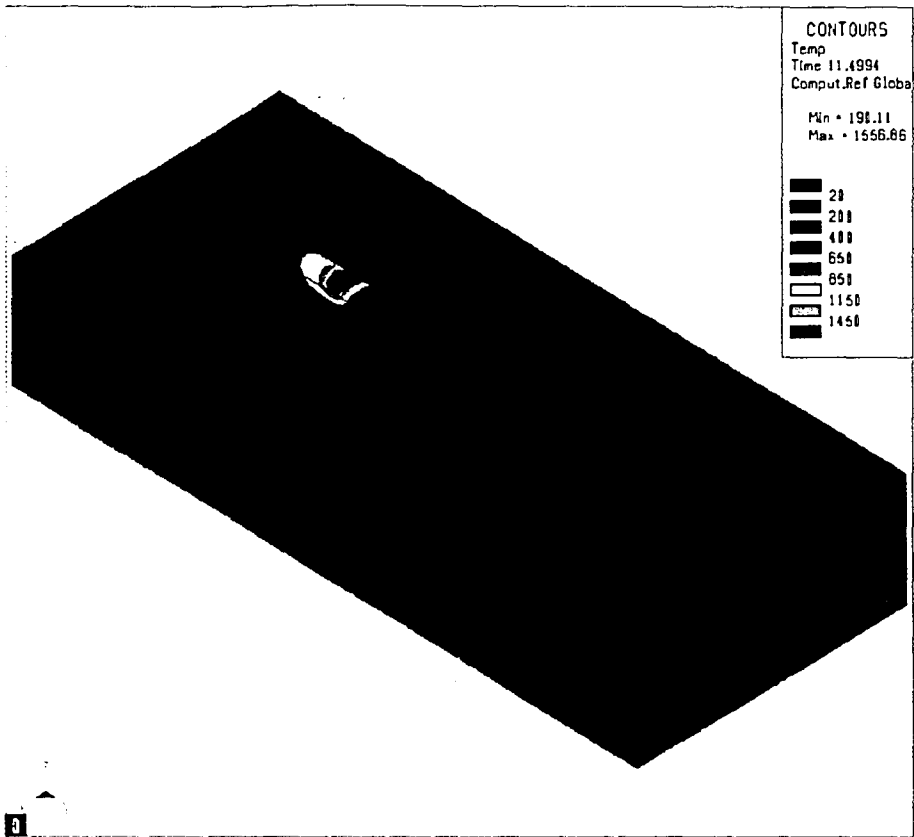


Figure 5.3 - S355J2G3 Simulation,  $t \sim 11.5$  s

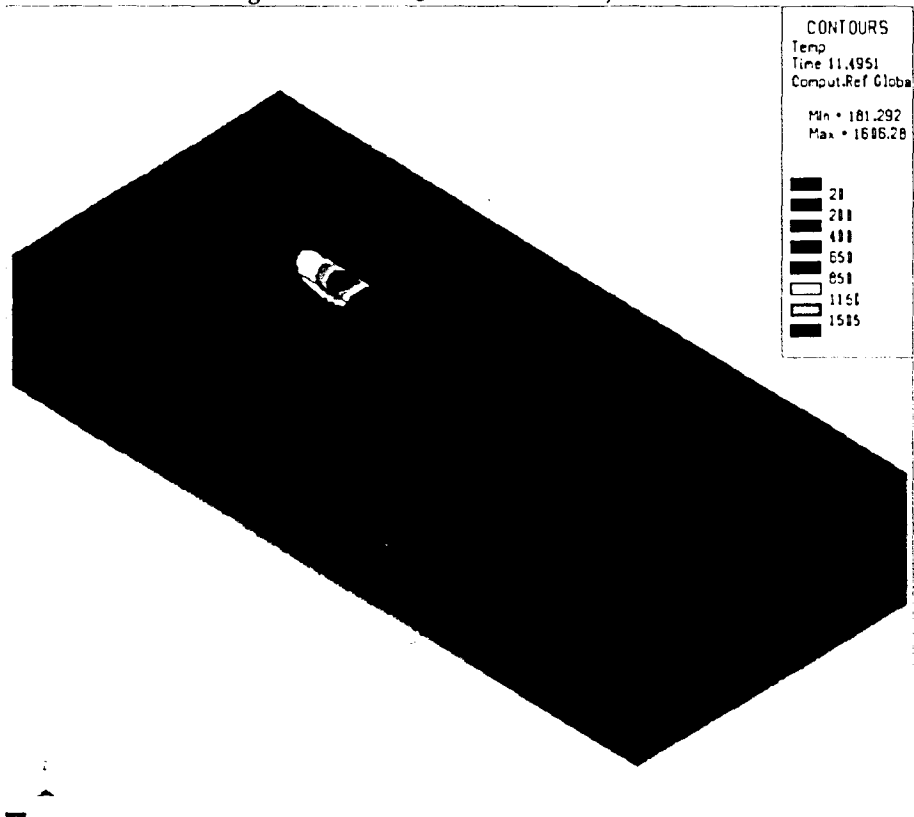
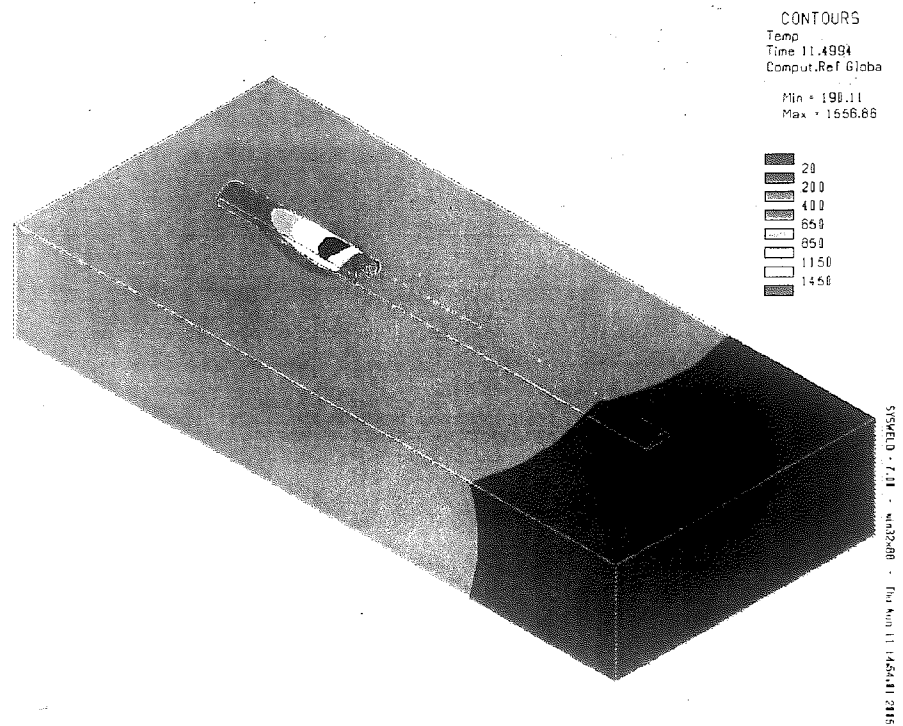
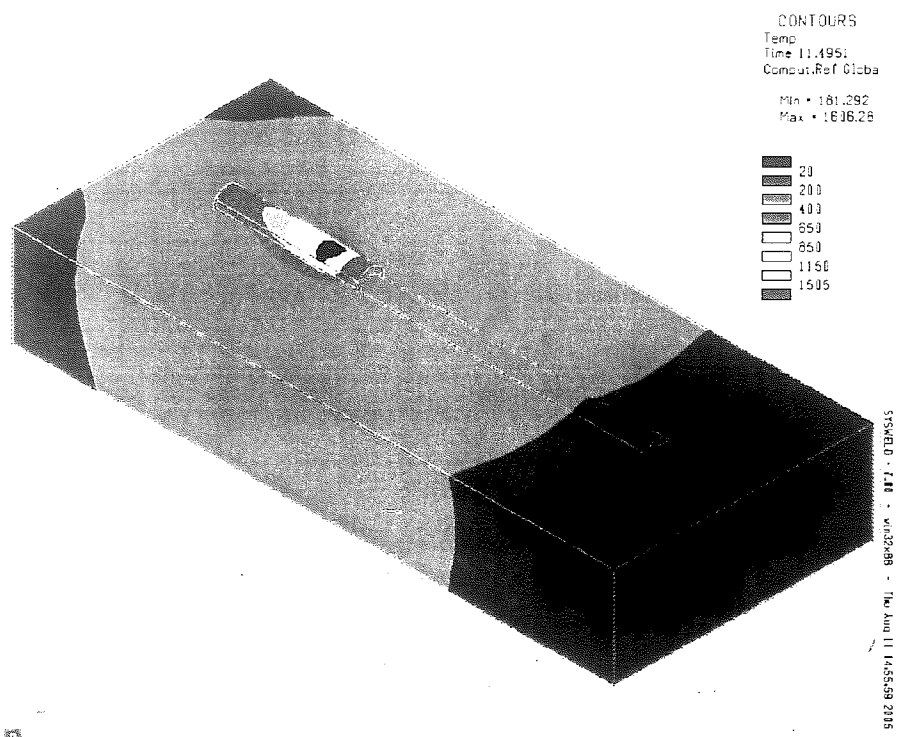


Figure 5.4 - DC04 Simulation,  $t \sim 11.5$  s



**Figure 5.3 - S355J2G3 Simulation, t ~ 11.5 s**



**Figure 5.4 - DC04 Simulation, t ~ 11.5**

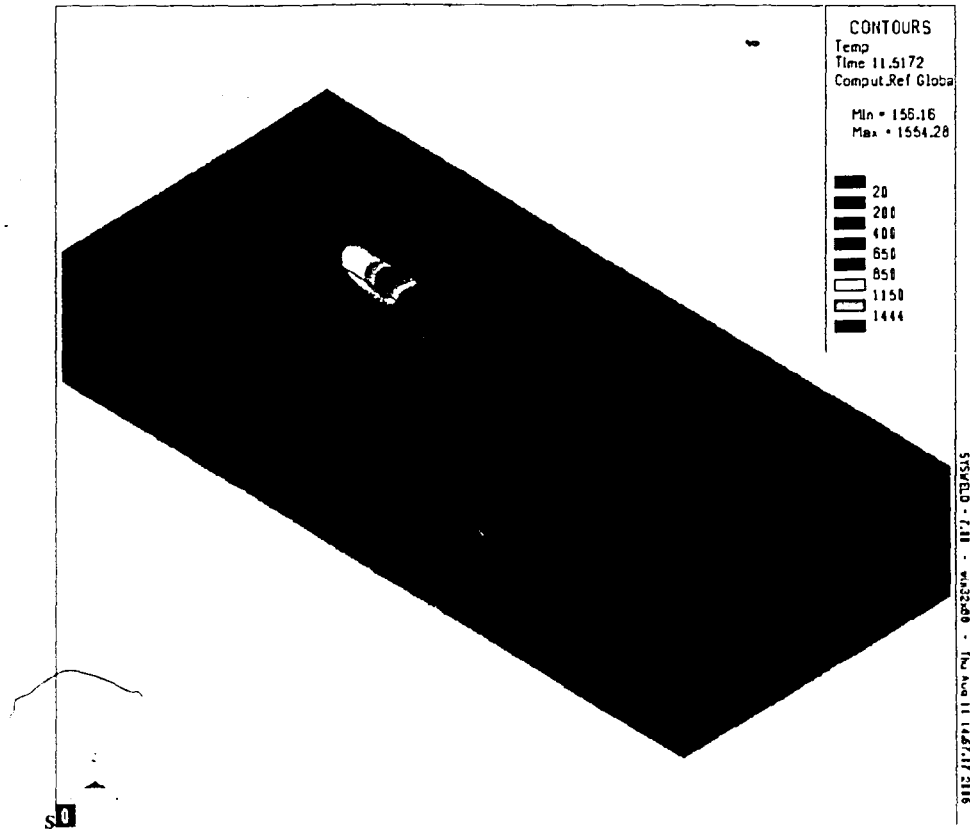


Figure 5.5 - X20Cr13 Simulation, t ~ 11.5 s

Material	S355J2G3	DC04	X20Cr13
Max Temp @ t ~ 5.00 s	1556.86°C	1606.28°C	1554.28°C
Melting Temp	1450°C	1505°C	1444°C
Difference	106.86°C	101.28°C	110.28°C
Time Step	11.4994 s	11.4951 s	11.5172 s

Table 5.3 - Temperature Data ~ 11.5 s

It is more important that the thermal history of the three models be comparable near the end of the simulation for two reasons. Primarily, similar thermal results near the end indicate that the early comparisons were not by chance. Furthermore, the final pass will have the largest weld pool, and most likely the largest influence on the residual stresses. The large impact on residual stresses is due mainly to the fact that the last pass will re-melt some of the material deposited by the previous pass, alleviating residual stresses already in the part. Figure 5.6 - Molten Pool size at t ~ 25 seconds

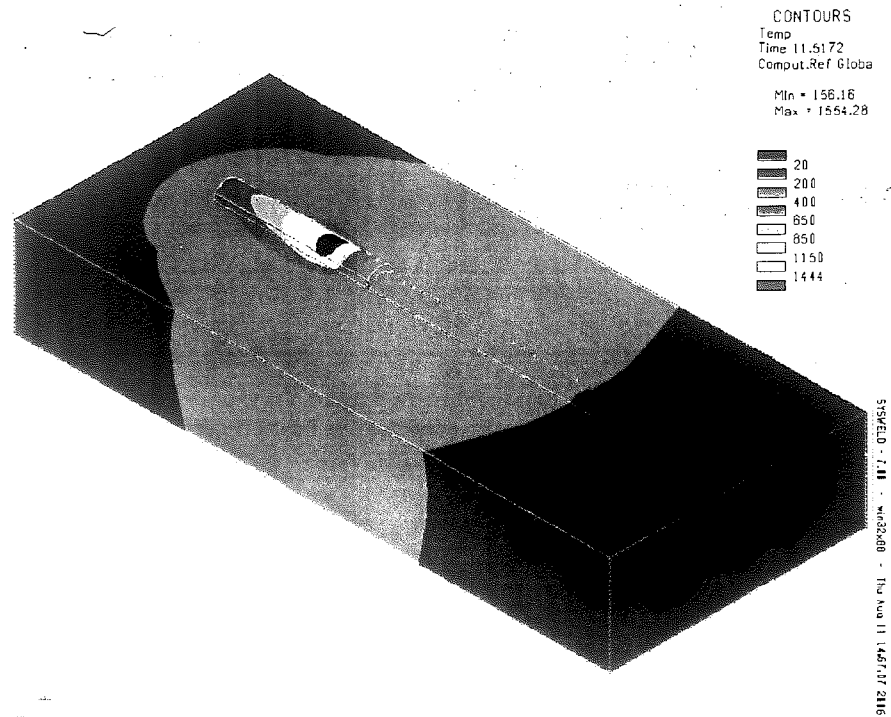


Figure 5.5 - X20Cr13 Simulation, t ~ 11.5 s

Material	S355J2G3	DC04	X20Cr13
Max Temp @ t ~ 5.00 s	1556.86°C	1606.28°C	1554.28°C
Melting Temp	1450°C	1505°C	1444°C
Difference	106.86°C	101.28°C	110.28°C
Time Step	11.4994 s	11.4951 s	11.5172 s

Table 5.3 - Temperature Data ~ 11.5 s

It is more important that the thermal history of the three models be comparable near the end of the simulation for two reasons. Primarily, similar thermal results near the end indicate that the early comparisons were not by chance. Furthermore, the final pass will have the largest weld pool, and most likely the largest influence on the residual stresses. The large impact on residual stresses is due mainly to the fact that the last pass will re-melt some of the material deposited by the previous pass, alleviating residual stresses already in the part. Figure 5.6 - Molten Pool size at t ~ 25 seconds



(S355J2G3, DC04 and X20Cr13 from left to right) shows a section view, at about 25 seconds, of all three material simulations. Figures 5.7 – 5.9 show a close up isometric view of the molten pool area and Table 5.4 details the temperature data. These results show very good comparability between the three material simulations. Even though the molten pool sizes are not exactly the same, this is still not cause for concern. The maximum temperature data is consistent and the overall isotherms compare very well. Overall, the thermal results provide good basis for comparison of the mechanical results because they vary very little from one material to another.

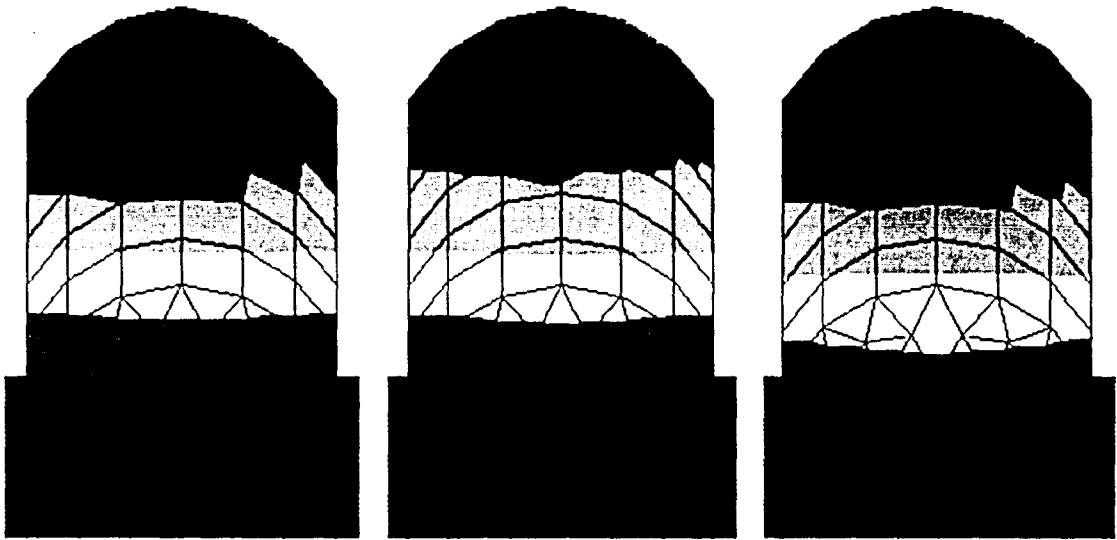


Figure 5.6 - Molten Pool size at  $t \sim 25$  seconds (S355J2G3, DC04 and X20Cr13 from left to right)

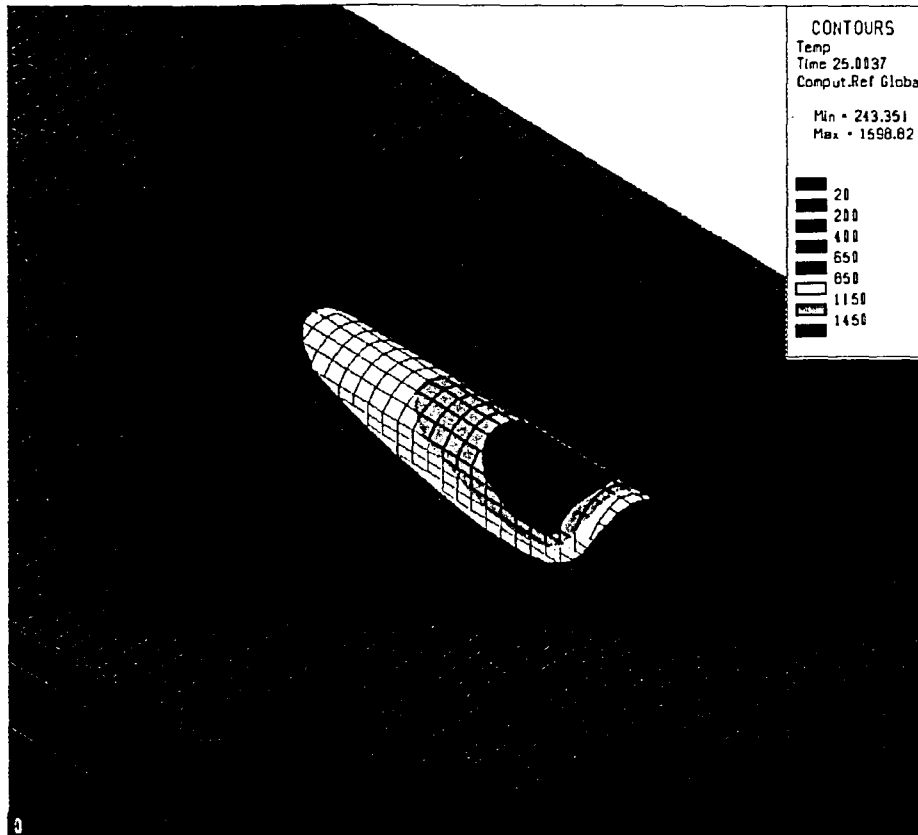


Figure 5.7 - S355J2G3 Simulation,  $t \sim 25.0$  s

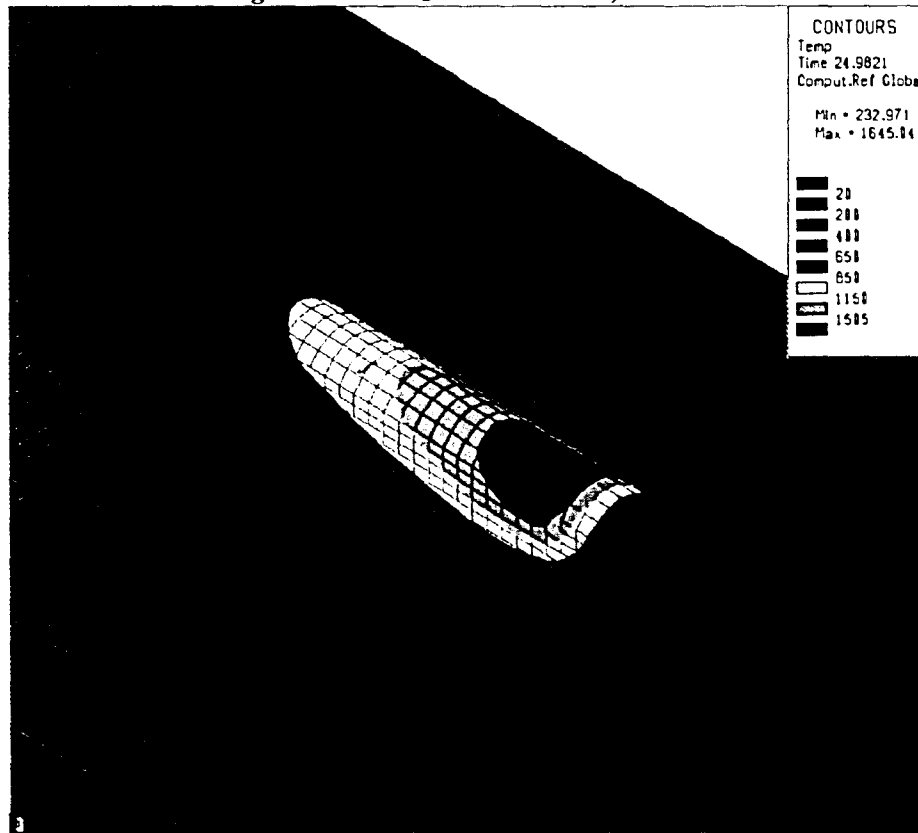


Figure 5.8 - DC04 Simulation,  $t \sim 25.0$  s

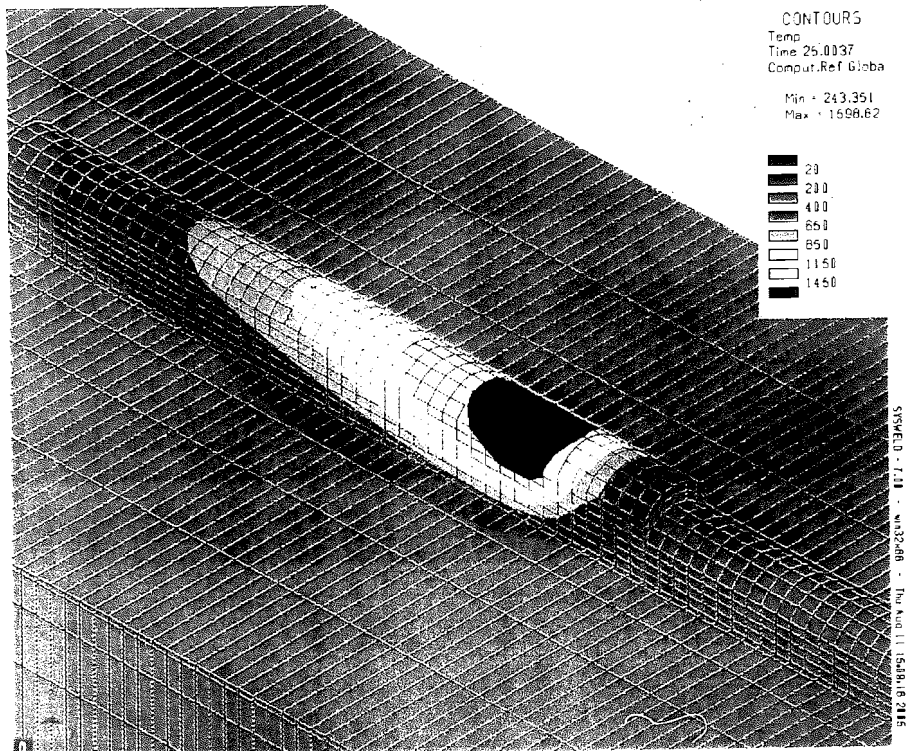


Figure 5.7 - S355J2G3 Simulation, t ~ 25.0 s

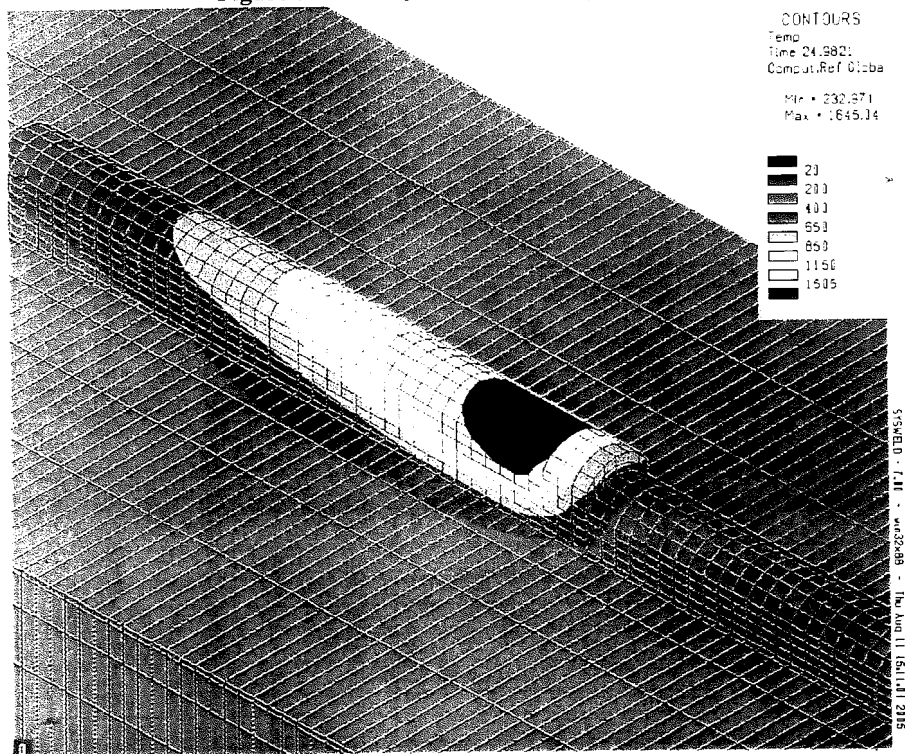


Figure 5.8 - DC04 Simulation, t ~ 25.0 s

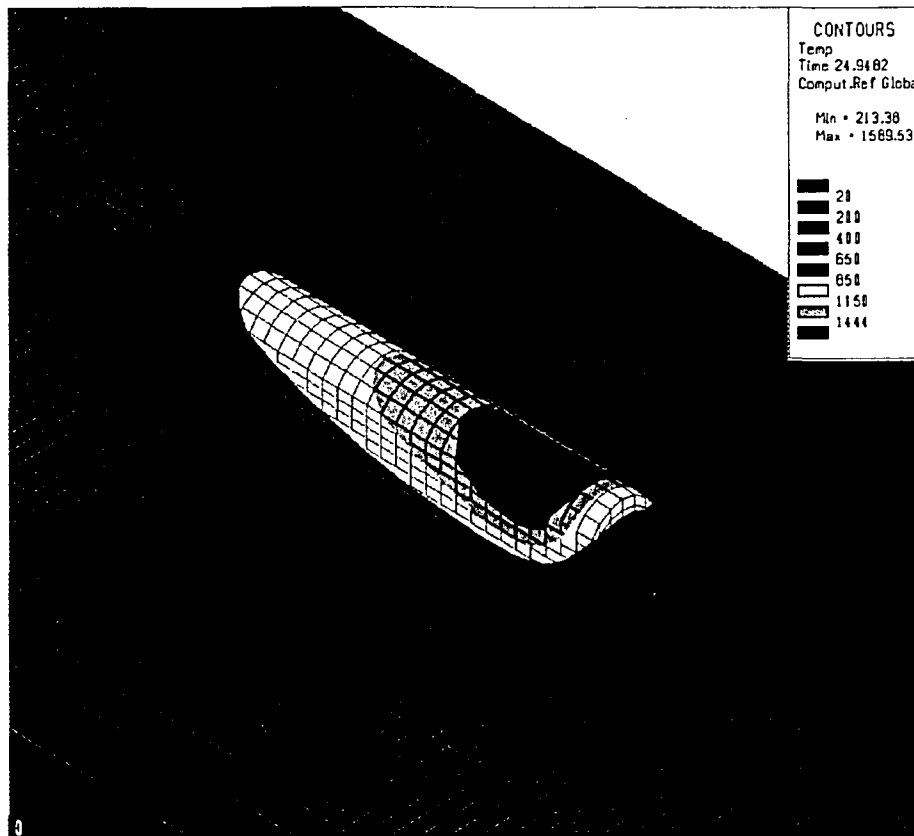


Figure 5.9 - X20Cr13 Simulation,  $t \sim 25.0$  s

Material	S355J2G3	DC04	X20Cr13
Max Temp @ $t \sim 5.00$ s	1598.82°C	1645.04°C	1589.53°C
Melting Temp	1450°C	1505°C	1444°C
Difference	148.82°C	140.04°C	145.53°C
Time Step	25.0037 s	24.9821 s	24.9482 s

Table 5.4 - Temperature Data  $\sim 25.0$  s

## 5.2 Mechanical Results

Once a satisfactory thermal simulation was achieved, the thermal results were used to produce a mechanical simulation for each of the material models. Comparison of the mechanical simulations is difficult because there are many different types of results that can be compared. The data available from the mechanical simulation includes: displacements in all three directions, normal and shear stresses in all three

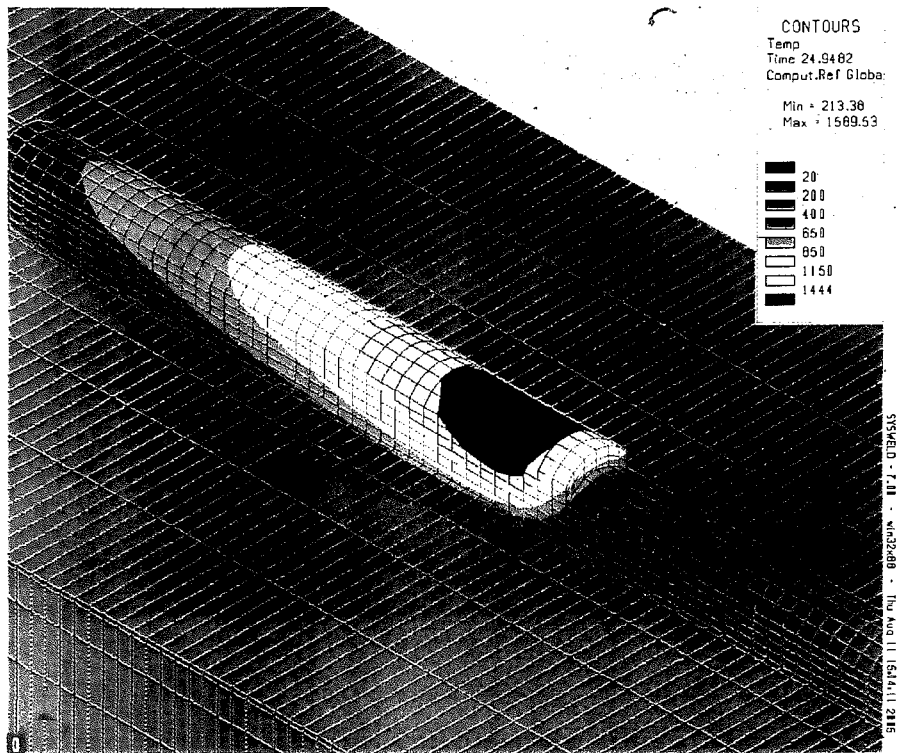


**Figure 5.9 - X20Cr13 Simulation, t ~ 25.0 s**

Material	S355J2G3	DC04	X20Cr13
Max Temp @ t ~ 5.00 s	1598.82°C	1645.04°C	1589.53°C
Melting Temp	1450°C	1505°C	1444°C
Difference	148.82°C	140.04°C	145.53°C
Time Step	25.0037 s	24.9821 s	24.9482 s

**Table 5.4 - Temperature Data ~ 25.0 s**

**5.2 Mechanical Results**

Once a satisfactory thermal simulation was achieved, the thermal results were used to produce a mechanical simulation for each of the material models. Comparison of the mechanical simulations is difficult because there are many different types of results that can be compared. The data available from the mechanical simulation includes: displacements in all three directions, normal and shear stresses in all three

directions, three principal stresses, and Von mises stress. Rather than compare the results for each of the three material simulations at each time step; select parameters will be compared in order to analyze the effect of the different materials in the simulation. Results from some intermediate time steps will be analyzed; however, most emphasis will be placed on the results from the very last time step since the final distortion and residual stress is of the greatest importance.

Figures 5.10 – 5.18 show the results from the mechanical simulation at time steps near 25.00 seconds. The results displayed are  $\sigma_{xx}$  (stress in the x-direction) and two images showing  $\sigma_{yy}$  (stress in the y-direction). Both of the images showing  $\sigma_{yy}$  have distorted shapes which indicate the deformation of the part. The actual distortion was multiplied by 10 to make the distortion easier to see. The y-direction is the welding direction and the x-direction faces the bottom left corner of each of the images. The results for stress in the x-direction show a very similar stress state throughout the part for all three materials. Some differences in magnitude exist among the materials, but most of the differences are not significant. Discrepancies in maximum stress are not significant in these simulations since this maximum can very easily be an anomaly. The stress in the y-direction also shows a similar stress state in the build simulations. The results show that the layer being deposited is under very little stress. The previous layer, which has had some time to cool, is in compression. Like the stresses, the distorted images do not show many differences in displacement between the simulation results for the three materials. The only pronounced difference is the large distortion seen at the right end of the bead for the DC04 and X20Cr13 builds. Most likely this is due to a small problem with bead activation.

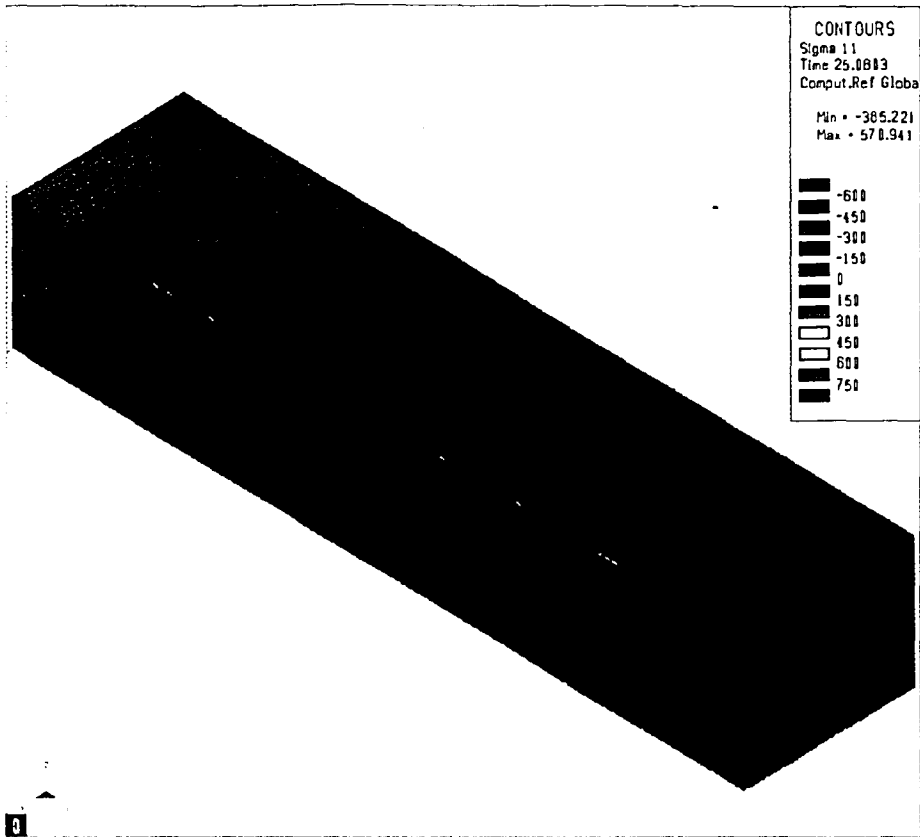


Figure 5.10 – S355J2G3 Simulation,  $t \sim 25.00$  s,  $\sigma_{xx}$  (MPa)

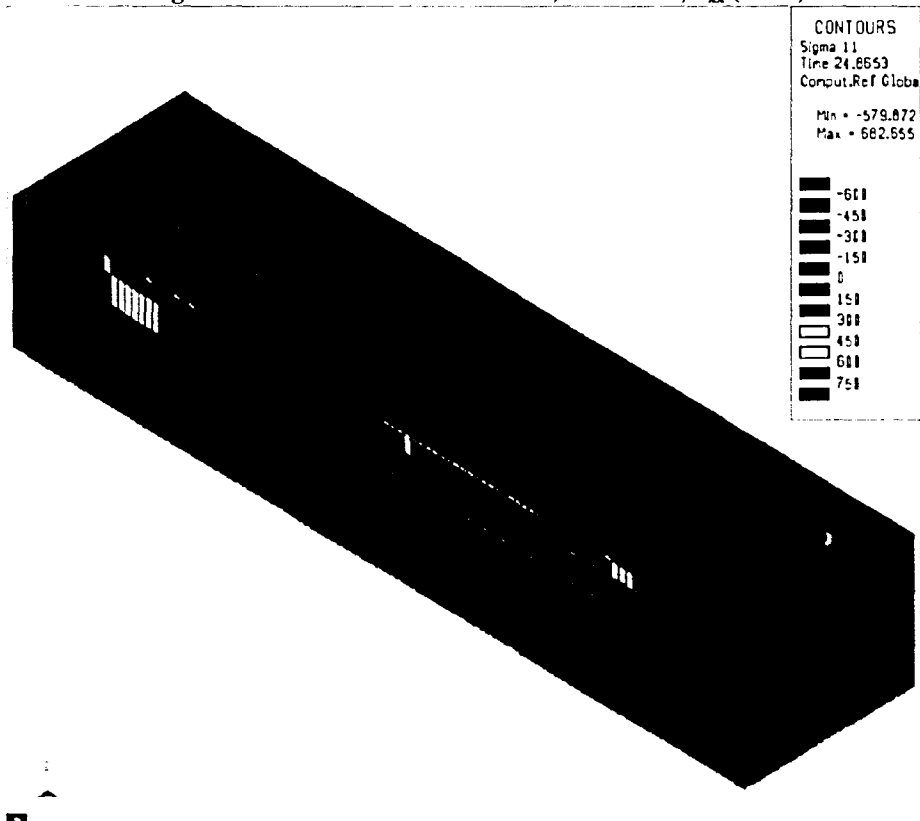


Figure 5.11 - DC04 Simulation,  $t \sim 25.00$  s,  $\sigma_{xx}$  (MPa)

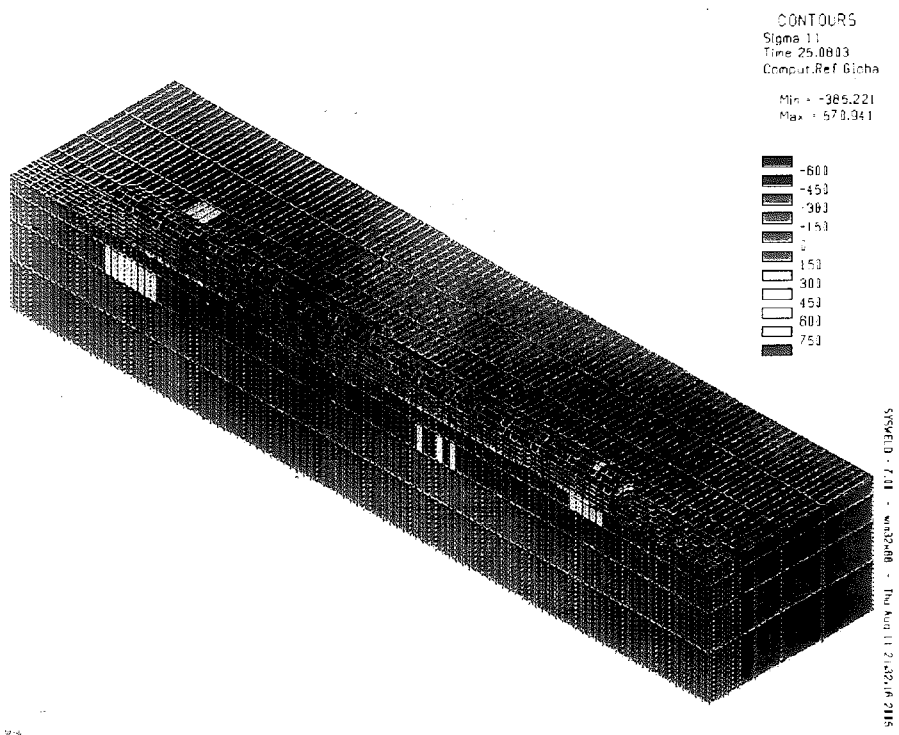


Figure 5.10 – S355J2G3 Simulation,  $t \sim 25.00$  s,  $\sigma_{xx}$  (MPa)

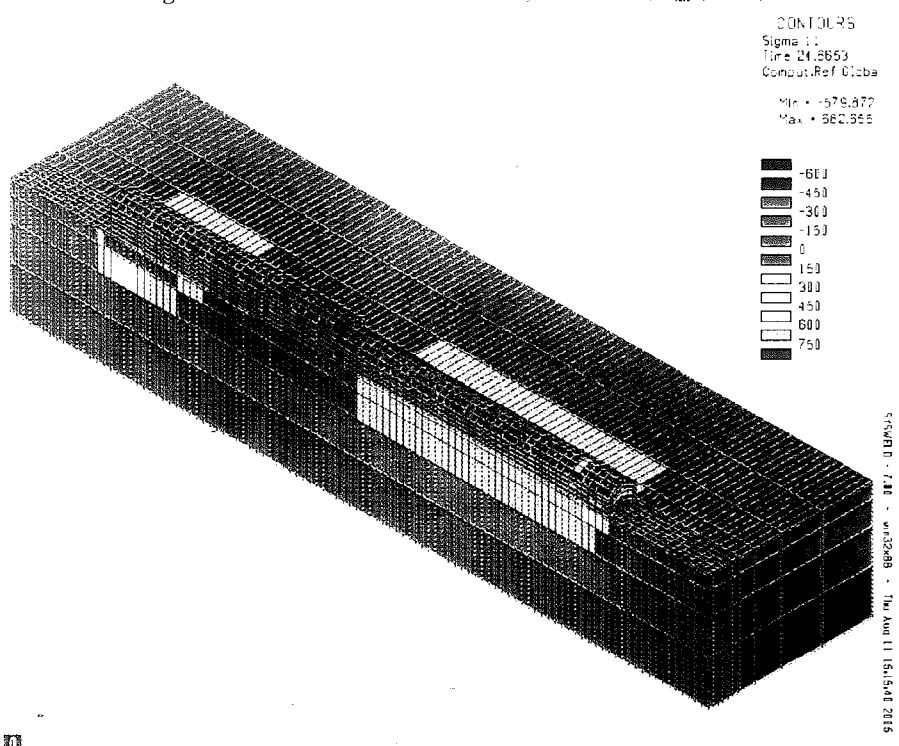


Figure 5.11 - DC04 Simulation,  $t \sim 25.00$  s,  $\sigma_{xx}$  (MPa)



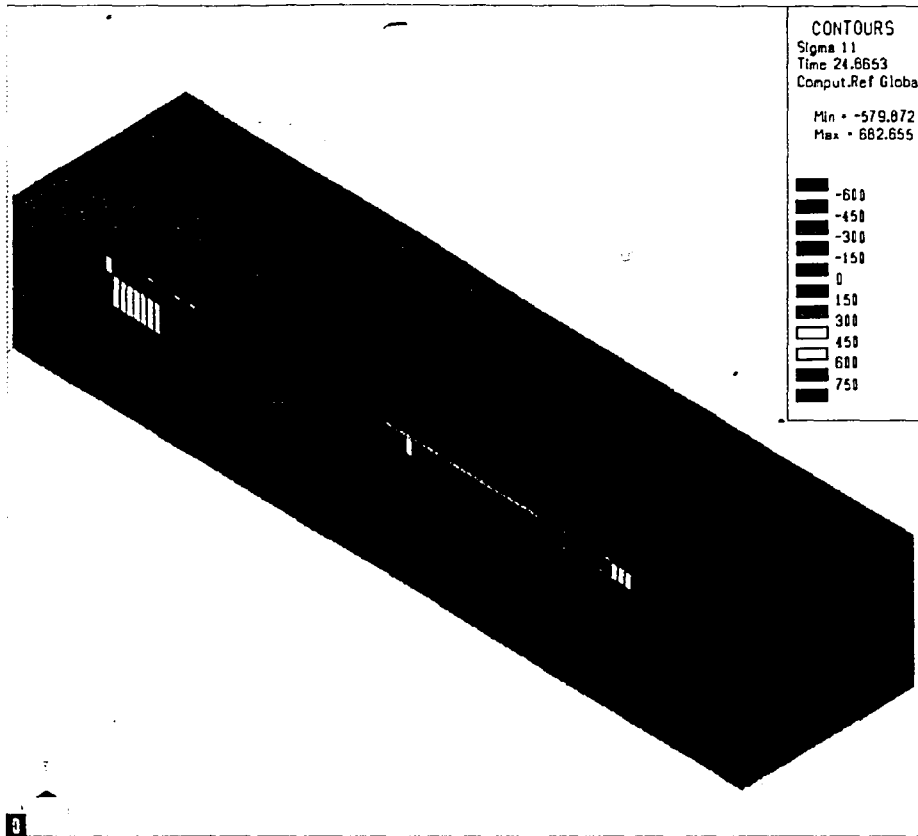


Figure 5.12 - X20Cr13 Simulation,  $t \sim 25.00$  s,  $\sigma_{xx}$  (MPa)

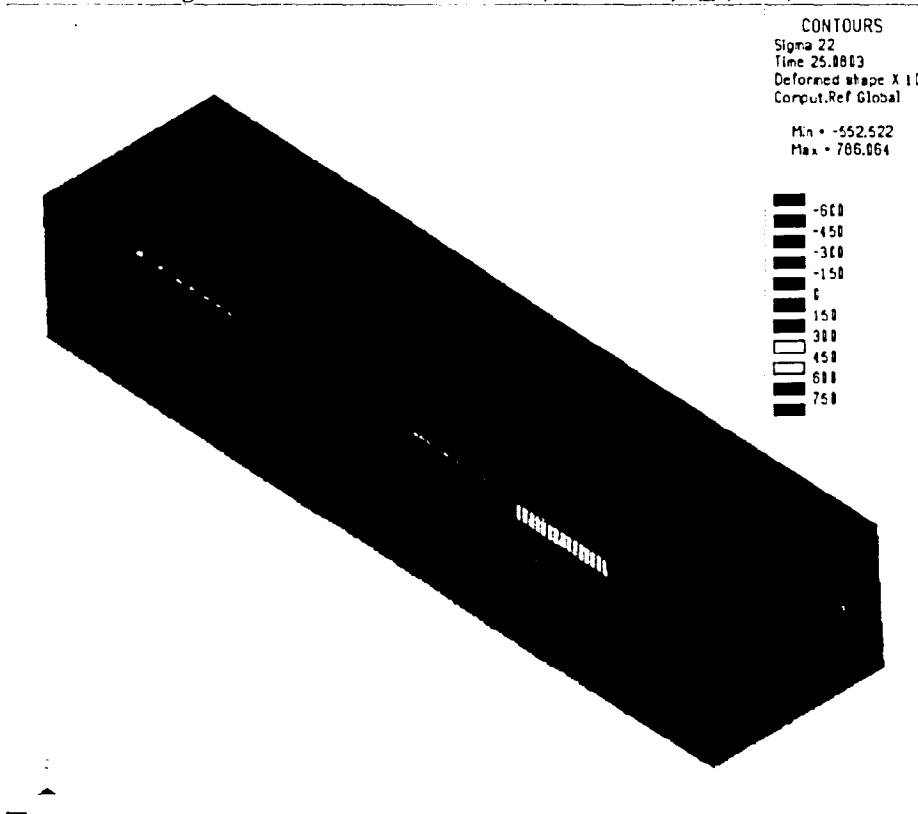


Figure 5.13 - S355J2G3 Simulation,  $t \sim 25.00$  s,  $\sigma_{yy}$  (MPa)

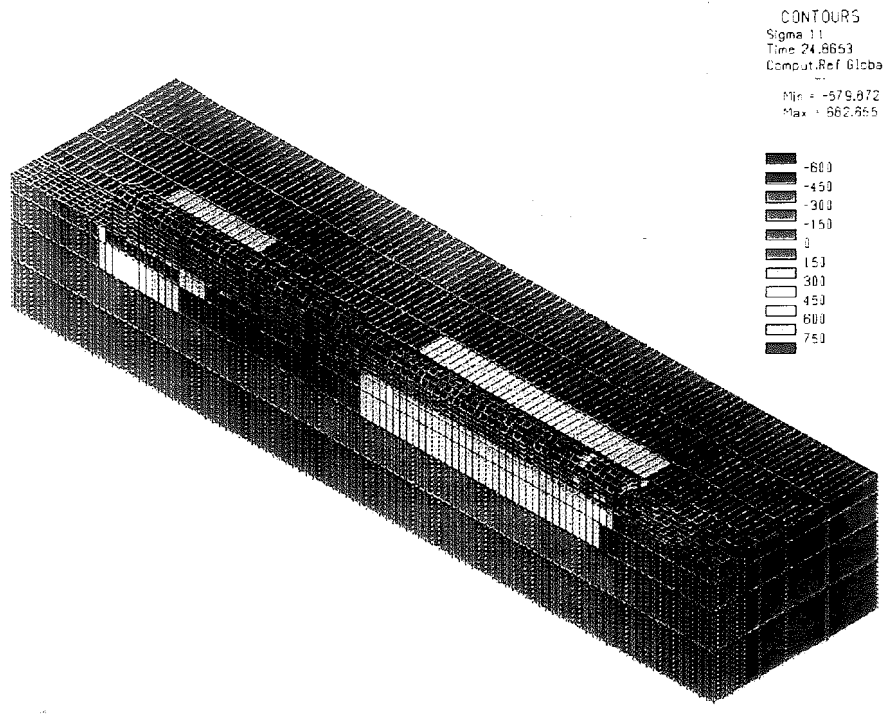


Figure 5.12 - X20Cr13 Simulation, t ~ 25.00 s,  $\sigma_{xx}$  (MPa)

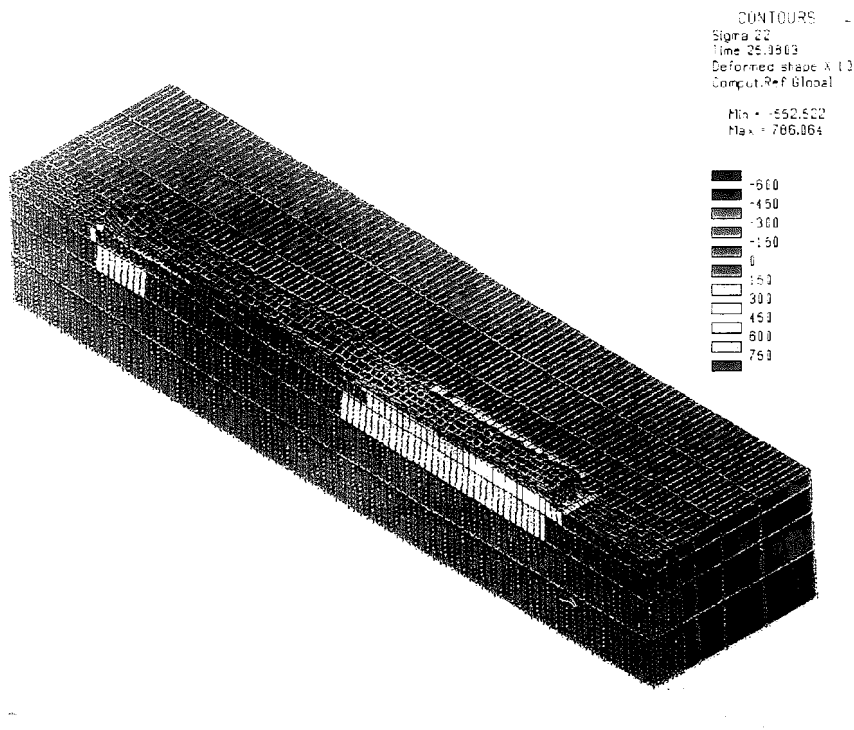


Figure 5.13 - S355J2G3 Simulation, t ~ 25.00 s,  $\sigma_{yy}$  (MPa)

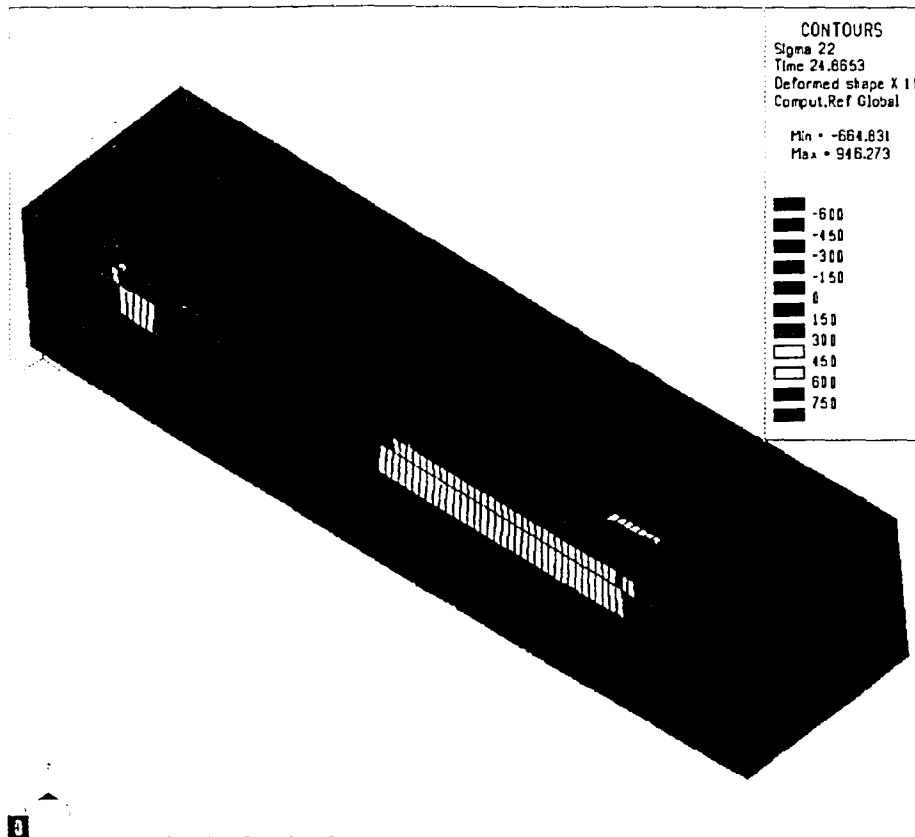


Figure 5.14 - DC04 Simulation,  $t \sim 25.00$  s,  $\sigma_{yy}$  (MPa)

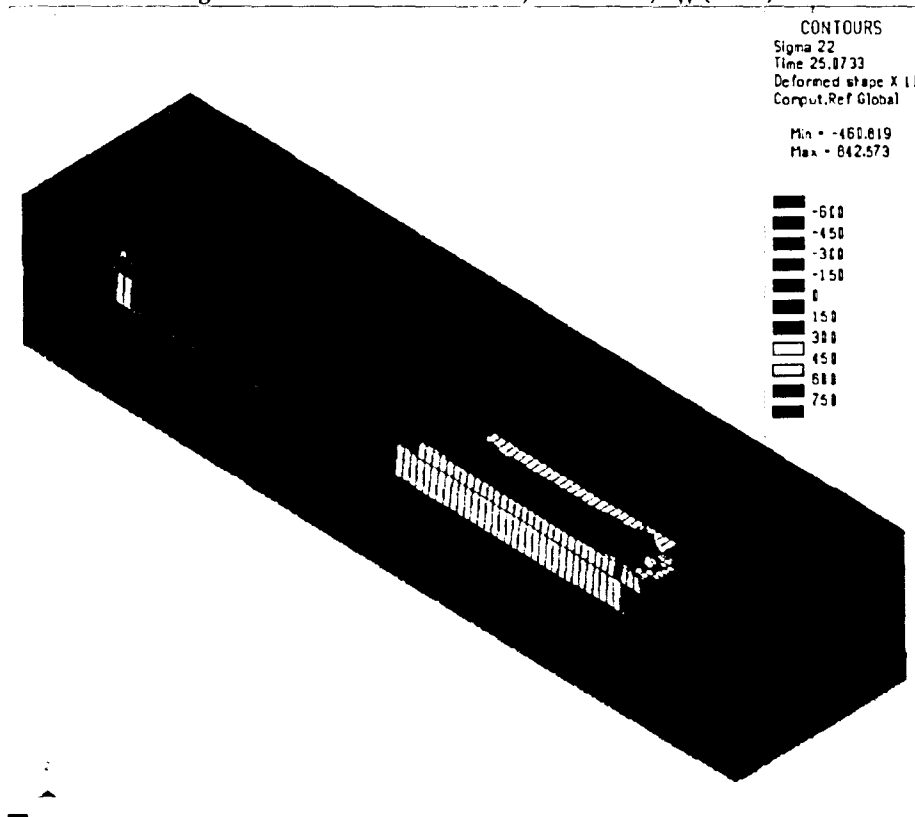


Figure 5.15 - X20Cr13 Simulation,  $t \sim 25.00$  s,  $\sigma_{yy}$  (MPa)

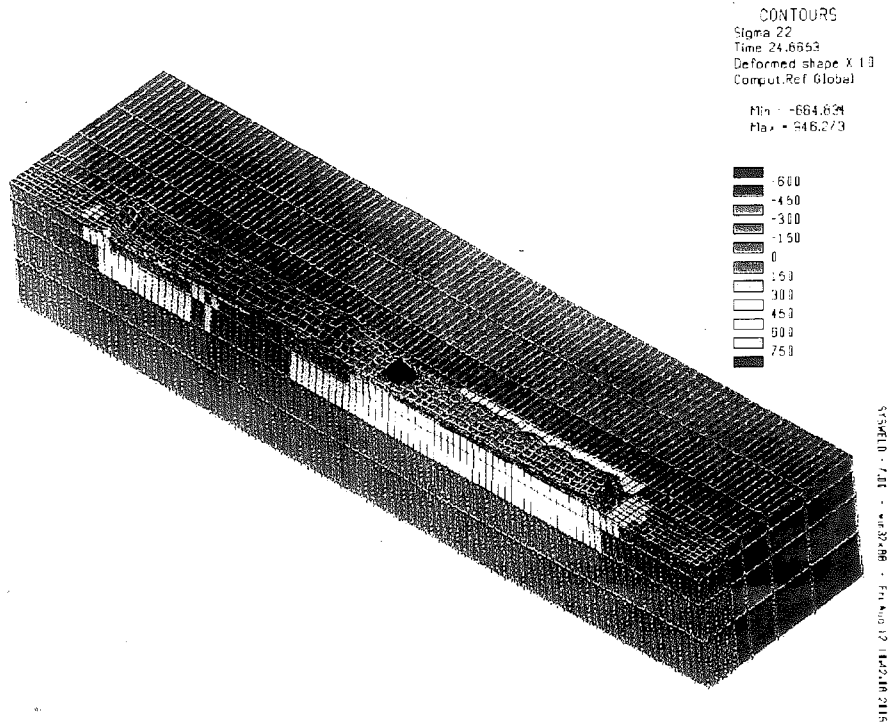


Figure 5.14 - DC04 Simulation, t ~ 25.00 s,  $\sigma_{yy}$  (MPa)

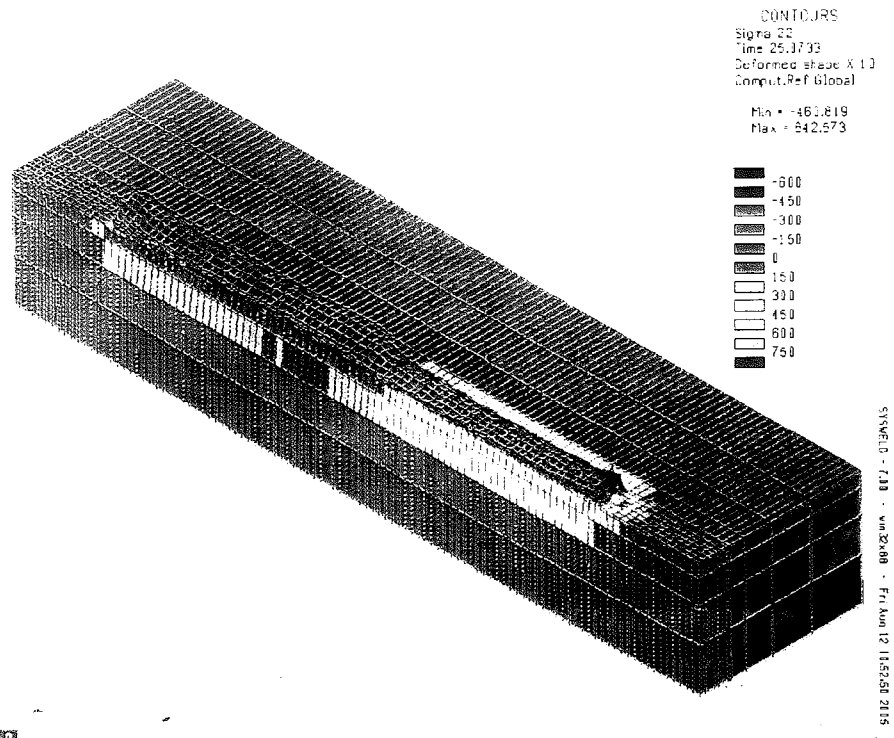


Figure 5.15 - X20Cr13 Simulation, t ~ 25.00 s,  $\sigma_{yy}$  (MPa)

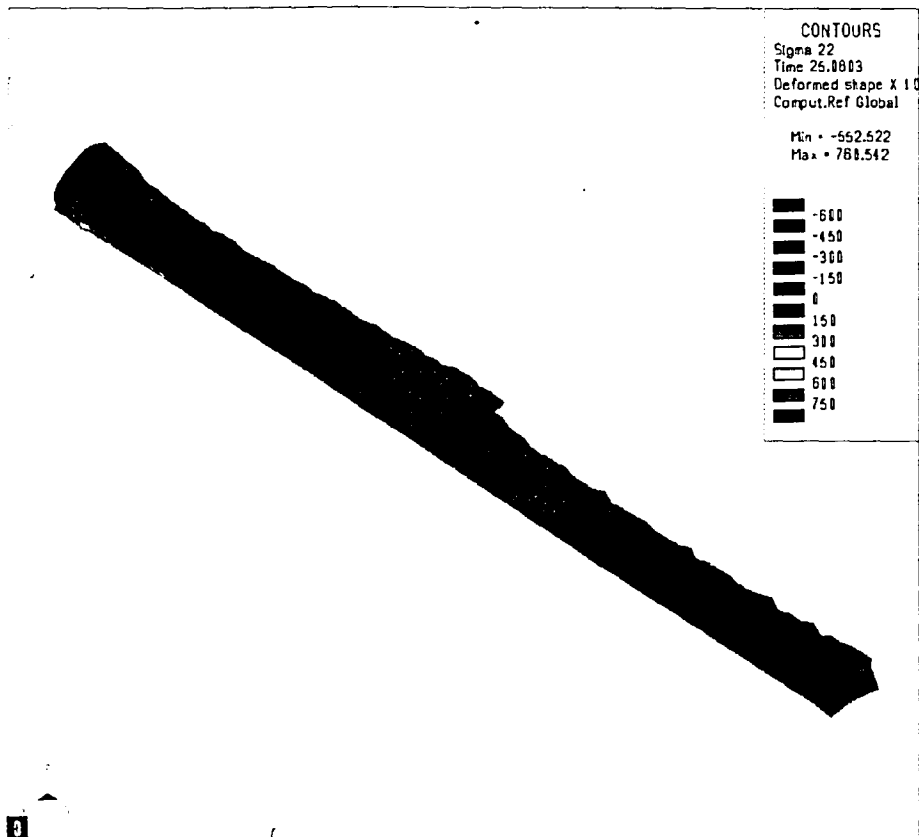


Figure 5.16 - S355J2G3 Simulation, t ~ 25.00 s,  $\sigma_{yy}$  (MPa), bead only

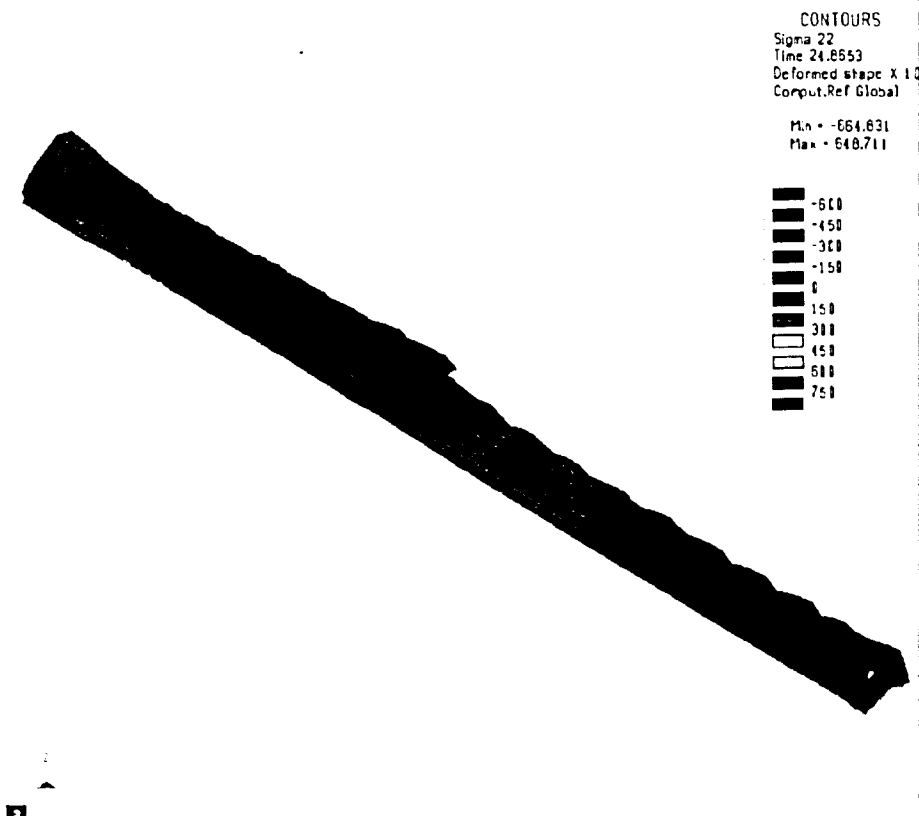


Figure 5.17 - DC04 Simulation, t ~ 25.00 s,  $\sigma_{yy}$  (MPa), bead only

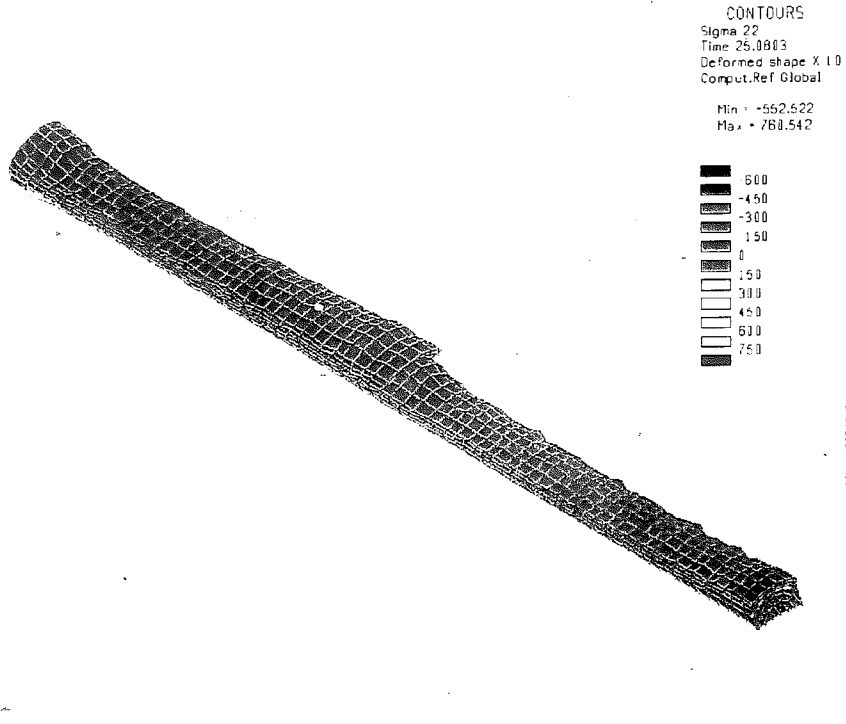


Figure 5.16 - S355J2G3 Simulation,  $t \sim 25.00$  s,  $\sigma_{yy}$  (MPa), bead only

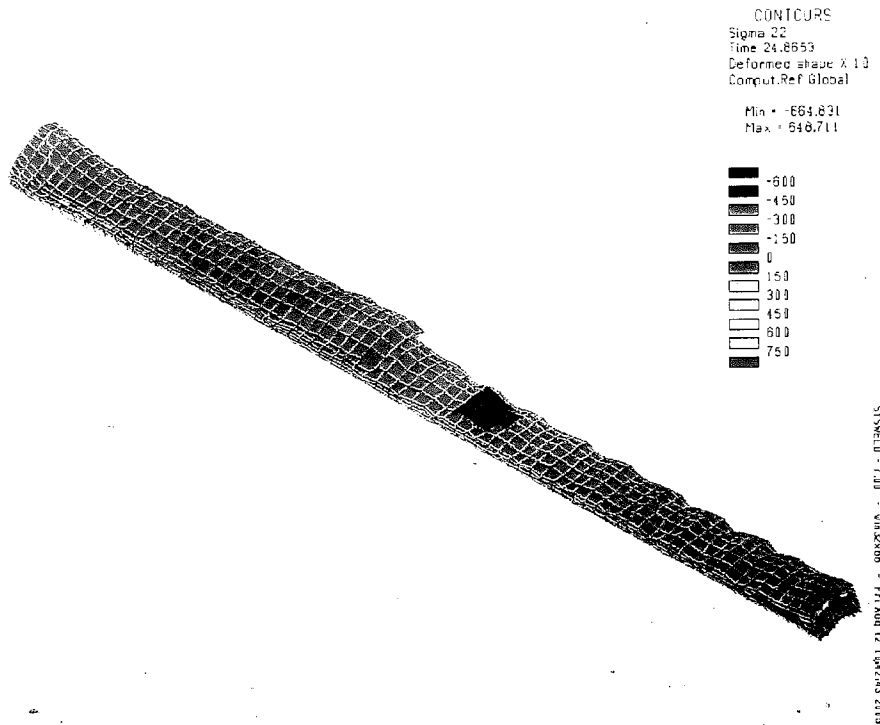


Figure 5.17 - DC04 Simulation,  $t \sim 25.00$  s,  $\sigma_{yy}$  (MPa), bead only

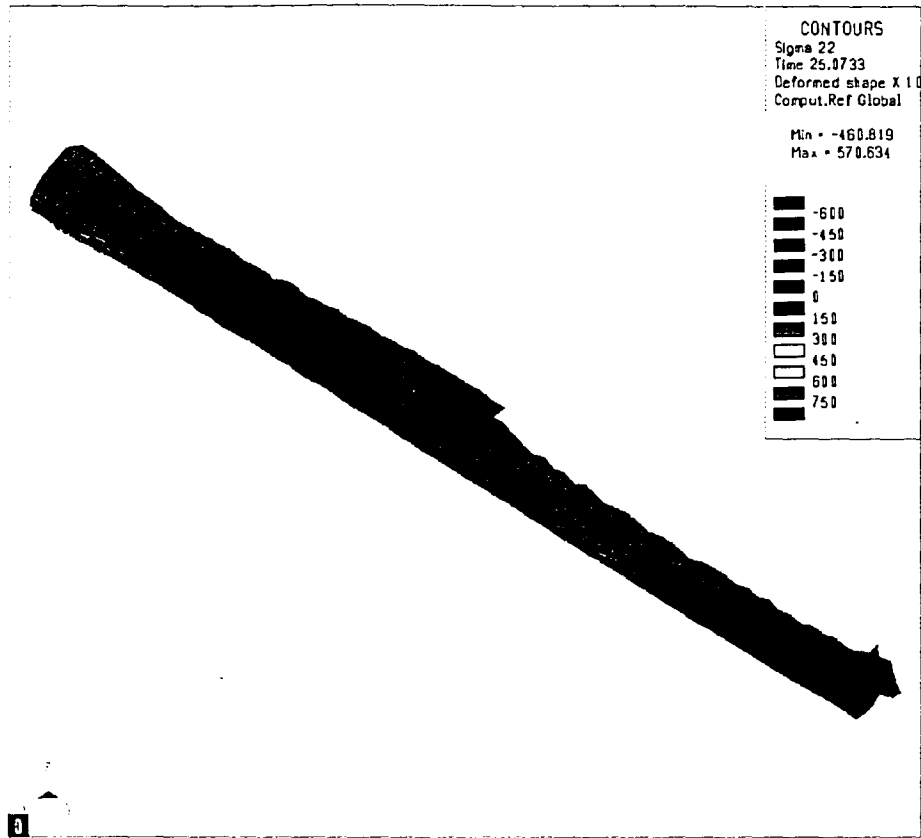


Figure 5.18 - S355J2G3 Simulation,  $t = 25.00$  s,  $\sigma_{yy}$  (MPa), bead only

Figure 5.19 – 5.27 show the results of mechanical simulation at 60.00 seconds. Again, data for  $\sigma_{xx}$ , and  $\sigma_{yy}$  is shown, with the  $\sigma_{yy}$  images distorted to show the displacement. The results for this time step follow a similar pattern to the results from the time steps near 25.00 seconds. The stresses in the x and y-directions, again, show very similar stress patterns and magnitudes for both the x and y-directions. The deposited layers still exhibit compressive stress after cooling. This is somewhat more pronounced in the results from 60.00 seconds than those from 25.00 seconds. The displacement trend seen in each of the materials is similar as well. The largest displacement occurs at the top left part of the last bead. The top right part of the last bead also shows some significant distortion. This trend is the same for all three material simulations.

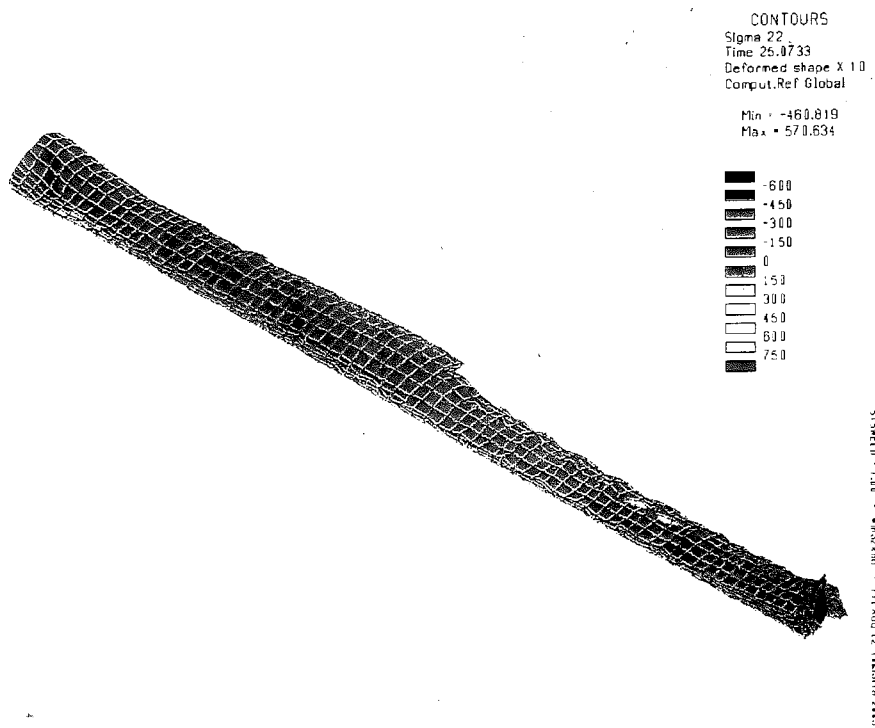


Figure 5.18 - S355J2G3 Simulation, t ~ 25.00 s,  $\sigma_{yy}$  (MPa), bead only

Figure 5.19 – 5.27 show the results of mechanical simulation at 60.00 seconds. Again, data for  $\sigma_{xx}$ , and  $\sigma_{yy}$  is shown, with the  $\sigma_{yy}$  images distorted to show the displacement. The results for this time step follow a similar pattern to the results from the time steps near 25.00 seconds. The stresses in the x and y-directions, again, show very similar stress patterns and magnitudes for both the x and y-directions. The deposited layers still exhibit compressive stress after cooling. This is somewhat more pronounced in the results from 60.00 seconds than those from 25.00 seconds. The displacement trend seen in each of the materials is similar as well. The largest displacement occurs at the top left part of the last bead. The top right part of the last bead also shows some significant distortion. This trend is the same for all three material simulations.



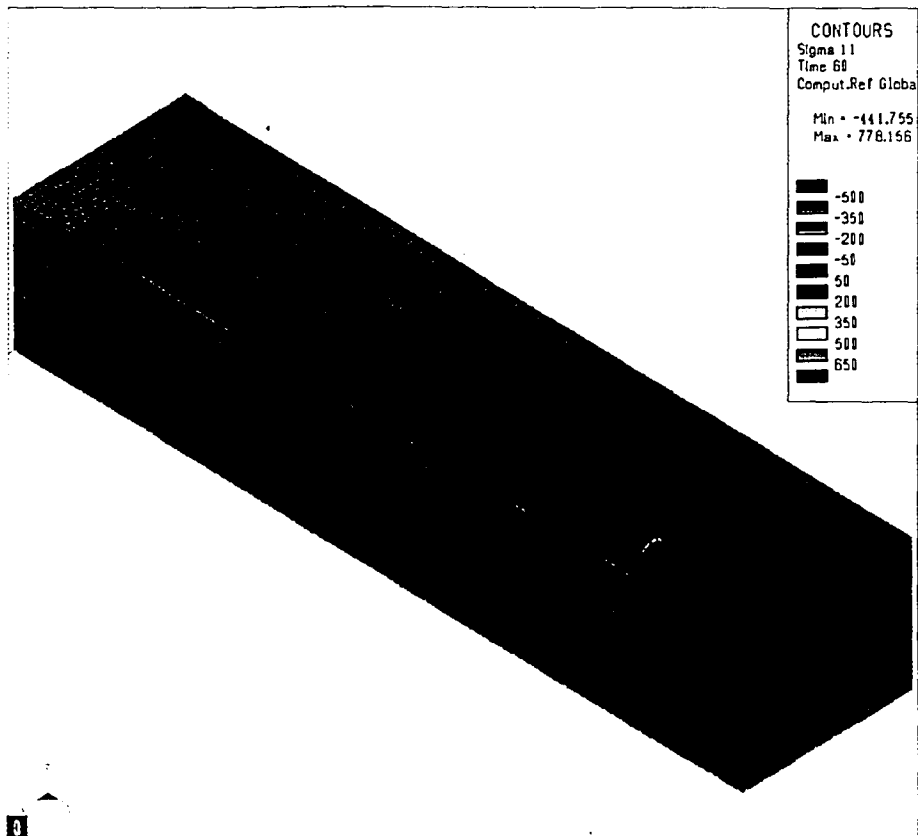


Figure 5.19 - S355J2G3 Simulation,  $t = 60.00$  s,  $\sigma_{xx}$  (MPa)

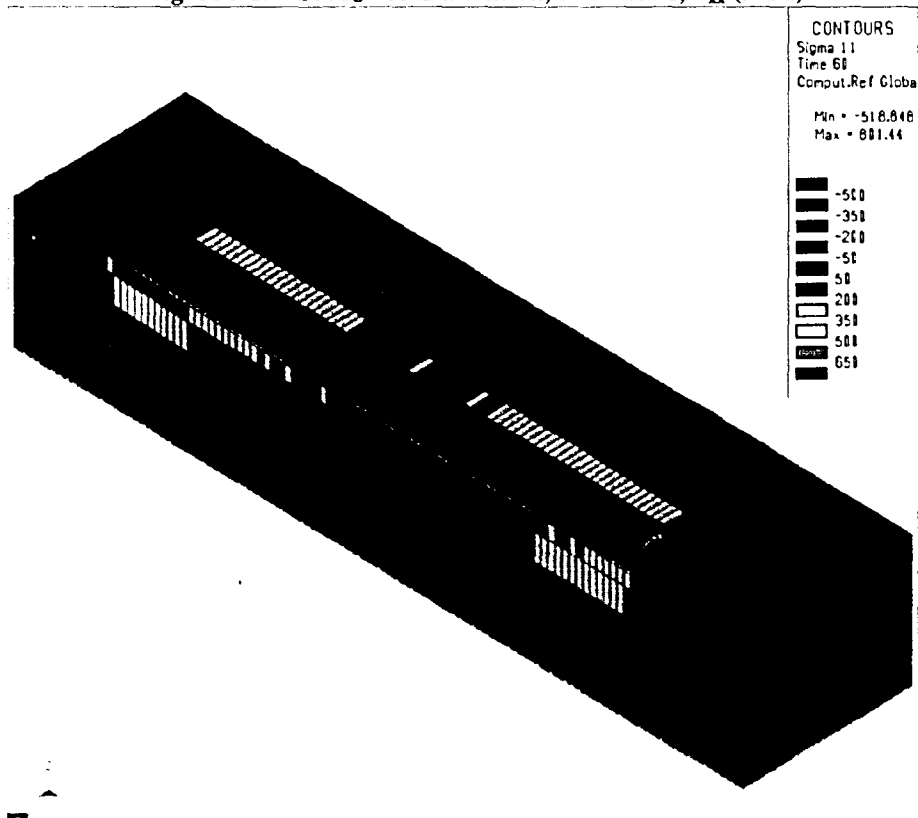


Figure 5.20 - DC04 Simulation,  $t = 60.00$  s,  $\sigma_{xx}$  (MPa)

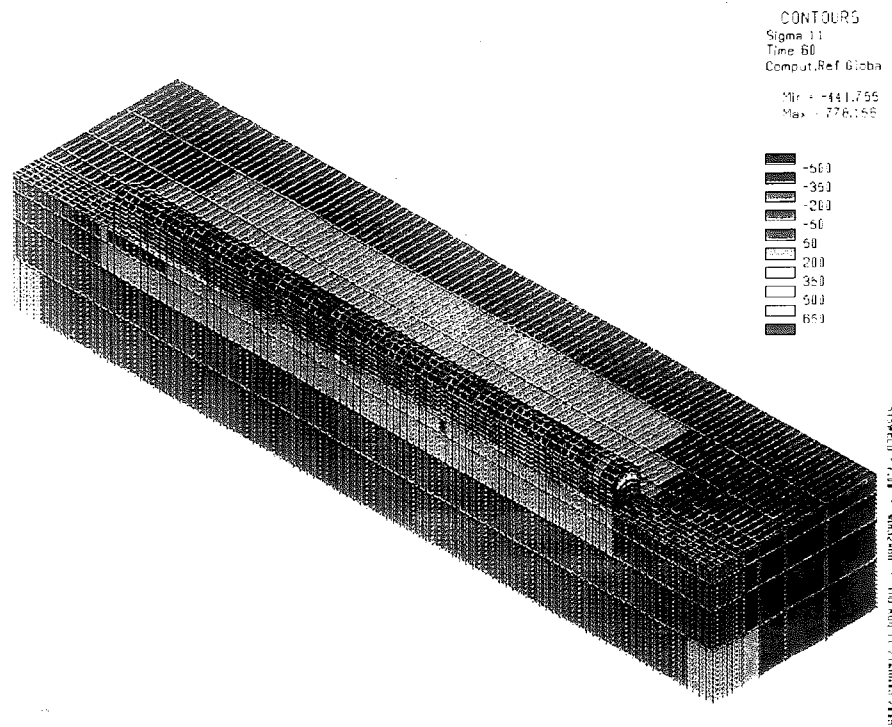


Figure 5.19 - S355J2G3 Simulation, t = 60.00 s,  $\sigma_{xx}$  (MPa)

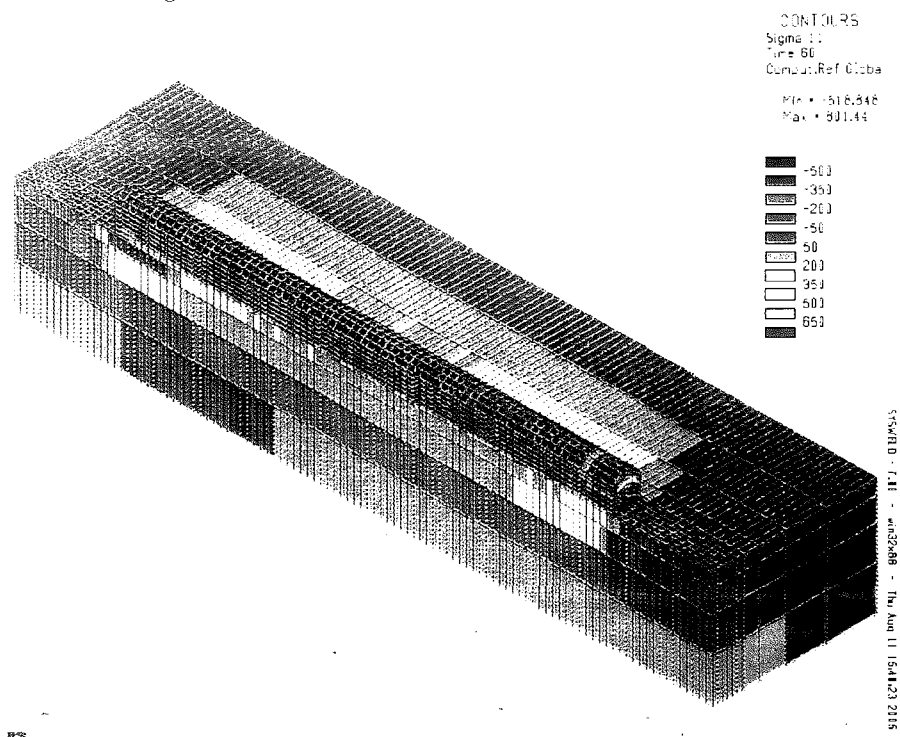


Figure 5.20 - DC04 Simulation, t = 60.00 s,  $\sigma_{xx}$  (MPa)

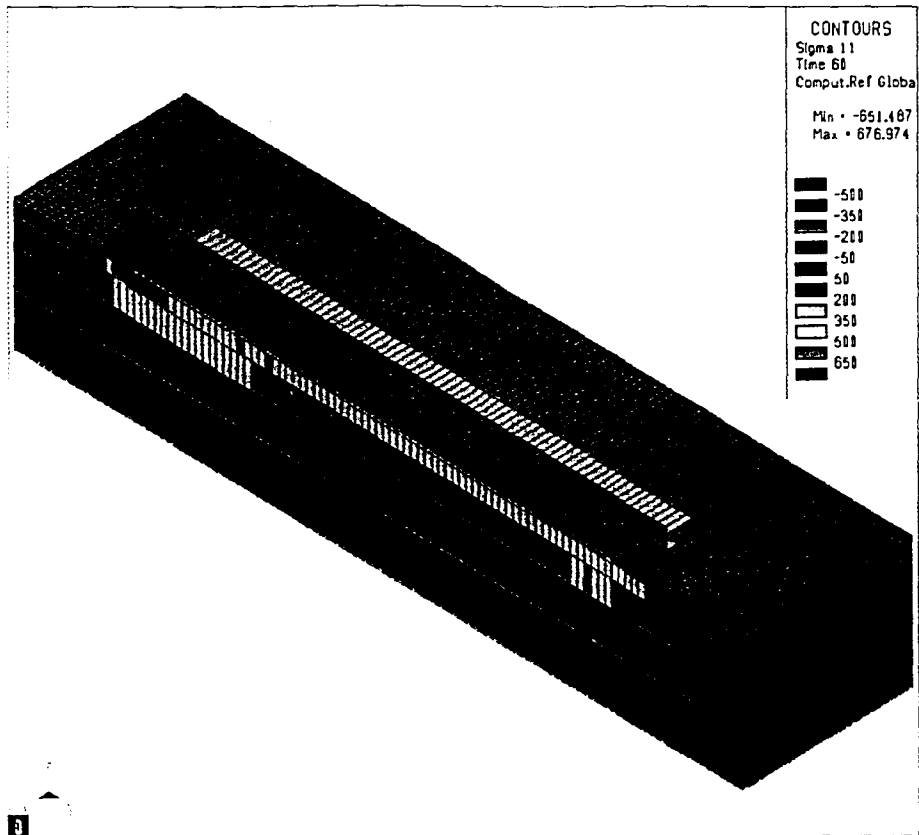


Figure 5.21 - X20Cr13 Simulation,  $t = 60.00$  s,  $\sigma_{xx}$  (MPa)

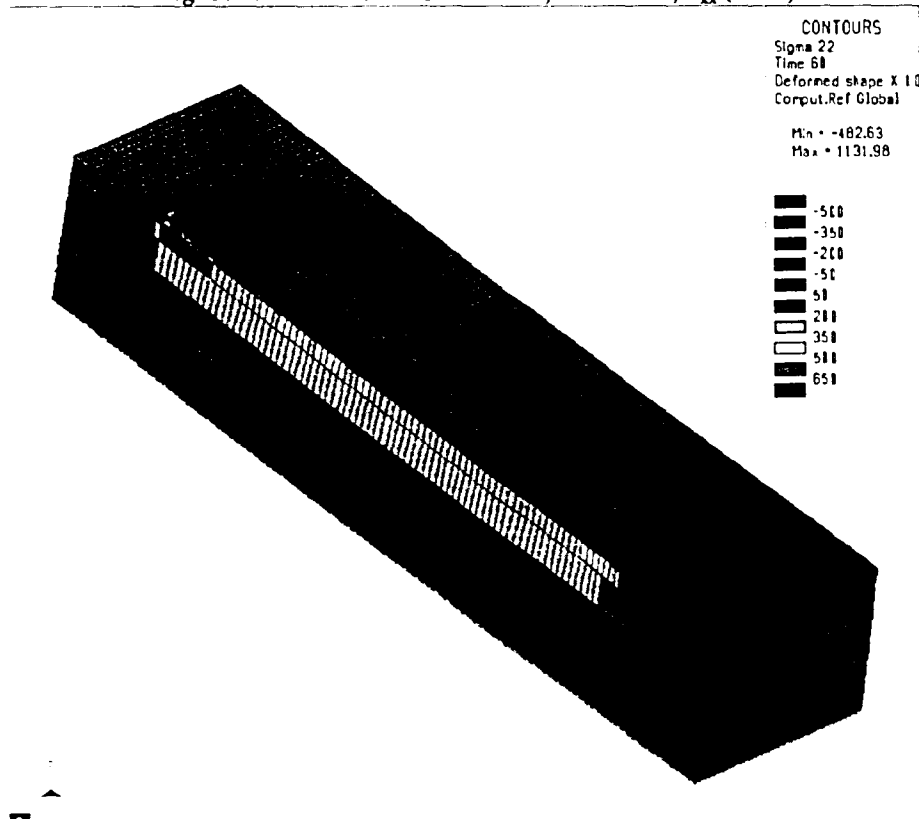


Figure 5.22 - S355J2G3 Simulation,  $t = 60.00$  s,  $\sigma_{yy}$  (MPa)

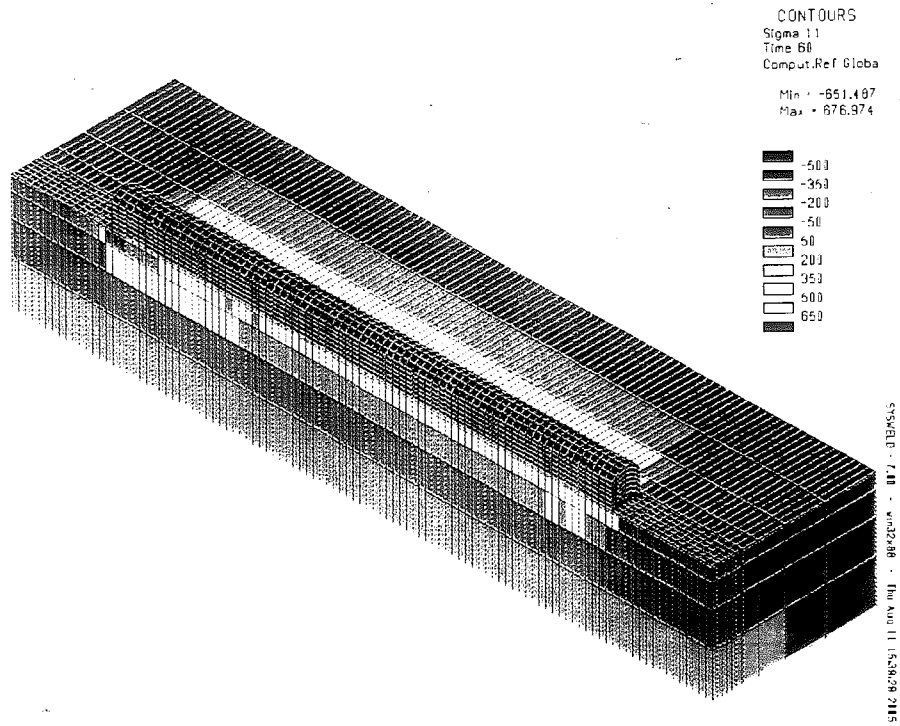


Figure 5.21 - X20Cr13 Simulation, t = 60.00 s,  $\sigma_{xx}$  (MPa)

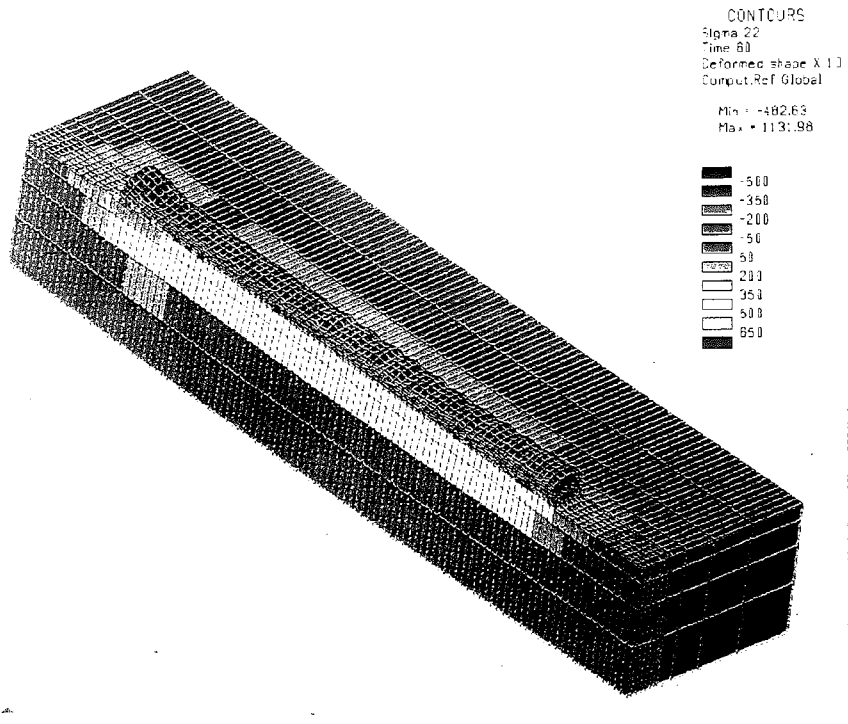


Figure 5.22 - S355J2G3 Simulation, t = 60.00 s,  $\sigma_{yy}$  (MPa)

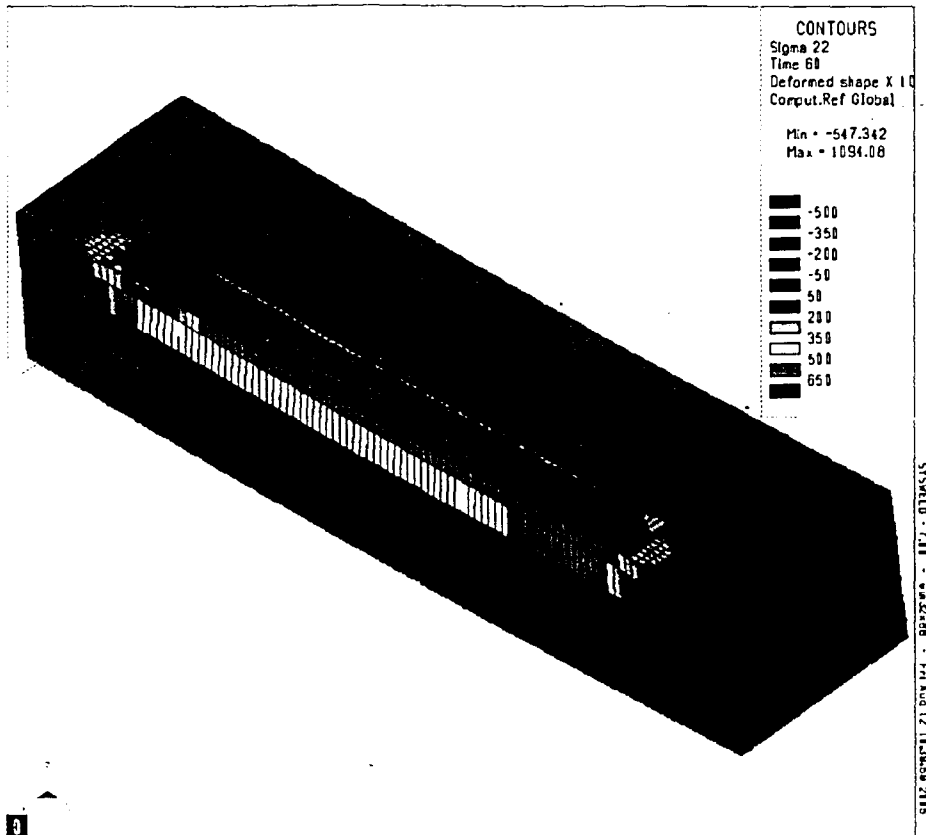


Figure 5.23 - DC04 Simulation,  $t = 60.00$  s,  $\sigma_{yy}$  (MPa)

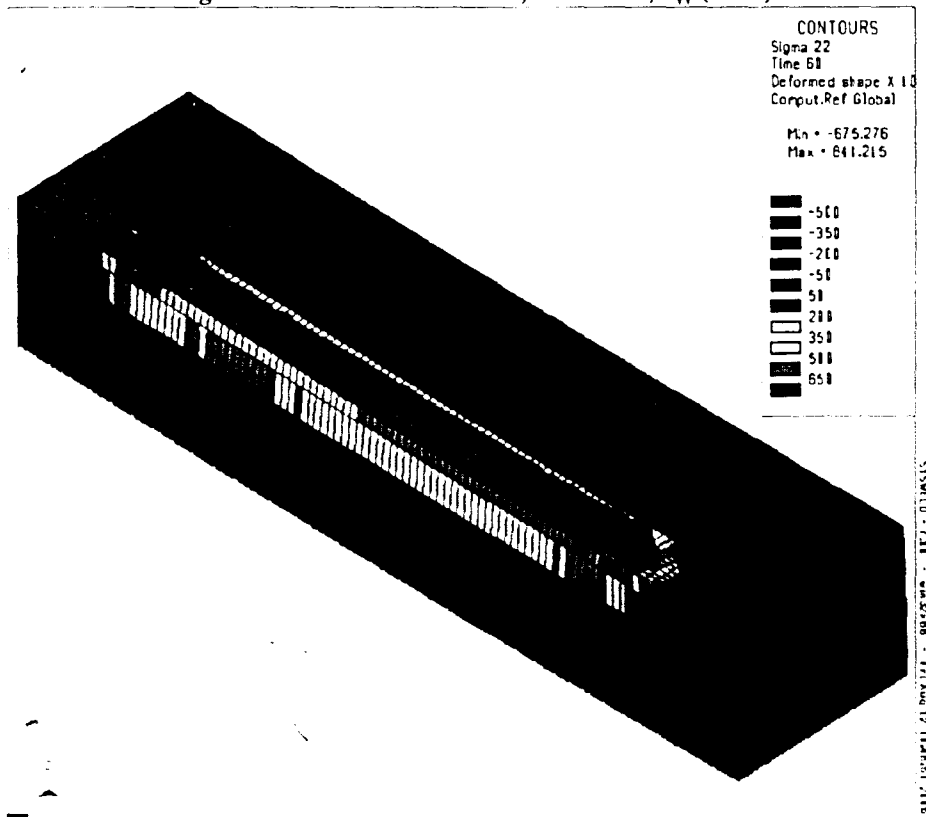


Figure 5.24 - X20Cr13 Simulation,  $t = 60.00$  s,  $\sigma_{yy}$  (MPa)

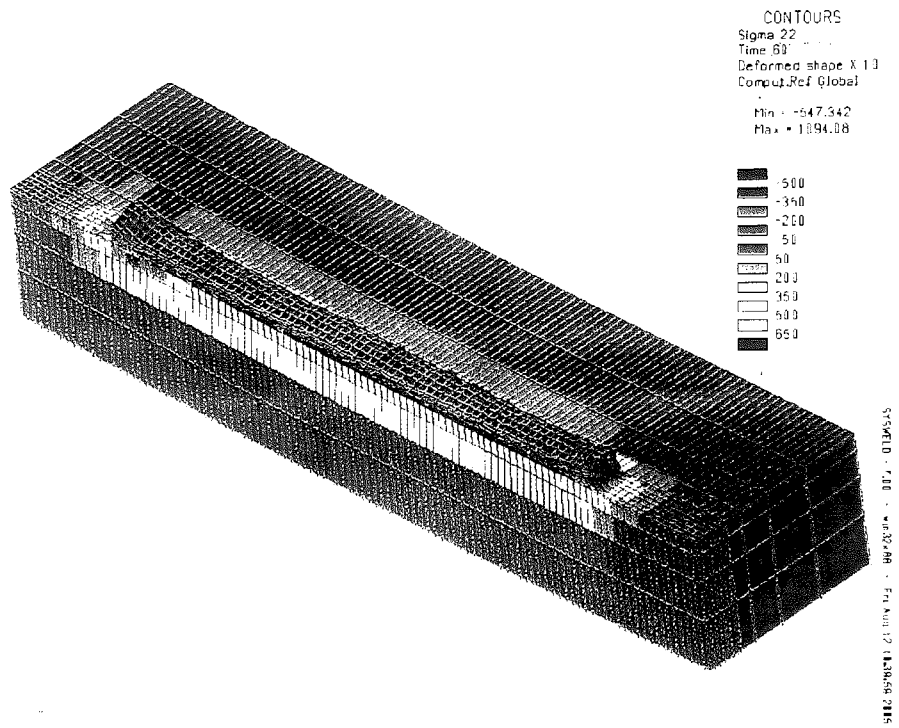


Figure 5.23 - DC04 Simulation, t = 60.00 s,  $\sigma_{yy}$  (MPa)

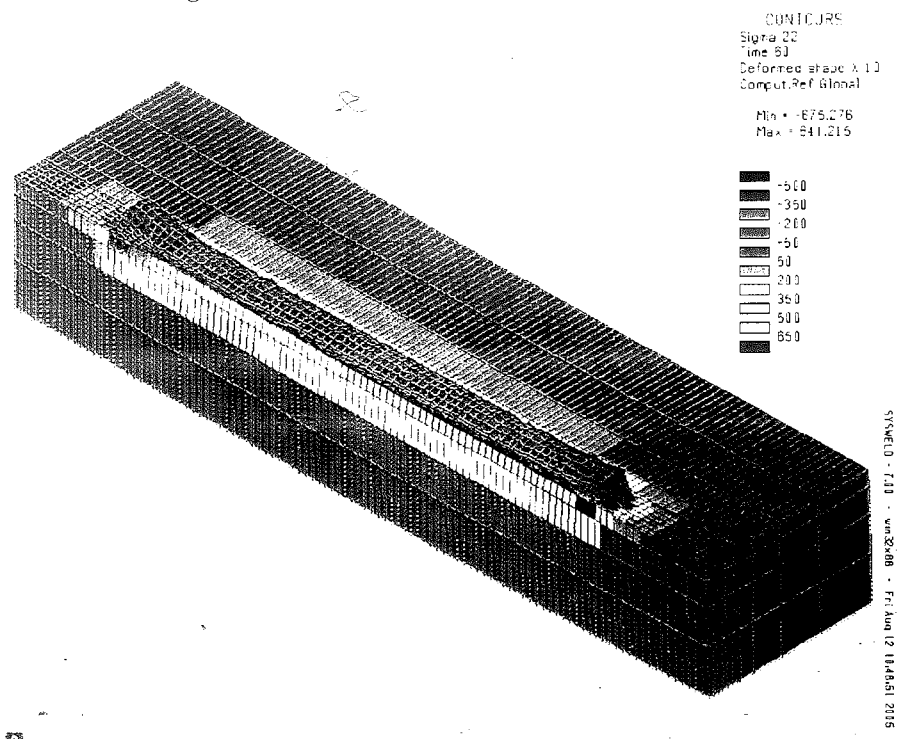


Figure 5.24 - X20Cr13 Simulation, t = 60.00 s,  $\sigma_{yy}$  (MPa)

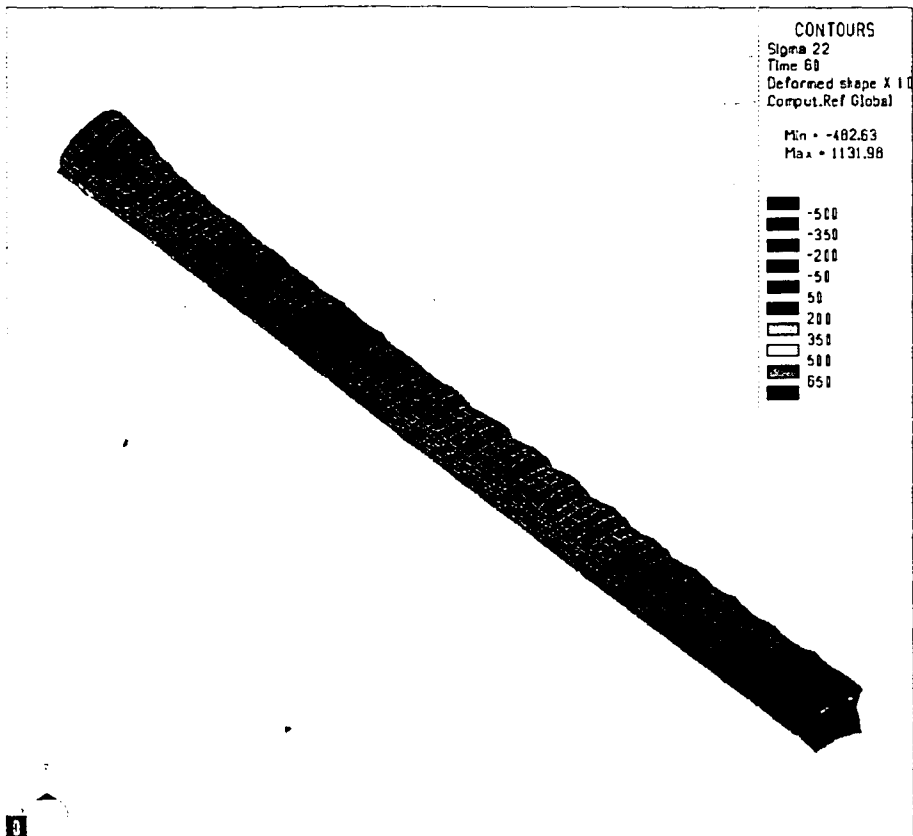


Figure 5.25 - S355J2G3 Simulation, Displacement in y direction (mm) (shifted scale)

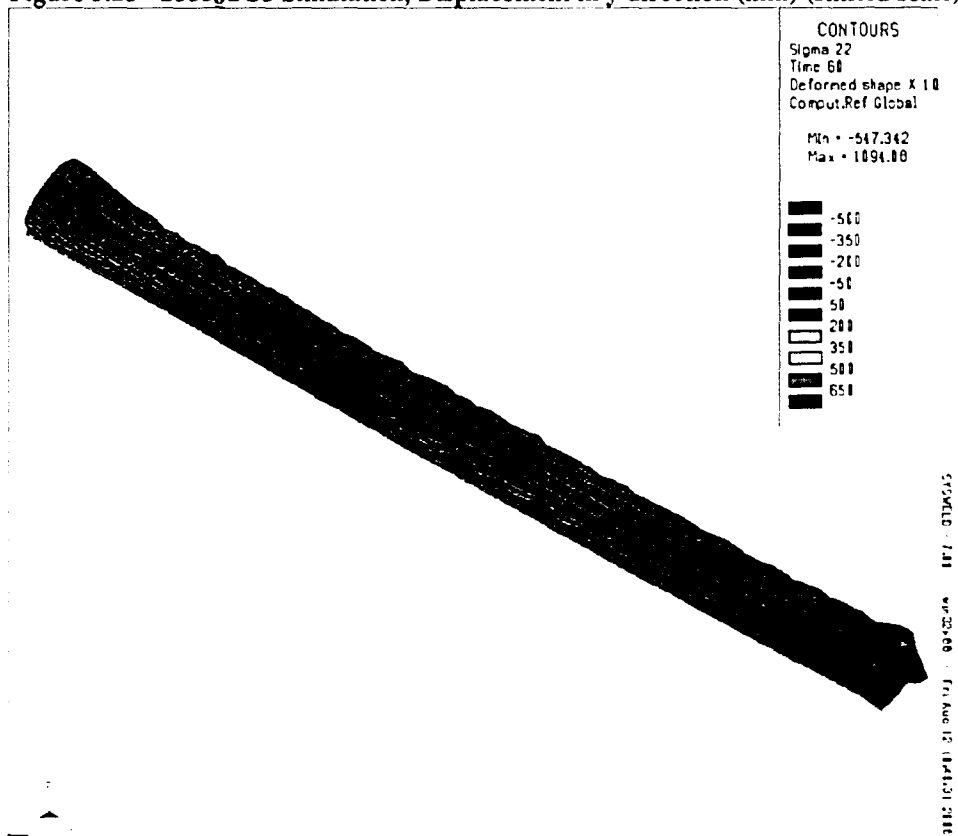


Figure 5.26 - DC04 Simulation, t = 60.00 s, Displacement in y direction (mm)

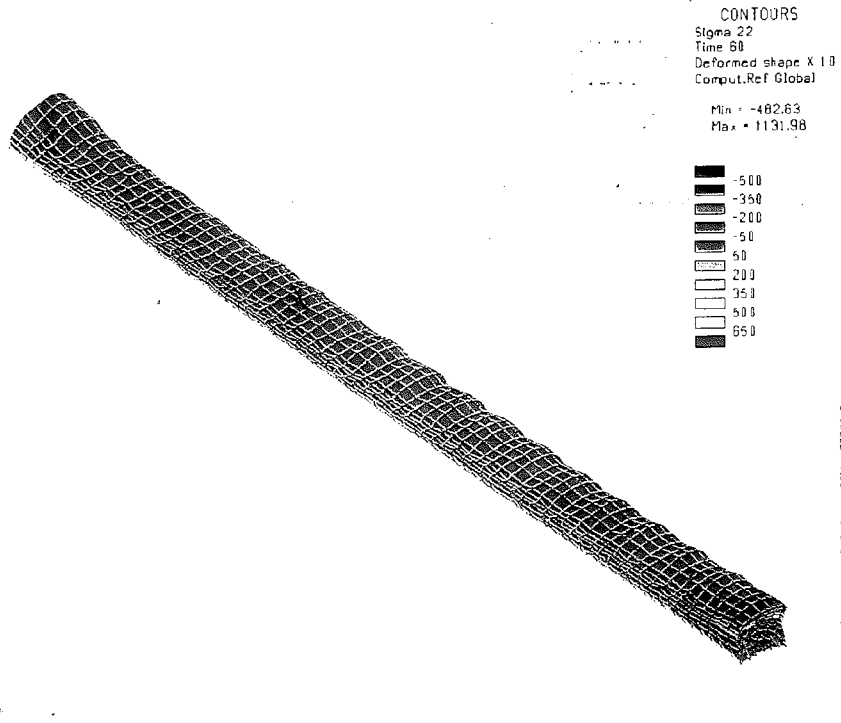


Figure 5.25 - S355J2G3 Simulation, Displacement in y direction (mm) (shifted scale)

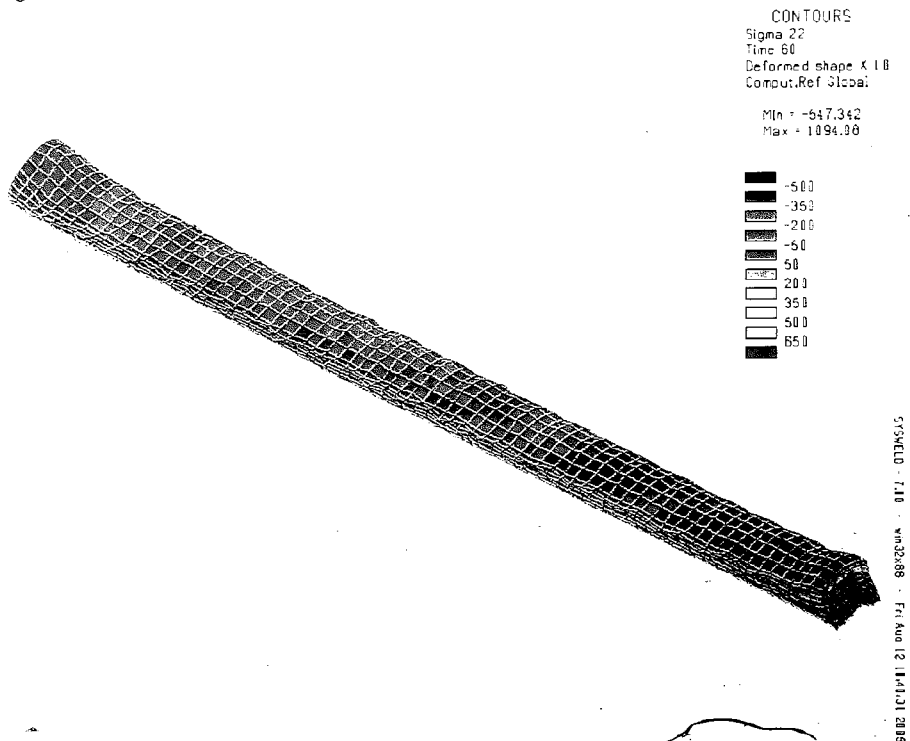


Figure 5.26 - DC04 Simulation, t = 60.00 s, Displacement in y direction (mm)



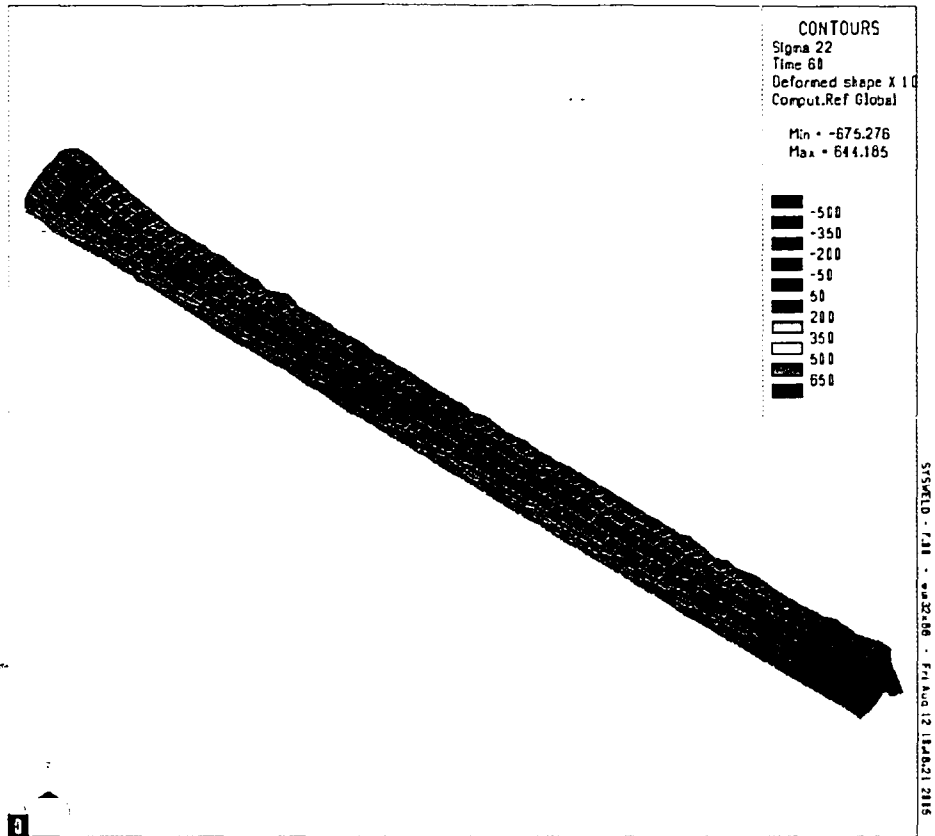


Figure 5.27 – X20Cr13 Simulation, t = 60.00 s, Displacement in y direction (mm)

## Chapter 6 - Conclusions and Recommendations

### 6.1 Conclusions

The thermal results show a very good correlation between all three material simulations. Although small differences do exist, the thermal histories are very similar in most aspects. At each of the time steps, the weld pool size and shape and the maximum temperature data for each of the three simulations match up very well. Overall, the thermal simulation provides a very good base to compare different mechanical simulations.

The results of the mechanical simulation, like the thermal results, are very consistent. The residual stresses and the stresses seen during deposition are all similar

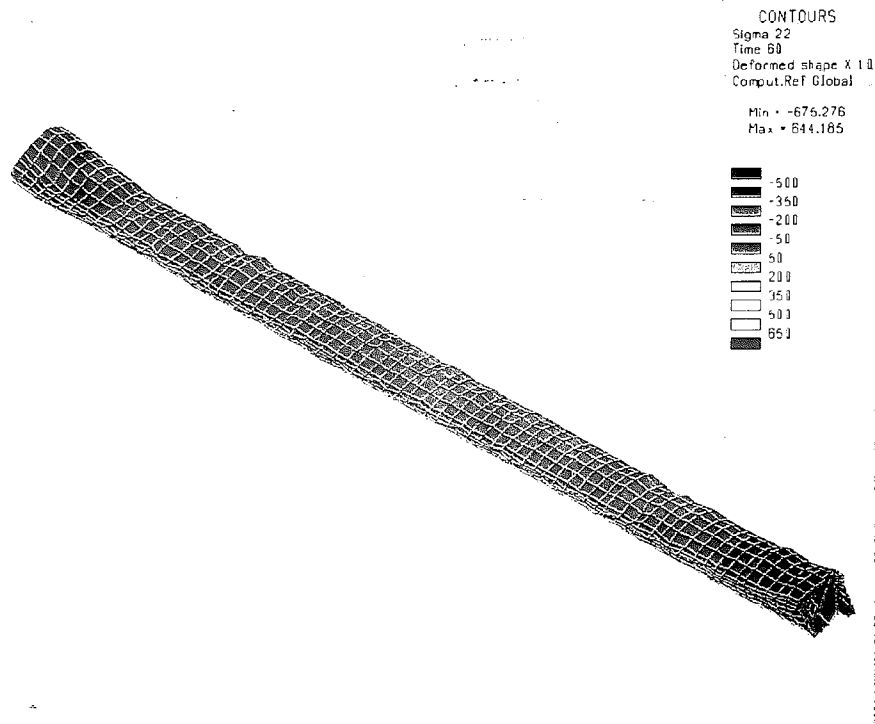


Figure 5.27 – X20Cr13 Simulation, t = 60.00 s, Displacement in y direction (mm)

## Chapter 6 - Conclusions and Recommendations

### 6.1 Conclusions

The thermal results show a very good correlation between all three material simulations. Although small differences do exist, the thermal histories are very similar in most aspects. At each of the time steps, the weld pool size and shape and the maximum temperature data for each of the three simulations match up very well. Overall, the thermal simulation provides a very good base to compare different mechanical simulations.

The results of the mechanical simulation, like the thermal results, are very consistent. The residual stresses and the stresses seen during deposition are all similar

from one material to the next. Also, the displacements show no large differing points between the materials. These results are somewhat unexpected because of the differences in the material models. Some of the major differences being the range of melting temperatures (1444°C to 1505°) and the range of the number of phases (2 to 6).

There are several possible explanations for the similar results from these three simulations. One possible explanation is the magnitude of the stress and displacement seen in this particular build was not sufficient to show the effect of solid phase transformations. Another possible explanation is the material properties for S355J2G3, DC04, and X20Cr13 are not detailed or accurate enough to demonstrate significant difference between the two. Lastly, it is possible that the effects of solid phase transformations simply do not have a large impact on residual stress and distortion when modeling LENS. In order to determine the specific effect of phase transformations, each of these possibilities needs to be examined.

One definitive conclusion can be made from this study however. When simulating LENS line builds using SYSWELD material models, phase transformations do not significantly affect the residual stress or distortion for these specific material models.

## ***6.2 Recommendations***

In order to improve future finite element models, several issues should be considered. As most parts made using LENS require more than four layers, it is evident that an increase in the number of simulated deposit layers is necessary for more accurate modeling. However, increasing the number of layers in the simulation causes problems

with lengthy computation times and inadequate storage space. One solution of this problem is setting up a computer cluster to run the simulations. This would allow multiple computers to process the same simulation, reducing computation time. Another possible solution is implementing a mesh refining technique in the simulations. This would change the mesh as the simulation progressed, using a fine mesh only in regions with high thermal gradients. This would reduce the number of elements and nodes in the simulation, which are the main cause of long computation times.

In addition to increasing the simulated depositing layers, it is necessary for future research to more accurately compare the simulations to experimental builds. Measuring the temperature during the experimental build is vital to an accurately simulated LENS build. Furthermore, the residual stress of the experimental builds should be measured and compared with the results of the simulations. Lastly, in an ideal situation, the material used in the experimental builds would be the same as the material used in the simulation.

Finally, different geometries need to be investigated. While a line build is a good starting point, most parts made with LENS will be significantly more complicated. A solid cube or tube shape would be most likely produce very different results than those seen with a line build. In order to fully understand the LENS process, these different geometries need to be studied.

## References

- [1] J. J. Beaman, J. W. Barlow, D. L. Bourell, R. H. Crawford, H. L. Marcus, and K. P. McAlea, *Solid Freeform Fabrication: A New Direction in Manufacturing*. Norwell: Kluwer Academic Publishers, 1997.
- [2] K. G. Cooper, *Rapid Prototyping Technology*. New York: Marcel Dekker, 2001.
- [3] A. Mengel, "Finite Element Modeling of LENS Deposition Using SYSWELD," in *Mechanical Engineering and Mechanics*. Bethlehem: Lehigh University, 2002.
- [4] "Optomec - Additive Manufacturing," 2005. Optomec Inc. May 15, 2005 [www.optomec.com](http://www.optomec.com)
- [5] T. Swain, "Optomec LENS Presentation," 2000.
- [6] D. Rosenthal, "The Theory of Moving Sources of Heat and Its Application to Metal Treatments," *Transactions of ASME*, pp. 849-866, 1946.
- [7] K. Masubuchi, *Analysis of welded structures: residual stresses, distortion, and their consequences*, 1st ed. New York: Pergamon Press, 1980.
- [8] P. S. Myers, O. A. Uyehara, and G. L. Borman, "Fundamentals of Heat Flow in Welding," *Welding Research Council Bulletin*, vol. 123, 1967.
- [9] V. Pavelic, R. Tanbakuchi, O. A. Uyehara, and P. S. Myers, "Experimental and Computed Temperature Histories in Gas Tungsten-Arc Welding of Thin Plates," *Welding Journal*, vol. 48, pp. 295s-305s, 1969.
- [10] G. R. Stoeckinger, R. A. Calabrese, and R. F. Menaul, "Computerized Prediction of Heat Distribution in Welding Tooling," *Welding Journal*, vol. 49, pp. 14s-26s, 1970.
- [11] Z. Paley and P. D. Hibbert, "Computation of Temperatures in Actual Weld Designs," *Welding Journal*, vol. 54, pp. 385s-392s, 1975.
- [12] J. Goldak, A. Chakravarti, and M. Bibby, "A New Finite Element Model for Welding Heat Sources," *Metallurgical Transactions B*, vol. 15B, pp. 299-305, 1984.
- [13] E. Software, "SYSWELD Reference Manual", 2004, E. Group.
- [14] E. Friedman, "Thermomechanical Analysis of the Welding Process Using the Finite Element Method," *Journal of Pressure Vessel Technology*, vol. 97, pp. 206-213, 1975.
- [15] G. W. Krutz and L. J. Segerlind, "Finite Element Analysis of Welded Structures," *Welding Journal*, vol. 48, pp. 295s-305s, 1978.
- [16] E. Software, "SYSWELD Help Manual", 2004, E. Group.
- [17] A. F. A. Hoadley and M. Rappaz, "A Thermal Model of Laser Cladding by Powder Injection," *Metallurgical Transactions B*, vol. 23B, pp. 631-641, 1992.
- [18] A. Kar and J. Mazumder, "One-dimensional diffusion model for extended solid solution in laser cladding," *Journal of Applied Physics*, vol. 61, pp. 2645-2655, 1987.

- [19] A. Nickel, D. Barnett, G. Link, and F. Prinz, "Residual Stress in Layered Manufacturing," presented at Solid Freeform Fabrication Symposium, Austin, Texas, 1999.
- [20] M. L. Griffith, M. E. Schlienger, L. D. Harwell, M. S. Oliver, M. D. Baldwin, M. T. Ensz, M. Essien, J. Brooks, C. V. Robino, J. E. Smugeresky, W. H. Hofmeister, M. J. Wert, and D. V. Nelson, "Understanding thermal behavior in the LENS process," *Materials and Design*, vol. 20, pp. 107-113, 1999.
- [21] W. Hofmeister, M. Wert, J. Smugeresky, J. A. Philliber, M. Griffith, and M. Ensz, "Investigating Solidification with the Laser-Engineered Net Shaping (LENS) Process," *Journal of Materials*, vol. 51, 1999.
- [22] A. Vasinonta, J. Beuth, and M. Griffith, "Process Maps for Laser Deposition of Thin-Walled Structures," presented at Solid Freeform Fabrication Symposium, Austin, Texas, 1999.
- [23] C. A. Brice, K. I. Schwendner, D. W. Mahaffey, E. H. Moore, and H. L. Fraser, "Process Variable Effects on Laser Deposited Ti-6Al-4V," presented at Solid Freeform Fabrication Symposium, Austin, Texas, 1999.
- [24] C. L. Chan, J. Mazumder, and M. M. Chen, "Effect of Surface Tension Gradient Driven Convection in a Laser Melt Pool: Three-dimension Perturbation Model," *Journal of Applied Physics*, vol. 64, pp. 6166-6174, 1988.
- [25] V. Babu, S. A. Korpela, and N. Ramanan, "Flow and Temperature Fields in a Weld Pool Formed by a Movign Laser," *Journal of Applied Physics*, vol. 67, pp. 3990-3998, 1990.
- [26] S. Murugan, P. V. Kumar, T. P. S. Gill, B. Raj, and M. S. C. Bose, "Numerical Modelling and Experimental Determination of Temperature Distribution During Manual Metal Arc Welding," *Science and Technology of Welding and Joining*, vol. 4, pp. 357-364, 1999.
- [27] C. K. Leung, R. J. Pick, and D. H. B. Mok, "Finite Element Modeling of a Single Pass Weld," *Welding Research Council Bulletin*, vol. 356, pp. 1-10, 1990.
- [28] E. Software, "SYSWELD Analysis Reference Manul", 2004, E. Group.
- [29] A. Mengel, M. Tomik, Ed., 2004, pp. (Personal E-mail).
- [30] C. Semetay and D. Truxell, "LENS Operating Manual." (Unpublished): Lehigh University.
- [31] "MEsteel," 2005. August 3, 2005 <http://www.mesteel.com/>
- [32] R. Beardmore, "RoyMech," 2005. August 03, 2005 <http://www.roymech.co.uk/>
- [33] "POCSO Steel-N.com," 2005. August 03, 2005 <http://www.steel-n.com/>

## Appendix

Included in this appendix are the data files used to run the three SYSWELD simulations. The group.dat and medium.dat files, used to name specific volumes, elements and nodes needed in the simulation, are left out of this appendix because they are rather long. The a#.dat files are for the thermal simulation and the m#.dat files are for the mechanical simulation. The first files to run are ap.dat and mp.dat, which are the preheat passes. They are followed by a1, a2 and so on. Only the run files for the first material will be included in the appendix. The entire thermal simulation is conducted before the mechanical simulation is started. The MAT#\_metallurgy.dat file contains the thermal information for each material. The metallurgy.dat files are directly from SYSWELD and the only change made was the thermal conductivity above the melting temperature. Files in this appendix: ap.dat, a1.dat, mat1\_metallurgy.dat and mp.dat.

## Material 1 – ap.dat

### DEFINITION

m1

OPTION THERMAL METALLURGY SPATIAL  
RESTART GEOMETRY

### MATERIAL PROPERTIES

ELEMENTS GROUPS \$PART\$ / MATE 1 TRAJ 1

ELEMENTS GROUPS \$BEAD1\$ / MATE 1

ELEMENTS GROUPS \$BEAD2\$ / MATE 1

ELEMENTS GROUPS \$BEAD3\$ / MATE 1

ELEMENTS GROUPS \$BEAD4\$ / MATE 1

ELEMENTS GROUPS \$BEAD5\$ / MATE 1

ELEMENTS GROUPS \$BEAD6\$ / MATE 1

ELEMENTS GROUPS \$BEAD7\$ / MATE 1

; The metallurgy option is necessary in order to use materials with phase  
; transformations. MATE 1 indicates that the properties of the material will be  
; obtained from the metallurgy.dat file.  
; It should be noted that Part refers to the weld base, Bead1 refers to the first deposit  
; layer and so on.

### MEDIUM

WELDLINE / GROUPS \$TRAJP\$ ELEMENTS \$fep\$ START \$fnp\$ ARRIVAL  
\$lnp\$ VELOCITY 6.000000 TINF 0.000000 MODEL 1

### CONSTRAINTS

ELEMENTS GROUPS \$SKINPART\$ / KT 1 VARIABLE 1

### LOAD

1

ELEMENTS GROUPS \$SKINPART\$ / TT 20.000

ELEMENTS GROUPS \$part\$ / QR 1 VARIABLE -10000 TRAJECTORY 1

; when using a trajectory, the weldline info must be done as shown above. the line  
; number (trajp), first element (fep), first node (fnp) and last node (lnp) are required  
; inputs. The VARIABLE 1 after ELEMENTS GROUPS \$SKINPART\$ indicates that  
; the data for that particular constraint will be found in Table 1/ below. This will be  
; used in the future for activating and deactivating elements.

### TABLE

1 / FORTRAN

function f(t)

c

c radiative losses :  $f = \text{sig} * e * (t + t_0)(t^{**2} + t_0^{**2})$



```

c
e = 1.0
sig = 5.67*-8
to = 20.
to = 20. + 273.15
t1 = t + 273.15
a = t1 * t1
b = to * to
c = a + b
d = t1 + to
d = d * c
d = d * e
d = d * sig

c
c convective losses = 25 W/m2
f = d + 25.
c change to W/mm2
d = 1*-6
f = f * d

c
return
END

```

2 / FORTRAN  
function f(t)

```

c
c heat flux bc  $h=k*(t-t_0)/L$ 
c

```

```

t0 = 20. + 273.15
t1 = t + 273.15
a = t1 - t0

```

```

c change to W/mm2
d = 1*-6
f = a * d

```

```

c
return
END

```

4 / FORTRAN  
FUNCTION F(X)  
DIMENSION X(5)  
xa = X(1)

```

ya = X(2)
za = X(3)
time = X(4)
C
f = -1

return
end
5 / FORTRAN
FUNCTION F(X)
DIMENSION X(5)
xa = X(1)
ya = X(2)
za = X(3)
time = X(4)
C
f = 1

return
end
3 / FORTRAN
FUNCTION F(X)
DIMENSION X(5)
xa = X(1)
ya = X(2)
za = X(3)
time = X(4)
C
f = 0
ro = 1.5
zlimit = 0.00
zllimit = -0.41
xx = xa * xa
yy = ya * ya

c
rr = xx + yy
rr = sqrt(rr)
c
if (rr. le. ro) f = 1
if (za. gt. zlimit) f = 0
if (za. lt. zllimit) f = 0

return
end

```

; this function, although not used here, activated beads as they become close to the heat  
; source.

```
10000 / FORTRAN  
FUNCTION F(X)
```

```
C  
C F = Q0 * exp( - R^2 / R0^2 ) with  
C R^2 = ( XX-X0 )^2 + ( YY-Y0-VY*T )^2  
C R0 = RE - ( RE-RI )*( ZE-ZZ+Z0 )/( ZE-ZI )  
C IF R0 < RI , R0 = 0. and return  
C IF R0 > RE , R0 = 0. and return
```

```
C  
C DIMENSION X(4)
```

```
C  
C Input
```

```
C  
C XX = X(1) ; X Coordinate  
C YY = X(2) ; Y Coordinate  
C ZZ = X(3) ; Z Coordinate  
C TT = X(4) ; Time
```

```
C  
C Variables
```

```
C  
C Q0 = 850 ; Maximal source intensity  
C RE = 0.70 ; Gaussian parameter  
C RI = 0.55 ; Gaussian parameter  
C ZE = -0.4 ; Upper plan  
C ZI = -0.8 ; Lower plan  
C M1 = -1
```

; Above is the heat source definition. The inputs follow those described in chapter 4.

```
C  
C R^2 computation
```

```
C  
C DE = ZZ - ZE  
C DI = ZZ - ZI  
C A1 = XX * XX  
C A2 = YY * YY  
C R2 = A1 + A2  
C A3 = DI * DI  
C IF( ZZ .LT. ZI ) R2 = R2 + A3
```

```
C  
C R0^2 computation
```

```
C
```

```
A1 = RE - RI
A2 = ZE - ZI
A3 = ZE - ZZ
R0 = A3 / A2
R0 = R0 * A1
R0 = RE - R0
IF( ZZ .LT. ZI ) R0 = RI
R02 = R0 * R0
```

C

C F computation

C

```
IF( R2 .GT. R02 ) RETURN
```

```
A1 = R2 / R02
```

```
A2 = M1 * A1
```

```
A2 = EXP( A2 )
```

```
F = Q0 * A2
```

C

```
RETURN
```

```
END
```

```
RETURN
```

```
SAVE DATA 1043
```

```
MEDIUM
```

```
EXTRACT MEDIUM
```

```
;
```

```
; Welding Wizard - Thermal Analysis
```

```
;
```

```
;
```

```
; Trajectory Medium - Heat Source
```

```
;
```

```
;
```

```
; Time Step 1
```

```
;
```

```
TRANSIENT NON-LINEAR
```

```
BEHAVIOUR METALLURGY 4 FILE MAT1_METALLURGY.DAT
```

```
ALGORITHM BFGS IMPLICIT 1 ITERATION 20
```

```
PRECISION ABSOLUTE FORCE 0.01 DISPLACEMENT 0.1 ENERGY 10*-20
```

```
METHOD SYMMETRICAL TEST 0 ITERATIVE PRECISION ABSOLUTE 1*-4
```

```
INITIAL CONDITIONS
```

```
NODES / TT 20.00
```

```
;
```

ELEMENTS GROUPS \$PART\$ / P 1. 0. 0. 0. 0. 0.  
ELEMENTS GROUPS \$BEAD1\$ / P 1. 0. 0. 0. 0. 0. is -1  
ELEMENTS GROUPS \$BEAD2\$ / P 1. 0. 0. 0. 0. 0. is -1  
ELEMENTS GROUPS \$BEAD3\$ / P 1. 0. 0. 0. 0. 0. is -1  
ELEMENTS GROUPS \$BEAD4\$ / P 1. 0. 0. 0. 0. 0. is -1  
ELEMENTS GROUPS \$BEAD5\$ / P 1. 0. 0. 0. 0. 0. is -1  
ELEMENTS GROUPS \$BEAD6\$ / P 1. 0. 0. 0. 0. 0. is -1  
ELEMENTS GROUPS \$BEAD7\$ / P 1. 0. 0. 0. 0. 0. is -1

; The number after "BEHAVIOUR METALLURGY" must be equivalent to the total  
; number of phases described in the metallurgy.dat file being used.  
; The P 1. 0. 0. 0. 0. 0. command is required to make all the elements in the simulation  
; begin in phase 1.

TIME INITIAL 0.  
0.01000 / STORE 1  
RETURN

SAVE DATA TRAN 1043

ASSIGN 19 TRAN1043.TIT

;  
TRANSIENT NON-LINEAR  
BEHAVIOUR METALLURGY 4 FILE MAT1\_METALLURGY.DAT  
ALGORITHM BFGS IMPLICIT 1 ITERATION 20  
PRECISION ABSOLUTE FORCE 0.01 DISPLACEMENT 0.1 ENERGY 10\*-20  
METHOD SYMMETRICAL TEST 0 ITERATIVE PRECISION ABSOLUTE 1\*-4  
STEP DTMINI 0.001 DTMAXI 0.500000 EPSF 10\*+20 EPSD 50. FACC 0.5 FACP  
1.2 FORCE  
INITIAL CONDITIONS RESTART CARD LAST  
TIME INITIAL RESTART  
4.2000000 STEP 0.02 / STORE 4  
RETURN

; Details on the different solver types and when they should be used are available in the  
; SYSWELD manual. DTMINI sets the minimum time step and DTMAXI sets the  
; maximum timestep.

## Material 1 – a1.dat

DEFINITION

m1

OPTION THERMAL METALLURGY SPATIAL

RESTART GEOMETRY

MATERIAL PROPERTIES

ELEMENTS GROUPS \$PART\$ / MATE 1

ELEMENTS GROUPS \$BEAD1\$ / MATE 1 status -3 TRAJ 1

ELEMENTS GROUPS \$BEAD2\$ / MATE 1

ELEMENTS GROUPS \$BEAD3\$ / MATE 1

ELEMENTS GROUPS \$BEAD4\$ / MATE 1

ELEMENTS GROUPS \$BEAD5\$ / MATE 1

ELEMENTS GROUPS \$BEAD6\$ / MATE 1

ELEMENTS GROUPS \$BEAD7\$ / MATE 1

; The status is set to -3 because it is the bead that is being build. Once the bead has  
; built, it's status is changed to -5, keeping it activated.

MEDIUM

WELDLINE / GROUPS \$TRAJ1\$ ELEMENTS \$fe1\$ START \$fn1\$ ARRIVAL  
\$ln1\$ VELOCITY 6.000000 TINF 4.2000000 MODEL 1

CONSTRAINTS

ELEMENTS GROUPS \$\$SKINPART\$ / KT 1 VARIABLE 1

LOAD

1

ELEMENTS GROUPS \$\$SKINPART\$ / TT 20.000

ELEMENTS GROUPS \$BEAD1\$ / QR 1 VARIABLE -10000 TRAJECTORY 1

; Notice the traj1, fe1, fn1 and ln1 have been changed, as has the TINF, which indicates  
; the start time for the heat source.

;The tables were deleted from this .dat file because they are identical to ap.dat

SAVE DATA 1043

MEDIUM

EXTRACT MEDIUM

DEASSIGN 19

ASSIGN 19 TRAN1043.TIT

:

TRANSIENT NON-LINEAR

BEHAVIOUR METALLURGY 4 FILE MAT1\_METALLURGY.DAT

ALGORITHM BFGS IMPLICIT 1 ITERATION 20  
PRECISION ABSOLUTE FORCE 0.01 DISPLACEMENT 0.1 ENERGY 10\*-20  
METHOD SYMMETRICAL TEST 0 ITERATIVE PRECISION ABSOLUTE 1\*-4  
STEP DTMINI 0.001 DTMAXI 0.500000 EPSF 10\*+20 EPSD 50. FACC 0.5 FACP  
1.2 FORCE  
INITIAL CONDITIONS RESTART CARD last  
TIME INITIAL 4.20  
10.45000000 STEP 0.02 / STORE 4  
RETURN  
SAVE DATA 1043

; The only changes here are the Time Initial and the final time (10.45).

## MAT1\_Metallurgy.dat

### MATERIAL 1 PHASE 4

KX(1) = KX(2) = KX(3) = TABLE 103

KX(4) = TABLE 104

C(1) = C(2) = C(3) = TABLE 105

C(4) = TABLE 106

RHO(1) = RHO(2) = RHO(3) = TABLE 107

RHO(4) = TABLE 108

### REACTION

1 4 HEATING PEQ table 11 TAU table 12

2 4 HEATING PEQ table 11 TAU table 12

3 4 HEATING PEQ table 11 TAU table 12

4 1 COOLING PEQ table 20 TAU table 21 F table 22

4 2 COOLING PEQ table 30 TAU table 31 F table 32

4 3 COOLING MS 475 KM 0.012

; KX is the thermal conductivity. C is the specific heat and RHO is the density.

; Each of these is defined for the 4 phases of this material.

; The reactions detail the change from one phase to another.

### TABLES

11 / 1 727 0 867 1

12 / 1 727 1 800 0.5 867 0.1 900 0.05 1000 0.01 1100 0.001

20 / 1 589 0 590 1 620 1 860 0

21 / 1 589 1\*6 590 1 620 1 700 1 780 10 860 100

22 / 1 -200 0.01 -100 0.14 -80 0.19 -40 0.26 -20 0.24 -12.5 0.21 -7 0.3

\* -5 0.7 -3.2 1 -0.1 1

30 / 1 479 0 480 1 595 0

31 / 1 479 1\*6 480 1 625 1

32 / 1 -280 0.01 -250 0.2 -200 0.5 -100 2 -80 3 -40 5 -20 2.5 -12.5 2

\* -7 3 -5 10

103 / 1 0 0.070 20 0.068 200 0.059 400 0.047 600 0.036 800 0.029

\* 900 0.027 1450 0.033

104 / 1 0 0.017 20 0.018 800 0.025 900 0.027 1450 0.033 1475 0.33

\* 1500 0.33 1550 0.33 1650 0.33 2500 0.33

; only the thermal conductivity for this liquidous phase should be multiplied by

; 10 to approximate convection in the molten pool. Also, the change should be made at

; a temperature just above the melting temperature. Changing the conductivity at 1450

; would make a slow increase in conductivity between 900°C and 1450°C, when a rapid

; increase is necessary.



105 / 1 0 475 20 480 100 502 200 544 300 569 400 624 500 682 700 800  
\* 800 909 900 649 1450 683

106 / 1 0 630 900 649 1450 683 1475 1220 1500 1850 1550 2480 1600 1850  
\* 1625 1220 1650 690 2500 700

107 / 1 0 7850\*-9 200 7800\*-9 400 7730\*-9 600 7653\*-9 700 7613\*-9  
\* 1600 7190\*-9

108 / 1 0 8104\*-9 800 7656\*-9 900 7600\*-9 1000 7548\*-9 1200 7443\*-9  
\* 1400 7320\*-9 1600 7190\*-9 2500 6940\*-9

END

## Material 1 – mp.dat

SEARCH DATA 1042

DEFINITION

m1

OPTION THREEDIMENSIONAL THERMOELASTICITY

RESTART GEOMETRY

MATERIAL PROPERTIES

ELEMENTS / INTE 2

ELEMENTS GROUPS \$PART\$ / E -10000 NU -10001 YIELD -10002 LX -10003 LY  
-10003 --

LZ -10003 SLOPE -10004 MODEL 2 PHAS 4 AUST 4 TF 1450 KY 0 TRAJ 1

ELEMENTS GROUPS \$BEAD1\$ / STATE=-3 E -10000 NU -10001 YIELD -10002  
LX -10003 LY -10003 --

LZ -10003 SLOPE -10004 MODEL 2 PHAS 4 AUST 4 TF 1450 KY 0

ELEMENTS GROUPS \$BEAD2\$ / STATE=-4 E -10000 NU -10001 YIELD -10002  
LX -10003 LY -10003 --

LZ -10003 SLOPE -10004 MODEL 2 PHAS 4 AUST 4 TF 1450 KY 0

ELEMENTS GROUPS \$BEAD3\$ / STATE=-4 E -10000 NU -10001 YIELD -10002  
LX -10003 LY -10003 --

LZ -10003 SLOPE -10004 MODEL 2 PHAS 4 AUST 4 TF 1450 KY 0

ELEMENTS GROUPS \$BEAD4\$ / STATE=-4 E -10000 NU -10001 YIELD -10002  
LX -10003 LY -10003 --

LZ -10003 SLOPE -10004 MODEL 2 PHAS 4 AUST 4 TF 1450 KY 0

ELEMENTS GROUPS \$BEAD5\$ / STATE=-4 E -10000 NU -10001 YIELD -10002  
LX -10003 LY -10003 --

LZ -10003 SLOPE -10004 MODEL 2 PHAS 4 AUST 4 TF 1450 KY 0

ELEMENTS GROUPS \$BEAD6\$ / STATE=-4 E -10000 NU -10001 YIELD -10002  
LX -10003 LY -10003 --

LZ -10003 SLOPE -10004 MODEL 2 PHAS 4 AUST 4 TF 1450 KY 0

ELEMENTS GROUPS \$BEAD7\$ / STATE=-4 E -10000 NU -10001 YIELD -10002  
LX -10003 LY -10003 --

LZ -10003 SLOPE -10004 MODEL 2 PHAS 4 AUST 4 TF 1450 KY 0

: Like the thermal simulation, the characteristics of the all the elements are defined  
: initially. Unlike the thermal simulation however, the properties are not defined in a  
: separate file, but direction in this file. However, the tables for these properties have  
: been removed in an attempt to conserve space. The state = -4 ensures that a bead  
: stay deactivated. The other variable are: E = Young's modulus, NU = Poisson's ratio,  
: YIELD = yield strength, LX, LY, LZ = coefficient of thermal expansion, and SLOPE  
: which refers to the slope of the stress/strain curve.

MEDIUM

WELDLINE / GROUPS \$TRAJp\$ ELEMENTS \$fep\$ START \$fnp\$ ARRIVAL  
\$lnp\$ VELOCITY 6.000000 TINF 0.000000 MODEL 1  
CONSTRAINTS

CONSTRAINTS  
NODES 1653/ UX UY UZ

; Constraints enables addition of constraints to the model at specific nodes

LOAD  
1 NOTHING

\*note: the tables defining the mechanical material properties have been removed due to their excessive length.

4 / FORTRAN  
FUNCTION F(X)  
DIMENSION X(5)  
xa = X(1)  
ya = X(2)  
za = X(3)  
time = X(4)

C  
f = -1

) return  
end  
5 / FORTRAN  
FUNCTION F(X)  
DIMENSION X(5)  
xa = X(1)  
ya = X(2)  
za = X(3)  
time = X(4)

C  
f = 1

return  
end  
3 / FORTRAN  
FUNCTION F(X)  
DIMENSION X(5)  
xa = X(1)  
ya = X(2)  
za = X(3)  
time = X(4)

C

```
f = 0
ro = 1.5
zlimit = 0.0
zllimit = -0.41
xx = xa * xa
yy = ya * ya
```

c

```
rr = xx + yy
rr = sqrt(rr)
```

c

```
if (ya.le.0) goto 6
goto 7
6 if (rr. le. ro) f=1
7 if (za. gt. zlimit) f = 0
if (za. lt. zllimit) f = 0
return
end
```

RETURN

SAVE DATA 1053

MEDIUM

EXTRACT MEDIUM

```
;  
; Welding Wizard - Thermo-mechanical Analyses
```

```
;  
; Load Thermal Analysis
```

```
;  
SEARCH DATA 1043
```

```
ASSIGN 19 TRAN1043.TIT
```

```
TEMPERATURE TRANSIENT METALLURGY CARD
```

```
DEASSIGN 19
```

```
;  
: Data Mechanics
```

```
;  
SEARCH DATA 1053
```

```
;  
: Time Step 1
```

```
;  
TRANSIENT NON-LINEAR STATIC ARCHIVATE
```

```

BEHAVIOUR PLASTIC METALLURGY 4
ALGORITHM OPTIMISE 1 1 20 IMPLICIT 1 ITERATION 20
PRECISION ABSOLUTE FORCE 5. DISPLACEMENT 10*-20 ENERGY 10*-20
UNIT
METHOD SYMMETRICAL TEST 0 ITERATIVE PRECISION ABSOLUTE 1*-6
INITIAL CONDITIONS
ELEMENTS GROUP $BEAD1$ / IS -1
ELEMENTS GROUP $BEAD2$ / IS -1
ELEMENTS GROUP $BEAD3$ / IS -1
ELEMENTS GROUP $BEAD4$ / IS -1
ELEMENTS GROUP $BEAD5$ / IS -1
ELEMENTS GROUP $BEAD6$ / IS -1
ELEMENTS GROUP $BEAD7$ / IS -1

;
TIME INITIAL 0.
0.01000 / STORE 1
RETURN
;
; Save as Files DATAyyyy.TIT, TRANyyyy.TIT And HISTyyyy.TIT
;
SAVE DATA TRAN HIST 1053
; File TRANyyyy.TIT And HISTyyyy.TIT

ASSIGN 25 HIST1053.TIT
ASSIGN 19 TRAN1053.TIT
;
TRANSIENT NON-LINEAR STATIC ARCHIVATE
BEHAVIOUR PLASTIC METALLURGY 4
ALGORITHM OPTIMISE 1 1 20 IMPLICIT 1 ITERATION 20
PRECISION ABSOLUTE FORCE 5. DISPLACEMENT 10*-20 ENERGY 10*-20
UNIT
METHOD SYMMETRICAL TEST 0 ITERATIVE PRECISION ABSOLUTE 1*-6
STEP DTMINI .001 DTMAXI 0.500000 EPSF 100. EPSD 10*+20 FACC .5 FACP 1.2
INITIAL CONDITIONS RESTART CARD LAST
TIME INITIAL RESTART
4.200000 STEP .02 / STORE 2
RETURN
SAVE DATA 1053
; Some minor differences occur in the format of the mechanical and thermal files.

```

## Vita

Matthew Tomik was born in Poughkeepsie, NY on December 2, 1980. He graduated from The Millbrook School in 1999. He then proceeded to Lafayette College, where he was awarded a Marquis Scholarship, and studied Mechanical Engineering. He graduated Cum-Laude from Lafayette in 2003. His next step was enrolling in Lehigh University to research finite element modeling of LENS. He graduated from Lehigh in 2005 with a Masters of Science in Mechanical Engineering and went on to pursue a career at Picatinny Arsenal, in Picatinny, New Jersey.



**END OF  
TITLE**